Fundamentals of Electronic Structure Theory (PHU.013)

WS 2018/19

Assoz.-Prof. Dr. Peter Puschnig
Institut für Physik, Fachbereich Theoretische Physik
Karl-Franzens-Universität Graz
Universitätsplatz 5, A-8010 Graz
peter.puschnig@uni-graz.at
http://physik.uni-graz.at/~pep

Graz, December 7, 2018

Contents

Chapter 1

Introduction

1.1 Quantum Mechanical Many-Electron Problem

We start with a quote from John P. Perdew [1] whose work on density functional theory has led to him being one of the world's most cited physicists. [1]

"The material world of everyday experience, as studied by chemistry and condensed-matter physics, is built up from electrons and a few (or at most a few hundred) kinds of nuclei. The basic interaction is electrostatic or Coulombic: An electron at position $\boldsymbol{r}$ *is attracted to a nucleus of charge* Z *at* $\boldsymbol{R}$ *by the potential energy* $-Z/|\boldsymbol{r}-\boldsymbol{R}|$*, a pair of electrons at* $\boldsymbol{r}$ *and* $\boldsymbol{r}'$ *repel one another by the potential energy* $1/|\boldsymbol{r}-\boldsymbol{r}'|$*, and two nuclei at* $\boldsymbol{R}$ *and* $\boldsymbol{R}'$ *repel one another as* $ZZ'/|\boldsymbol{R}-\boldsymbol{R}'|$*. The electrons must be described by quantum mechanics, while the more massive nuclei can sometimes be regarded as classical particles. All of the electrons in the lighter elements, and the chemically important valence electrons in most elements, move at speeds much less than the speed of light, and so are non-relativistic.*

In essence, that is the simple story of practically everything. But there is still a long path from these general principles to theoretical prediction of the structures and properties of atoms, molecules, and solids, and eventually to the design of new chemicals or materials. If we restrict our focus to the important class of ground-state properties, we can take a shortcut through density functional theory."

Let us now consider the Hamiltonian of a system of N electrons with spatial and spin coordinates $\boldsymbol{r}_i$ and σ_i, respectively, and K atomic nuclei with coordinates $\boldsymbol{R}_k$, charge numbers Z_k and masses M_k. Here, and throughout these lecture notes, we will use *atomic units*, thus formally we set Planck's reduced constant $\hbar = 1$, the electron mass $m = 1$, and the term $\frac{e^2}{4\pi\varepsilon_0} = 1$. As a consequence, we will measure units in the natural units for electrons, thus the length unit is the Bohr radius $a_0 = 0.52917721092(17)$ Å, the energy unit is called 1 Hartree (Ha) = 27.211385 eV, and the unit of time

[1] See, for instance, https://en.wikipedia.org/wiki/John_Perdew

is $t_0 = 2.418884326505(16) \times 10^{-17}$ seconds.[2] Then, the non-relativistic Hamiltonian consisting of the following five terms takes the form:

$$\hat{H} = \underbrace{-\frac{1}{2}\sum_{i=1}^{N}\Delta_i}_{\hat{T}} + \underbrace{\frac{1}{2}\sum_{i,j\neq i}\frac{1}{|\boldsymbol{r}_i - \boldsymbol{r}_j|}}_{\hat{V}_{ee}} \underbrace{-\sum_{i=1}^{N}\sum_{k=1}^{K}\frac{Z_k}{|\boldsymbol{r}_i - \boldsymbol{R}_k|}}_{\hat{V}_{en}} \underbrace{-\frac{1}{2M_k}\sum_{k=1}^{K}\Delta_k}_{\hat{T}_n} + \underbrace{\frac{1}{2}\sum_{k,l\neq k}\frac{Z_k Z_l}{|\boldsymbol{R}_k - \boldsymbol{R}_l|}}_{\hat{V}_{nn}}. \tag{1.1}$$

The first term, $\hat{T}$, denotes the kinetic energy of the electrons, the second one, $\hat{V}_{ee}$ is the electron-electron Coulomb repulsion. Note that with $\sum_{i,j\neq i}$ we denote a double summation over all electrons excluding $i = j$ since a given electron obviously cannot interact with itself. To counterbalance the double counting of interactions of electron i with j, and j with i, in the double sum, we introduce the factor $\frac{1}{2}$. The third term, $\hat{V}_{en}$, is the attractive electron-nuclei interaction. The remaining two terms, $\hat{T}_n$ and $\hat{V}_{nn}$, respectively, are the kinetic energy of the atomic nuclei and the Coulombic nuclei-nuclei interaction. Stationary states are obtained from the time-independent Schrödinger equation

$$\hat{H}\Psi\left(\{\boldsymbol{r}_i\},\{\boldsymbol{R}_k\}\right) = E\Psi\left(\{\boldsymbol{r}_i\},\{\boldsymbol{R}_k\}\right), \tag{1.2}$$

where E is the energy of a stationary state and $\Psi\left(\{\boldsymbol{r}_i\},\{\boldsymbol{R}_k\}\right)$ a wave function containing all electron and nuclear degrees of freedom as coordinates. This is an immensely difficult problem, that can only be solved for atoms or very simple molecules.

In order to simplify this complex many-electron / many-nuclei problem, we will introduce the *Born-Oppenheimer approximation* (BO) [2]. The BO approximation is ubiquitous in quantum chemical calculations of molecular wavefunctions and, even more so, for "band structure calculations" in solid-state physics. Due to the much larger mass of the atomic nuclei compared to the electron mass, the nuclear kinetic energy $\hat{T}_n$ can be neglected. In the remaining electronic Hamiltonian $\hat{H}_e$, the nuclear positions only enter as parameters. The electron-nucleus interactions are not removed, and the electrons still "feel" the Coulomb potential of the nuclei, however, the nuclei are clamped (fixed) at certain positions in space. Therefore, this is often referred to as the clamped-nuclei approximation, and the Hamiltonian takes the form

$$\hat{H}_e = \underbrace{-\frac{1}{2}\sum_{i=1}^{N}\Delta_i}_{\hat{T}} + \underbrace{\frac{1}{2}\sum_{i,j\neq i}\frac{1}{|\boldsymbol{r}_i - \boldsymbol{r}_j|}}_{\hat{V}_{ee}} + \underbrace{\sum_{i=1}^{N} v(\boldsymbol{r}_i)}_{\hat{V}_{\text{ext}}}. \tag{1.3}$$

Here we have renamed the electron-nucleus interaction as the "external" potential $\hat{V}_{\text{ext}}$ which can be written as a sum over the local potential $v(\boldsymbol{r})$ that is felt by a given electron in the electro-static field

[2] The speed of light in atomic units is $c = 1/\alpha \approx 137$.

of all nuclei at the clamped positions $\boldsymbol{R}_k$

$$v(\boldsymbol{r}) = -\sum_{k=1}^{K} \frac{Z_k}{|\boldsymbol{r} - \boldsymbol{R}_k|}. \tag{1.4}$$

The stationary Schrödinger equation for the electronic problem then reads

$$\hat{H}_e \psi_q \left(\{\boldsymbol{r}_i \sigma_i\}; \{\boldsymbol{R}_k\}\right) = E_q(\{\boldsymbol{R}_k\}) \psi_q \left(\{\boldsymbol{r}_i \sigma_i\}; \{\boldsymbol{R}_k\}\right). \tag{1.5}$$

Here, ψ_q is the many-electron wave function with the set of quantum numbers abbreviated as q, which depends on the N electron coordinates $\boldsymbol{r}_i \sigma_i$ and contains, *as parameters*, the fixed nuclear positions $\boldsymbol{R}_k$. Thus, also the energy E_q can be viewed as a function of the nuclear coordinates, which is referred to as the $3K$-dimensional Born-Oppenheimer surface.

The full solution of Eq. 1.5 leading to the N-electron wave function can, however, be only achieved for sufficiently small molecules. This is because, as can be shown, the numerical complexity of the problem scales *exponentially* with the number of electrons N. This has been nicely illustrated in the Nobel Lecture of Walter Kohn and is also referred to as Van Vleck's catastrophy [3]. On the other hand, a theory based on the electron density $n_\sigma(\boldsymbol{r})$,

$$n_\sigma(\boldsymbol{r}) = N \sum_{\sigma_2 \cdots \sigma_N} \int \mathrm{d}^3 r_2 \cdots \int \mathrm{d}^3 r_N \left|\psi(\boldsymbol{r}\sigma, \boldsymbol{r}_2 \sigma_2, \cdots, \boldsymbol{r}_N \sigma_N)\right|^2, \tag{1.6}$$

rather than on the N-electron wave function does not encounter such an "exponential wall", but scales only as N^3. Because of the normalization of the wave function

$$\langle \psi \,|\psi\rangle = \sum_{\sigma_1 \sigma_2 \cdots \sigma_N} \int \mathrm{d}^3 r_1 \int \mathrm{d}^3 r_2 \cdots \int \mathrm{d}^3 r_N \left|\psi(\boldsymbol{r}_1 \sigma_1, \boldsymbol{r}_2 \sigma_2, \cdots, \boldsymbol{r}_N \sigma_N)\right|^2 = 1, \tag{1.7}$$

it is easy to see that the integration over $\boldsymbol{r}$ and the summation over the spin channels σ for the spin density $n_\sigma(\boldsymbol{r})$ yields the total number of electrons N:

$$\sum_\sigma \int \mathrm{d}^3 r n_\sigma(\boldsymbol{r}) = N. \tag{1.8}$$

Based on the theorems by Hohenberg and Kohn to be discussed in detail in Chapter 3, it is indeed possible to find an equivalent description of the electronic structure problem solely in terms on the density. As always, there is no free lunch, and in this case the price to be paid is that the so-called *density functional theory* (DFT) is a *ground state theory*. This means that, rather than having access to all states E_q of the many-electron system, DFT only yields the energetically lowest possible state E_0, that is the electronic ground state.

1.2 Density Functional Theory in a Nutshell

Applied scientific research depends on the existence of accurate theoretical models. In particular, highly reliable *ab-initio* methods are in-dispensable for designing novel materials as well as for a detailed understanding of their properties. The development of such theories describing the electronic structure of atoms, molecules, and solids has been one of the success stories of physics in the 20$^{\text{th}}$ century. Among these, density functional theory (DFT) [3–6] has proven to yield *ground state* properties for a vast number of systems in a very precise manner.[3]

DFT [3–5, 7] provides a rigorous framework to reduce the interacting many-electron problem to an effective system of non-interacting electrons which will be the topic of Chapter 3. There it will be shown that the quantum-mechanical, i.e. *ab-initio*, treatment of materials properties becomes tractable by solving the so-called Kohn-Sham equations. These equations are essentially *single*-particle Schrödinger equations with an effective potential.

$$\left[-\frac{1}{2}\Delta + v_s(\boldsymbol{r})\right]\varphi_j(\boldsymbol{r}) = \varepsilon_j\varphi_j(\boldsymbol{r}). \tag{1.9}$$

Here $v_s(\boldsymbol{r})$ is an effective potential, the Kohn-Sham potential,

$$v_s(\boldsymbol{r}) = v(\boldsymbol{r}) + v_H(\boldsymbol{r}) + v_{xc}(\boldsymbol{r}), \tag{1.10}$$

comprised of the *external* potential $v(\boldsymbol{r})$ due to the atomic nuclei as defined in Eq. 1.4, the *Hartree* potential $v_H(\boldsymbol{r})$ and the so-called *exchange-correlation* potential $v_{xc}(\boldsymbol{r})$. The eigenvalues ε_j of Eq. 1.9 are the Kohn-Sham energies, and the eigenfunctions $\varphi_j(\boldsymbol{r})$ the Kohn-Sham orbitals. The density $n(\boldsymbol{r})$ is constructed from the single particle orbitals $\varphi_j(\boldsymbol{r})$, as

$$n(\boldsymbol{r}) = \sum_{j=1}^{N} \left|\varphi_j(\boldsymbol{r})\right|^2. \tag{1.11}$$

It is important to note that Eqs. 1.9 and 1.11 have to be solved *self-consistently*, i.e. iteratively, since the Hartree as well as the exchange-correlation potential depend on the density.

Recommended Literature. (i) A Primer in Density Functional Theory, Fiolhais et al. (Editors) [1]; (ii) Electronic Structure: Basic Theory and Practical Methods, Richard M. Martin [8]; (iii) Density Functional Theory: A Practical Introduction, Sholl and Steckel [9].

[3]The Nobel Prize in Chemistry 1998 was awarded to Walter Kohn for his development of the density-functional theory.

1.3 Typical Applications of DFT

Before we continue in Chapter 2 to review the theoretical foundations of density functional theory and discuss in some detail the fundamental equations of DFT in Chapter 3, the remaining section of the first introductory Chapter aims at presenting typical applications of actual DFT calculations for molecules, surfaces and solids. Thus, this section serves as a motivation for what follows and may also be skipped at this time.

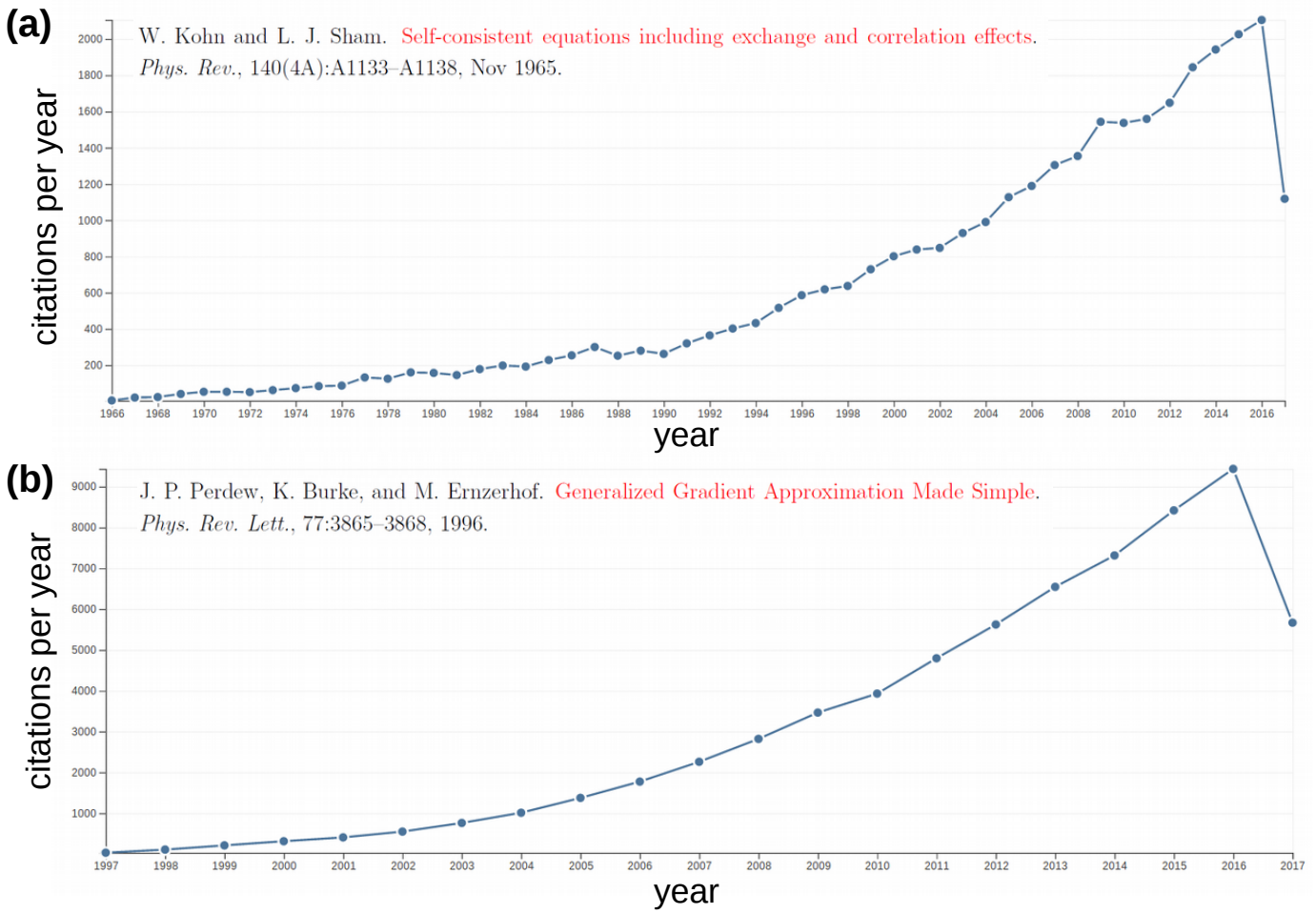

Figure 1.1: Citation report from August, 9th 2017 for two fundamental papers in the field of density functional theory, (a) the Kohn-Sham paper from 1965 [5], and (b) Perdew's paper about the generalized gradient approximation for exchange and correlation effects from 1996 [10].

To demonstrate the importance of DFT for theoretical solid state physics and quantum chemistry (but indeed also for related fields such as materials science, biochemistry, ...) Fig. 1.1 shows recent citation reports of two fundamental papers, namely the original Kohn-Sham paper from 1965 [5], and Perdew's famous paper about the generalized gradient paper for exchange-correlation effects from

1996. Both citation reports demonstrate the steadily growing interest in DFT. On the one hand this is due to the availability modern computer hardware which enables larger and larger systems to be computed. Nowadays, structures containing a few hundred atoms, translating typically into a few thousand electrons N, are routinely possible. On the other hand, the accuracy of the numerical results and thereby the capability to predict materials properties with sufficient precision has also grown owing to continuous improvements in theory (exchange-correlation functional) and numerics (basis sets, parallelization).

1.3.1 Equilibrium Geometries and Hellmann-Feynman Theorem

The self-consistent solution of Eqs. 1.9 and 1.11 leads to the ground state electron density $n(\boldsymbol{r})$ and the corresponding *ground state total energy* E. Because the total energy depends on the coordinates of the clamped nuclei

$$E = E(\boldsymbol{R}_1, \boldsymbol{R}_2, \cdots \boldsymbol{R}_K), \tag{1.12}$$

one can determine the equilibrium geometry of molecules and solids by varying the coordinates $(\boldsymbol{R}_1, \boldsymbol{R}_2, \cdots \boldsymbol{R}_K)$ and searching for the minimum in the total energy. This is illustrated in Fig. 1.2 for the most simple molecule, the H_2 molecule.

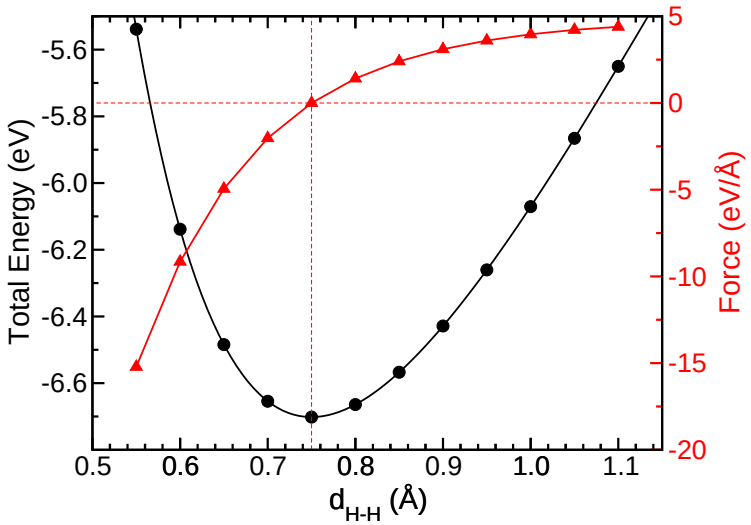

Figure 1.2: Total energy (black circles, left axis) and force on hydrogen atom (red triangles, right axis) for the hydrogen molecule H_2.

For the hydrogen molecule, there is only one internal degree of freedom, namely the bond distance $d_{\mathrm{H-H}}$. In Fig. 1.2 results of a DFT calculation for the total energy is shown where $d_{\mathrm{H-H}}$ has been

varied between 0.55 and 1.10 Å in steps of 0.05 Å. Clearly, there is a minimum at 0.75 Å which corresponds to the predicted equilibrium bond length of the H_2 molecule. This value compares quite well to the experimental value of 0.74144 Å as taken from the NISTChemistryWebBook. The remaining difference between the DFT prediction and the experimental value is due to certain approximations in the exchange correlation potential which will be discussed in detail in Sec. 3.5.

For molecules with more nuclear degrees of freedom, the search for the equilibrium geometry merely based on the total energy would be quite cumbersome. Fortunately, one can make use of the *Hellmann-Feynman theorem* (or equivalently the force theorem) which allows for much more efficient geometry relaxations. Assuming that the Hamiltonian $\hat{H}$ of a quantum mechanical system depends on a parameter λ and obeys the eigenvalue equation

$$\hat{H}(\lambda)\,|\psi(\lambda)\rangle = E(\lambda)\,|\psi(\lambda)\rangle\,, \tag{1.13}$$

the Hellmann-Feynman theorem relates the derivative of the total energy with respect to λ, to the expectation value of the derivative of the Hamiltonian with respect to that same parameter

$$\frac{\mathrm{d}E(\lambda)}{\mathrm{d}\lambda} = \left\langle \psi(\lambda) \middle| \frac{\mathrm{d}\hat{H}(\lambda)}{\mathrm{d}\lambda} \middle| \psi(\lambda) \right\rangle. \tag{1.14}$$

The proof of the Hellmann-Feynman theorem uses the fact that the wavefunction $|\psi(\lambda)\rangle$ is normalized, thus

$$\langle \psi(\lambda)\,|\,\psi(\lambda)\rangle = 1 \quad \Rightarrow \quad \frac{\mathrm{d}}{\mathrm{d}\lambda}\,\langle \psi(\lambda)\,|\,\psi(\lambda)\rangle = 0. \tag{1.15}$$

Applying the product rule of for differentiation and making use of the eigenvalue equation 1.13, we can proof the Hellmann-Feynman theorem

$$\begin{aligned}
\frac{\mathrm{d}E(\lambda)}{\mathrm{d}\lambda} &= \frac{\mathrm{d}}{\mathrm{d}\lambda}\left\langle \psi(\lambda) \middle| \hat{H}(\lambda) \middle| \psi(\lambda) \right\rangle \\
&= \left\langle \frac{\mathrm{d}\psi(\lambda)}{\mathrm{d}\lambda} \middle| \hat{H}(\lambda) \middle| \psi(\lambda) \right\rangle + \left\langle \psi(\lambda) \middle| \hat{H}(\lambda) \middle| \frac{\mathrm{d}\psi(\lambda)}{\mathrm{d}\lambda} \right\rangle + \left\langle \psi(\lambda) \middle| \frac{\mathrm{d}\hat{H}(\lambda)}{\mathrm{d}\lambda} \middle| \psi(\lambda) \right\rangle \\
&= E(\lambda)\left\langle \frac{\mathrm{d}\psi(\lambda)}{\mathrm{d}\lambda} \middle| \psi(\lambda) \right\rangle + E(\lambda)\left\langle \psi(\lambda) \middle| \frac{\mathrm{d}\psi(\lambda)}{\mathrm{d}\lambda} \right\rangle + \left\langle \psi(\lambda) \middle| \frac{\mathrm{d}\hat{H}(\lambda)}{\mathrm{d}\lambda} \middle| \psi(\lambda) \right\rangle \\
&= E(\lambda)\underbrace{\frac{\mathrm{d}}{\mathrm{d}\lambda}\,\langle \psi(\lambda)\,|\,\psi(\lambda)\rangle}_{=0} + \left\langle \psi(\lambda) \middle| \frac{\mathrm{d}\hat{H}(\lambda)}{\mathrm{d}\lambda} \middle| \psi(\lambda) \right\rangle \\
&= \left\langle \psi(\lambda) \middle| \frac{\mathrm{d}\hat{H}(\lambda)}{\mathrm{d}\lambda} \middle| \psi(\lambda) \right\rangle.
\end{aligned}$$

The general Hellmann-Feynman theorem stated above can be utilized to derive the electro-static force theorem [1, 8]. Within the Born-Oppenheimer approximation, the electronic Hamilitonian depends parametrically on the positions $(\boldsymbol{R}_1, \boldsymbol{R}_2, \cdots \boldsymbol{R}_K)$ of the atomic nuclei

$$\hat{H}(\boldsymbol{R}_1, \boldsymbol{R}_2, \cdots \boldsymbol{R}_K) = -\frac{1}{2}\sum_{i=1}^{N}\Delta_i + \frac{1}{2}\sum_{i,j\neq i}\frac{1}{|\boldsymbol{r}_i - \boldsymbol{r}_j|} - \sum_{i=1}^{N}\sum_{k=1}^{K}\frac{Z_k}{|\boldsymbol{r}_i - \boldsymbol{R}_k|} + \frac{1}{2}\sum_{k,l\neq k}\frac{Z_k Z_l}{|\boldsymbol{R}_k - \boldsymbol{R}_l|}. \quad (1.16)$$

Thus, with the help of the Hellmann-Feynman theorem 1.14, we obtain for the force $\boldsymbol{F}_k$ acting on the k-th atomic nucleus

$$\boldsymbol{F}_k = -\frac{\partial E}{\partial \boldsymbol{R}_k} = \left\langle \psi \left| -\frac{\partial \hat{H}}{\partial \boldsymbol{R}_k} \right| \psi \right\rangle = \int \mathrm{d}^3 r\, n(\boldsymbol{r}) \frac{Z_k(\boldsymbol{r} - \boldsymbol{R}_k)}{|\boldsymbol{r} - \boldsymbol{R}_k|^3} + \sum_{l\neq k}\frac{Z_k Z_l(\boldsymbol{R}_k - \boldsymbol{R}_l)}{|\boldsymbol{R}_k - \boldsymbol{R}_l|^3}. \quad (1.17)$$

According to the electro-static force theorem, once the spatial distribution of the electrons $n(\boldsymbol{r})$ has been determined by solving Kohn-Sham equations, all the forces in the system can be calculated using classical electrostatics. Note that for deriving the first term in 1.17 involving the integral, we have made use of 1.6, and that the summation $\sum_{l\neq k}$ in the second term denotes a single sum excluding the case where $l = k$.

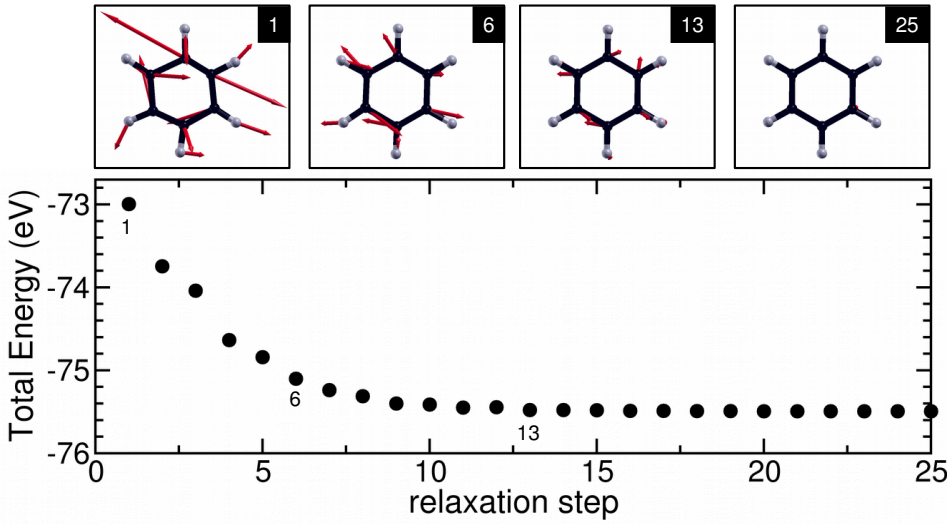

Figure 1.3: Snapshots of the geometry relaxation of a benzene ring making use of the Hellman-Feynman forces (red arrows).

The calculation of the forces acting on atomic nuclei based on 1.17 proves extremely useful when searching for the equilibrium geometry of structures such as a molecule. This is illustrated already in Fig. 1.2 for the H_2 molecule and in Fig. 1.3 for the more complicated benzene molecule with $3K = 36$ nuclear degrees of freedom. In this example, it takes about 25 geometry steps to find the equilibrium

geometry. At each step, the Kohn-Sham equations need to be solved self-consistently leading to the density $n(\boldsymbol{r})$ from which, according to 1.17, the atomic forces (red arrows) can be obtained. The snapshots of the relaxation procedure shown in Fig. 1.3 nicely demonstrate how forces are getting smaller and smaller accompanied by a steady decrease in the total energy.

1.3.2 Equilibrium Lattice Parameters of Bulk Crystals

Similar to the bond length variation previously shown for the H_2 molecules, we can apply an analogous procedure to periodic structures, that is crystalline solids, and determine their so-called *equation of state*. Thus, we solve the Kohn-Sham equations for a series of lattice parameters and plot the resulting total energies as a function of the unit cell volume.

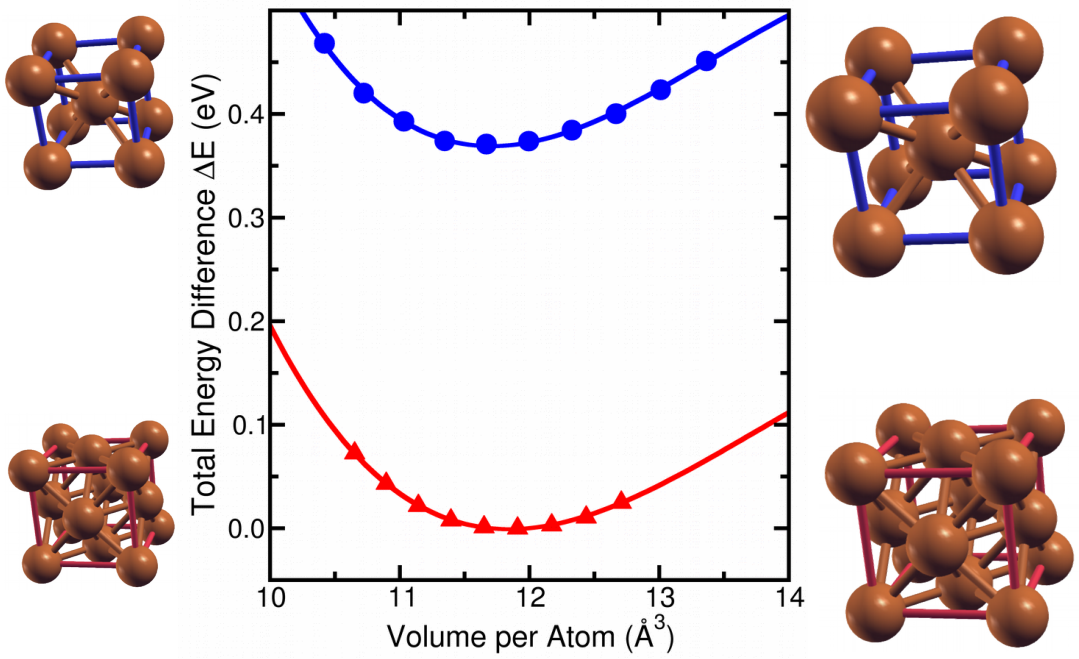

Figure 1.4: Equation of state for bulk copper in the face centered cubic (fcc) and body centered cubic (bcc) structures.

This is illustrated in Fig. 1.4 for bulk copper assuming, on the one hand, a face centred cubic structure (red color), or a body centred cubic structure (blue color), on the other. Without any empirical input, the results thus suggest that copper prefers to crystallize in the fcc structure with an equilibrium volume of about $V_0 = 11.85$ Å^3 per atom which translates into an equilibrium lattice parameter of $a_0 = \sqrt[3]{4V_0} \approx 3.63$ Å. This number compares quite well to the experimental value of 3.60 Å, the deviation is again due to the specific approximation used for exchange-correlation effects (see Sec. 3.5 for more details).

1.3.3 Bulk Modulus and Elastic Properties

Energy versus volume plots such as depicted in Fig. 1.4 also allow the bulk modulus to be determined from the second derivative of $E(V)$. The bulk modulus B is defined as the derivative of pressure p with respect to volume via

$$B = -V \left(\frac{\partial p}{\partial V} \right)_T , \tag{1.18}$$

where in turn pressure is given the the volume derivative of the total energy as

$$p = - \left(\frac{\partial E}{\partial V} \right)_S . \tag{1.19}$$

Combining these two equations shows that the bulk modulus can be obtained from the curvature of the equation of state $E(V)$ multiplied by the volume

$$B = V \left(\frac{\partial^2 E}{\partial V^2} \right) . \tag{1.20}$$

It is common to fit the numerically obtained points $(V_1, E_1), (V_2, E_2), \cdots$ to a functional form which is based on some physical assumptions. One commonly used equation of state is the one suggested by Murnaghan [11]. By assuming that the bulk modulus is a linear function of pressure

$$B(p) = B_0 + B_0' p \tag{1.21}$$

one can derive the following expression[4] for the total energy

$$E(V) = E_0 + \frac{B_0 (V - V_0)}{B_0' - 1} + \frac{B_0 V}{B_0' (B_0' - 1)} \left[\left(\frac{V_0}{V} \right)^{B_0'} - 1 \right] . \tag{1.22}$$

This equation of state contains four (fit) parameters, where B_0 and V_0, respectively, denote the zero pressure bulk modulus and unit cell volume, B_0' is the pressure derivative of the bulk modulus, and E_0 is the energy at zero pressure. When fitting 1.22 to the data points for fcc Cu leading to the solid red line, one obtains a value of $B_0 = 139$ GPa which is only slightly smaller than the measured value of 142 GPa.

The bulk modulus is only a particular example for one elastic modulus. Most generally, the linear elastic properties of crystals are described by the generalization of Hooke's law ($F = -kx$)

$$\sigma_{ij} = C_{ijkl} \varepsilon_{kl} . \tag{1.23}$$

[4] Although this is not the recommended practice, in this case wikipedia may be consulted for the derivation of the Murnaghan_equation_of_state.

Here, ε_{kl} is the *strain tensor* and σ_{ij} denotes the *stress tensor* which are both symmetric tensors of second rank. Therefore, the proportionality constant is a tensor of 4^{th} rank and is called the elastic tensor C_{ijkl}, its elements are the elastic constants. The dimensionless strain tensor describes how a point in space $\boldsymbol{r}$, or specifically the unit cell of a crystal, is deformed under a given strain to yield the point $\boldsymbol{r}'$

$$r_i' = (\delta_{ij} + \varepsilon_{ij}) r_j. \tag{1.24}$$

The stress tensor can be defined as the derivative of the total energy with respect to the strain

$$\sigma_{ij} = \frac{1}{V} \frac{\partial E}{\partial \varepsilon_{ij}}. \tag{1.25}$$

Thus it has units of energy/volume or equivalently force/area representing a pressure. Numerically, the components of the stress tensor can be obtained by choosing an appropriate type of strain and computing the total energy for various magnitudes of the strain. Finally, the elastic constants are related to the second derivative of the total energy with respect to strain in the following manner

$$C_{ijkl} = \frac{1}{V} \frac{\partial^2 E}{\partial \varepsilon_{ij} \partial \varepsilon_{kl}}. \tag{1.26}$$

For technical details on how to obtain the elastic constant of crystals from density functional calculations in practice the following reference is recommended: Golesorkhtabar et al. [12].

1.3.4 Surfaces of Crystals and Adsorption of Molecules

DFT calculations cannot only be used to study the properties of bulk crystals, but also crystal defects can be investigated. This includes point defects [14] as well as extended defects such as dislocations [15], grain boundaries [16] and crystal surfaces [13]. Here we will give a brief example for DFT results for crystal surfaces.

As will be described in detail in Chapter 4, most DFT implementations for solid state applications utilize basis functions which describe Bloch waves, that is, there are periodic boundary conditions in all three spatial directions. In order to perform calculations for a crystal surface, the so-called *repeated slab approach* is commonly used. Thus, instead of a semi-infinite crystal terminated by a single crystal surface, one approximates a surface by a crystal slab of finite thickness terminated by two planes at top and bottom of the slab. A typical unit cell for such a repeated slab calculation is illustrated in panel (a) of Fig. 1.5 for a (100) surface of an fcc crystal. It contains 15 atomic layers and an additional vacuum layer which is used to decouple the slab from its periodic images in z-direction.

Using the Hellmann-Feynman forces and relaxing the geometry of the slab, one observes that the topmost (and bottom most) atomic layers turn out to exhibit interlayer spacings d_{ij} which differ from

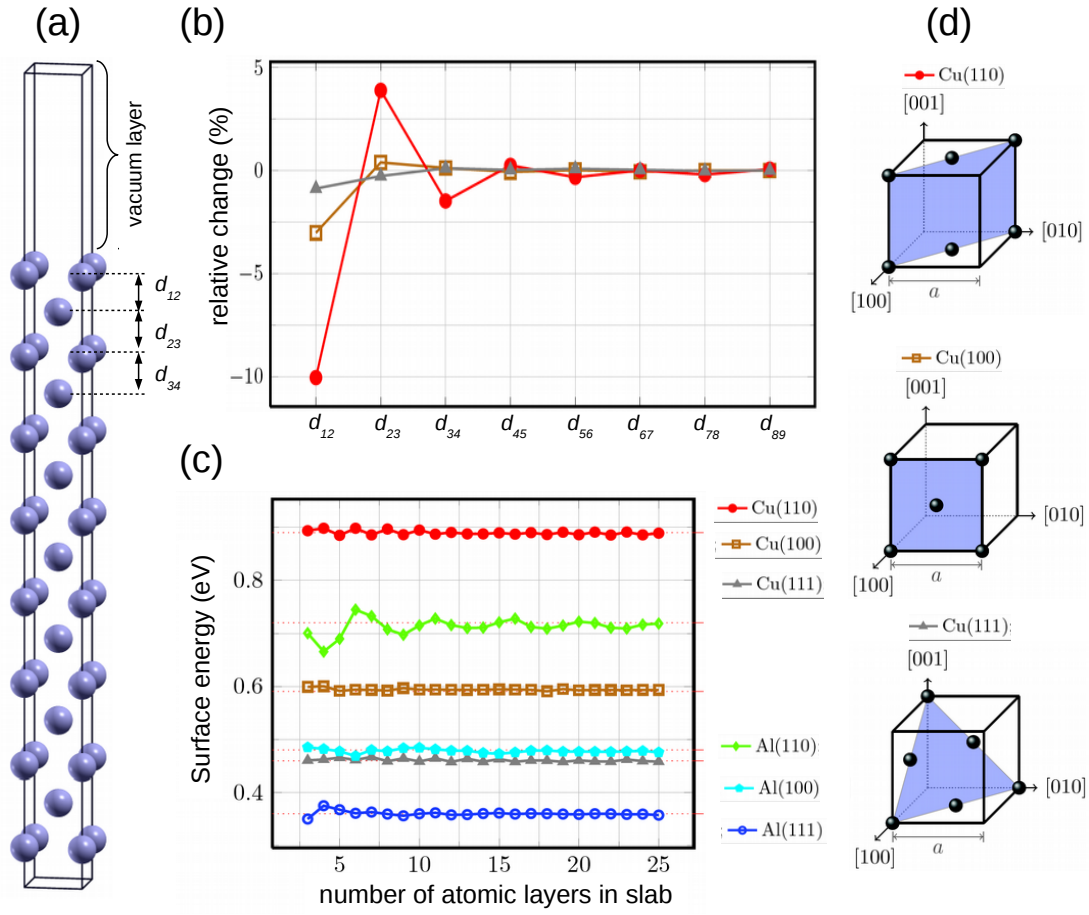

Figure 1.5: (a) Unit cell in the repeated slab approach for surface calculations containing 15 atomic layers. (b) Relaxation of the interlayer distances of the topmost atomic layers. (c) Convergence of the surface energy with respect to the number of atomic layers in the slab for the (110), (100) and (111) crystal faces of Cu and Al schematically depicted in panel (d). The figure is reproduced from the Master Thesis of Dario Knebl [13].

the interlayer spacing calculated for a bulk crystal (Fig. 1.5b). This relaxation is most pronounced for the first layers, $d_{12}, d_{23}, \cdots$ and approaches rather quickly the bulk value. Comparing the three crystal planes (110), (100), (111) of copper, it is found that the most open (110) surface shows the largest relaxations while the close-packed (111) surface retains interlayer spacings quite similar to the bulk crystal.

Fig. 1.5c shows the surface energy E_{surf} of the (110), (100) and (111) crystal faces of Cu and Al which is defined in the following way

$$E_{\text{surf}} = -\frac{1}{2}\left(E_{\text{slab}} - n \cdot E_{\text{bulk}}\right). \tag{1.27}$$

Here, E_{slab} is the total energy of the slab containing n atomic layers and E_{bulk} is the energy of the bulk

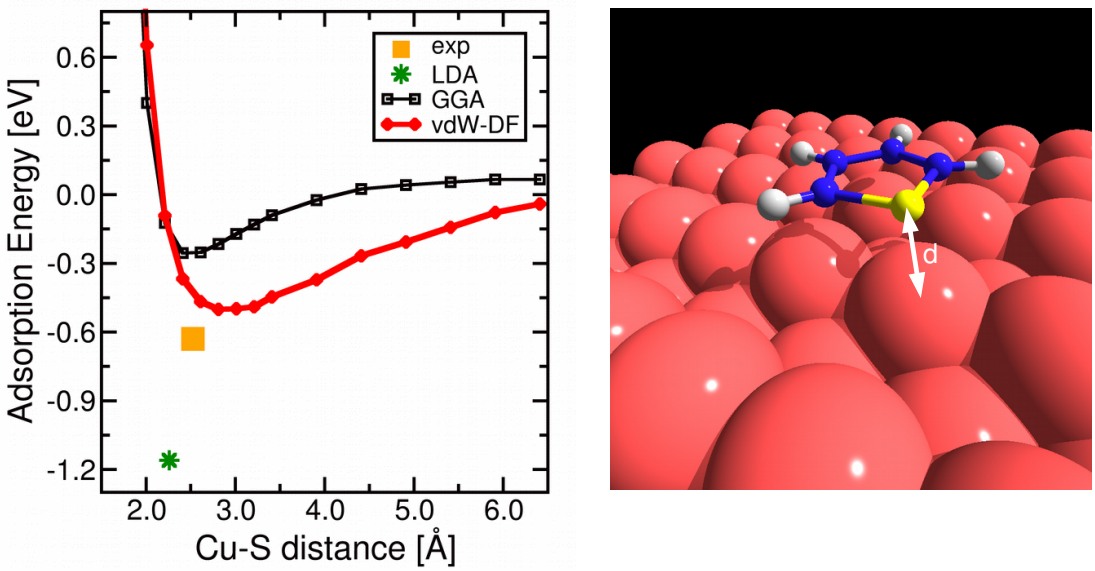

Figure 1.6: Adsorption energy E_{ad} of a thiophene molecule (C_4H_4S) on a Cu(110) surface as a function of the adsorption height d for various exchange-correlation functionals (see text for details) and comparison with equilibrium geometry from experiment. Data is reproduced from Ref. [17].

crystal. Note that the factor $\frac{1}{2}$ arises because of the two surfaces in the repeated slab approach, and the minus sign is convention to yield a positive number for the surface energy. Fig. 1.5c illustrates how the computed values for the surface energy converges towards a given value when adding more and more layers to the slab. It also demonstrates that the (111) surfaces have the lowest surface energies followed by the (100) and finally by the (110) face which can be explained by the bonding coordination of atoms on the respective surfaces.

An important application of DFT calculations for surfaces regards the question of how molecules interact with surfaces which is important in fields ranging from organic electronics to catalysis. Here, we briefly present a study of the adsorption of the organic molecule thiophene, C_4H_4S, on the (110) surface of copper (see Fig. 1.6). Of particular interest here is the precise adsorption geometry (height of the molecule above the surface, lateral position of the molecule with respect to the substrate atoms) and the interaction strength, the adsorption energy, which is defined in the following way:

$$E_{\mathrm{ad}} = E_{\mathrm{full}} - (E_{\mathrm{surface}} + E_{\mathrm{molecule}}). \tag{1.28}$$

Thus one needs to perform DFT calculations for three structures: (i) for the full system containing the molecule interacting with the surface, (ii) for the surface without the molecule, and (iii) for the molecule without the surface. The result of such calculations is shown in Fig. 1.6 where this adsorption energy E_{ad} has been plotted as a function of the Cu–S distance [17].

As already mentioned earlier, the exchange-correlation potential appearing as one term in the effective Kohn-Sham potential (see Eq. 1.10) needs to be approximated in some way. Now, it turns out that the most common approximations, namely the local density approximation (LDA) to be discussed in Sec. 3.5.3 as well as the generalized gradient approximation (GGA) to be discussed in Sec. 3.5.4, are both severely in error when compared to experiment when it comes to such molecule/metal interfaces. The reason is that so-called *van der Waals* dispersion forces, which are due to non-local quantum-mechanical electron correlations are absent in LDA and GGA. This can be seen by the red curve in Fig. 1.6 where a so-called van-der-Waals density functional has been employed. The development and further improvement of exchange-correlation functionals to accurately account for such van der Waals forces has in fact been an extremely active field of research in the past decade [18, 19], and we will briefly touch this issue in Section 3.5.6.

1.3.5 Vibrational Frequencies and Phonons

Density functional calculations can also be used to compute vibrational frequencies of molecules and the phonon dispersion relation of crystals within the so-called *frozen phonon approach*. Basically, starting from the equilibrium geometry of a molecule or solid (see above), the atomic nuclei are displaced and the total energy and the atomic forces are computed. The second derivative of the total energy with respect to a displacement then leads to the spring constant, or for systems with many degrees of freedom, to the *dynamical matrix* whose eigenvalues are the vibrational frequencies for the normal modes of vibration. Below we review the derivation of the dynamical matrix describing nuclear motion in a crystal.

Let us assume a perfect crystal with periodic boundary conditions at 0 Kelvin. We define $\boldsymbol{R}_\alpha$ as the position vectors to the α-th atom within an arbitrarily chosen "zero" unit cell, and the position vector to the n-th unit cell is denoted by $\boldsymbol{R}_n$. Hence the equilibrium position of atom α in unit cell n can be written as $\boldsymbol{R}_{n\alpha} = \boldsymbol{R}_n + \boldsymbol{R}_\alpha$. If we denote the Cartesian components of the displacement vector of atom α in unit cell n with $s_{n\alpha i}$, where i takes the three values x, y, z, we can write for the kinetic energy of the nuclear motion:

$$T = \sum_{n=1}^{N} \sum_{\alpha=1}^{r} \sum_{i=1}^{3} \frac{M_\alpha}{2} \left(\frac{\mathrm{d}s_{n\alpha\, i}\,(t)}{\mathrm{d}t} \right)^2 . \tag{1.29}$$

Here, M_α is the mass of atom α, and N is the number of unit cells in the crystal, r the number of atoms per unit cell, and i stands for the three Cartesian coordinates x, y, z. Hence the total number of degrees of freedom is $3rN$. The potential energy W can be expanded into a Taylor series in the

atomic coordinates.

$$W(s_{n\alpha i}) = W(0) + \sum_{n\alpha i} \underbrace{\frac{\partial W}{\partial s_{n\alpha i}}}_{=0} s_{n\alpha i} + \frac{1}{2} \sum_{n\alpha i} \sum_{n'\alpha' i'} \underbrace{\frac{\partial^2 W}{\partial s_{n\alpha i} \partial s_{n'\alpha' i'}}}_{\Phi^{n'\alpha' i'}_{n\alpha i}} s_{n\alpha i} s_{n'\alpha' i'} + \cdots \tag{1.30}$$

The linear terms in s vanish since we expand around the equilibrium configuration (vanishing forces), and we have introduced the force constant matrix $\Phi^{n'\alpha' i'}_{n\alpha i}$. They can be interpreted as the i-th Cartesian component of the force on atom α in unit cell n, when atom α' in unit cell n' is displaced a unit distance in i'-direction. Note also that we have neglected higher terms than the harmonic ones. The equations of motion can be derived from the the Euler–Lagrange equations

$$\frac{\mathrm{d}}{\mathrm{d}t} \frac{\partial \mathcal{L}}{\partial\, \dot{s}_{n\alpha i}} - \frac{\partial \mathcal{L}}{\partial s_{n\alpha i}} = 0. \tag{1.31}$$

Inserting $\mathcal{L} = T - W$ and taking account of the symmetry of the force constants $\Phi^{n'\alpha' i'}_{n\alpha i} = \Phi^{n\alpha i}_{n'\alpha' i'}$ leads to:

$$M_\alpha \frac{\mathrm{d}^2 s_{n\alpha i}}{\mathrm{d}t^2} = - \sum_{n'\alpha' i'} \Phi^{n'\alpha' i'}_{n\alpha i}\, s_{n'\alpha' i'}. \tag{1.32}$$

This can be solved with the harmonic ansatz

$$s_{n\alpha i}\,(t) = \frac{1}{\sqrt{M_\alpha}} u_{n\alpha i}\, e^{-i\omega t} \tag{1.33}$$

we obtain

$$\omega^2 u_{n\alpha i} = \sum_{n'\alpha' i'} \frac{\Phi^{n'\alpha' i'}_{n\alpha i}}{\sqrt{M_\alpha M_{\alpha'}}} u_{n'\alpha' i'} \tag{1.34}$$

which is an eigenvalue equation for the $3rN$ normal frequencies ω. On account of the translational symmetry in a periodic crystal, $\Phi^{n'\alpha' i'}_{n\alpha i}$ only depend on the difference $n - n'$, i.e. $\Phi^{n'\alpha' i'}_{n\alpha i} = \Phi^{\alpha' i'}_{\alpha i}(n - n')$. The translational symmetry is taken into account by the Fourier ansatz:

$$u_{n\alpha i} = c_{\alpha i} e^{i\boldsymbol{q}\boldsymbol{R}_n}, \tag{1.35}$$

where $\boldsymbol{q}$ is a momentum vector inside the first Brillouin zone. It leads to

$$\sum_{\alpha' i'} D^{\alpha' i'}_{\alpha i}(\boldsymbol{q}) c_{\alpha' i'} = \omega^2(\boldsymbol{q}) c_{\alpha i} \qquad \text{with} \qquad D^{\alpha' i'}_{\alpha i}(\boldsymbol{q}) = \sum_n \frac{\Phi^{\alpha' i'}_{\alpha i}(n)}{\sqrt{M_\alpha M_{\alpha'}}} e^{i\boldsymbol{q}\boldsymbol{R}_n}, \tag{1.36}$$

where we have introduced the dynamical matrix $D^{\alpha' i'}_{\alpha i}(\boldsymbol{q})$. We thus have arrived at an eigenvalue equation (1.36) which is only $3r$–dimensional. The phonon frequencies ω are functions of the wave vector $\boldsymbol{q}$ and are the square roots of the eigenvalue of the dynamical matrix.

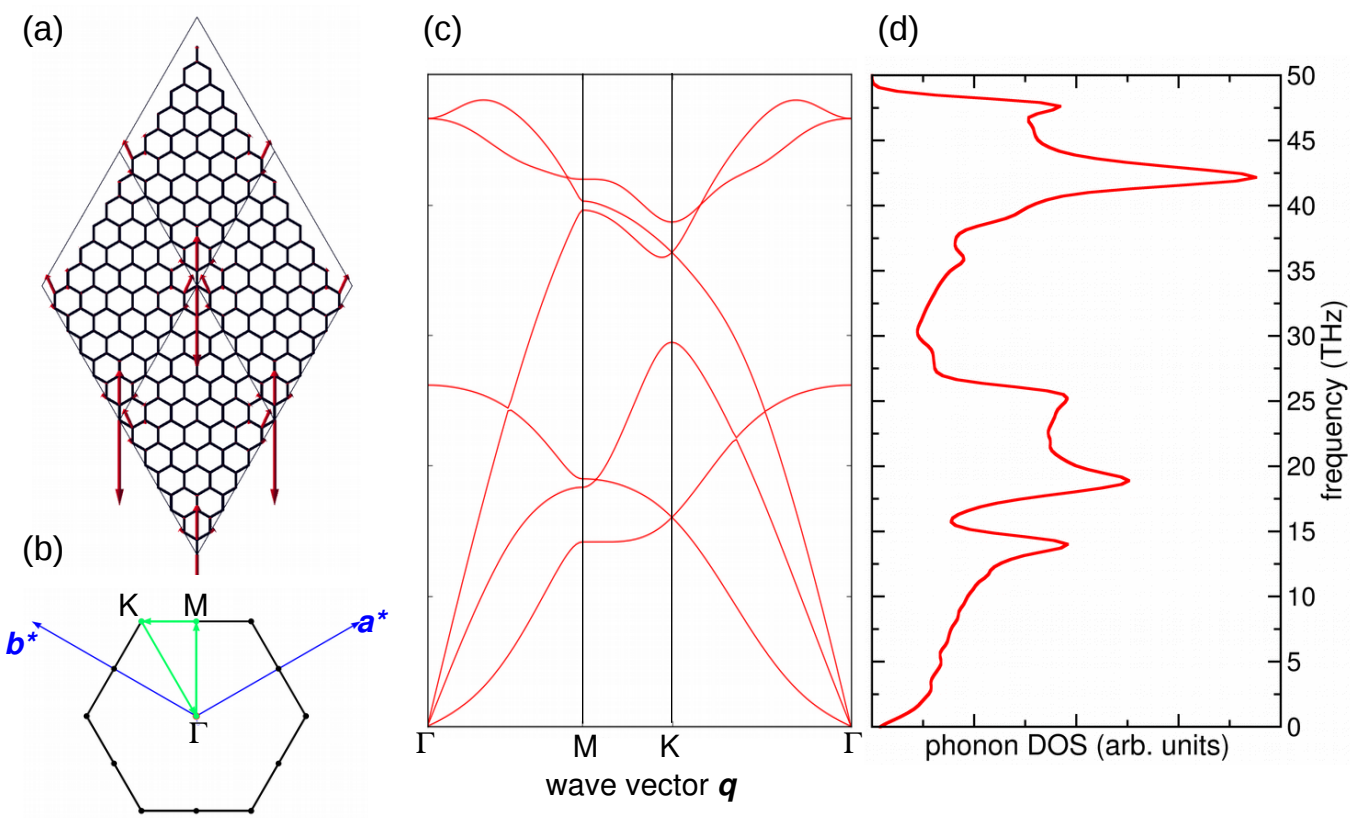

Figure 1.7: (a) 6×6 supercell of graphene with the central atom displaced in y direction, atomic forces are shown by the red arrows. (b) Brillouin zone of graphene with high symmetry points and reciprocal lattice vectors indicated. (c) Phonon band structure and (d) phonon density of states for graphene.

Fig. 1.7 depicts a frozen phonon calculation for graphene which is a two-dimensional layer of carbon atoms arranged in a honey-comb structure with a hexagonal unit cell containing $r = 2$ carbon atoms. In the *finite-displacement supercell* approach, a superstructure containing 6×6 unit cells, thus 72 carbon atoms, is formed as illustrated in Fig. 1.7a. The force constant matrix $\Phi_{\alpha i}^{\alpha' i'}(n)$ is computed by displacing one atom of this supercell and analyzing the Hellmann-Feynman forces on all atoms in the supercell indicated by the red arrows. According to 1.36, the $2r \times 2r = 6 \times 6$ dimensional dynamical matrix $D_{\alpha i}^{\alpha' i'}(\boldsymbol{q})$ is set up for a given wave vector $\boldsymbol{q}$ and its eigenvalues are calculated. Sampling the Brillouin zone (BZ) depicted in panel (b) along high symmetry directions (green lines) leads to the phonon band structure plot presented in Fig. 1.7c. Due to the two inequivalent atoms in the graphene unit cell, there are three acoustic phonon branches ($\omega \to 0$ for $|\boldsymbol{q}| \to 0$) and three optical phonon bands ($\omega > 0$ for $|\boldsymbol{q}| \to 0$). They are further distinguished into in-plane and out-of-plane modes which becomes evident when analyzing the eigen*vectors* of the dynamical matrix. We also show the phonon density of states in panel (d) which can be obtained by densely sampling the entire BZ with a $\boldsymbol{q}$-grid and counting the number of frequencies $\omega(\boldsymbol{q})$ in a certain frequency interval $(\omega, \omega + \Delta\omega)$.

Chapter 2

Theoretical Background

2.1 Periodic Solids and Electron Bands

Within this lecture, we will mainly deal with crystalline solids. In this section we will briefly introduce our nomenclature and review the most important relations for solids with translational symmetry. For more information we refer to standard text books on this topic such as the book by Ashcroft and Mermin [20].

We denote the primitive lattice vectors which span the unit cell of volume Ω_0 as

$$\boldsymbol{a}_1,\, \boldsymbol{a}_2,\, \boldsymbol{a}_3, \qquad \Omega_0 = (\boldsymbol{a}_1 \times \boldsymbol{a}_2) \cdot \boldsymbol{a}_3. \tag{2.1}$$

Any direct lattice vector $\boldsymbol{R}$ is then given as a linear combination of the basis vectors

$$\boldsymbol{R} = n_1\boldsymbol{a}_1 + n_2\boldsymbol{a}_2 + n_3\boldsymbol{a}_3, \tag{2.2}$$

with integer numbers n_1, n_2 and n_3. The reciprocal lattice is defined by the three vectors

$$\boldsymbol{b}_1 = \frac{2\pi}{\Omega_0}\boldsymbol{a}_2 \times \boldsymbol{a}_3, \qquad \boldsymbol{b}_2 = \frac{2\pi}{\Omega_0}\boldsymbol{a}_3 \times \boldsymbol{a}_1, \qquad \boldsymbol{b}_3 = \frac{2\pi}{\Omega_0}\boldsymbol{a}_1 \times \boldsymbol{a}_2. \tag{2.3}$$

Thus, the relation between the direct and the reciprocal basis vectors can be summarized as follows

$$\boldsymbol{a}_i \cdot \boldsymbol{b}_j = 2\pi\delta_{ij}. \tag{2.4}$$

In analogy to the direct lattice vectors $\boldsymbol{R}$, the reciprocal basis vectors $\boldsymbol{b}_1$, $\boldsymbol{b}_2$, and $\boldsymbol{b}_3$ span the reciprocal

lattice vectors which we denote by $\boldsymbol{G}$ as

$$\boldsymbol{G} = m_1\boldsymbol{b}_1 + m_2\boldsymbol{b}_2 + m_3\boldsymbol{b}_3, \tag{2.5}$$

with integer numbers m_1, m_2 and m_3. Thus, we have the important relation

$$\boldsymbol{G}\cdot\boldsymbol{R} = \sum_{i=1}^{3}\sum_{j=1}^{3} n_i m_j \boldsymbol{a}_i\cdot\boldsymbol{b}_j = 2\pi\sum_{i=1}^{3} n_i m_i \quad \Rightarrow \quad e^{i\boldsymbol{G}\cdot\boldsymbol{R}} = 1. \tag{2.6}$$

2.1.1 Bloch Theorem

Consider the eigenstates and eigenvalues of an effective one-electron Schrödinger equation, such as the Kohn-Sham equations 1.9, for a periodic solid

$$\hat{H}\varphi_j(\boldsymbol{r}) = \left[-\frac{1}{2}\Delta + v_s(\boldsymbol{r})\right]\varphi_j(\boldsymbol{r}) = \varepsilon_j\varphi_j(\boldsymbol{r}). \tag{2.7}$$

Because the effective potential is invariant under lattice translations

$$\hat{T}_{\boldsymbol{R}} v_s(\boldsymbol{r}) \equiv v_s(\boldsymbol{r}+\boldsymbol{R}) = v_s(\boldsymbol{r}) \tag{2.8}$$

and also the kinetic energy operator $-\frac{1}{2}\Delta$ is translationally invariant, the Hamilton operator $\hat{H}$ commutes with the translation operator $\hat{T}_{\boldsymbol{R}}$. Note that the action of the translation operator $\hat{T}_{\boldsymbol{R}}$ on a function $f(\boldsymbol{r})$ is given by $\hat{T}_{\boldsymbol{R}} f(\boldsymbol{r}) = f(\boldsymbol{r}+\boldsymbol{R})$.

$$\left[\hat{H}, \hat{T}_{\boldsymbol{R}}\right] = 0 \quad \Rightarrow \quad \hat{H}\hat{T}_{\boldsymbol{R}} = \hat{T}_{\boldsymbol{R}}\hat{H}. \tag{2.9}$$

Thus, the eigenstates of $\hat{H}$ can be chosen to be also eigenstates of all $\hat{T}_{\boldsymbol{R}}$ simultaneously. The eigenstates of the translation operator can be readily determined, independent of any details of the crystal, thereby rigorously classifying the states of the Hamiltonian $\hat{H}$ by the eigenvalues of the translation operator. This, in essence, leads to the Bloch theorem.

The key point to derive the Bloch theorem (see e.g. Ref. [21]) is to notice that the product of any two translation operators corresponding to the translations $\boldsymbol{R}_1$ and $\boldsymbol{R}_2$, respectively, corresponds to the translation $\boldsymbol{R}_1 + \boldsymbol{R}_2$. Thus, we can write

$$\hat{T}_{\boldsymbol{R}_1}\hat{T}_{\boldsymbol{R}_2} = \hat{T}_{\boldsymbol{R}_1+\boldsymbol{R}_2}. \tag{2.10}$$

and the eigenvalue equation of the translation operator $\hat{T}_{\boldsymbol{R}}$ demands

$$\hat{T}_{\boldsymbol{R}}\psi(\boldsymbol{r}) = \alpha_{\boldsymbol{R}}\psi(\boldsymbol{r}) \quad \Rightarrow \quad \hat{T}_{\boldsymbol{R}_1}\hat{T}_{\boldsymbol{R}_2}\psi(\boldsymbol{r}) = \alpha_{\boldsymbol{R}_1}\alpha_{\boldsymbol{R}_2}\psi(\boldsymbol{r}) = \alpha_{\boldsymbol{R}_1+\boldsymbol{R}_2}\psi(\boldsymbol{r}) \quad \Rightarrow \quad \alpha_{\boldsymbol{R}_1+\boldsymbol{R}_2} = \alpha_{\boldsymbol{R}_1}\alpha_{\boldsymbol{R}_2}. \tag{2.11}$$

On the other hand, because the charge density associated with the wave function must be translationally invariant

$$|\psi(\boldsymbol{r})|^2 = |\psi(\boldsymbol{r}+\boldsymbol{R})|^2 \quad \Rightarrow \quad |\alpha_{\boldsymbol{R}}|^2 = 1. \tag{2.12}$$

Eqs. 2.11 and 2.12 can be fulfilled by the following ansatz

$$\alpha_{\boldsymbol{R}} = e^{i\boldsymbol{k}\cdot\boldsymbol{R}}, \tag{2.13}$$

where $\boldsymbol{k}$ is a real-valued vector of reciprocal space that can be restricted to the first Brillouin zone because $e^{i(\boldsymbol{k}+\boldsymbol{G})\cdot\boldsymbol{R}} = e^{i\boldsymbol{k}\cdot\boldsymbol{R}}$. This directly leads to the Bloch ansatz for the wave function

$$\psi_{\boldsymbol{k}}(\boldsymbol{r}) = e^{i\boldsymbol{k}\cdot\boldsymbol{r}}u_{\boldsymbol{k}}(\boldsymbol{r}) \qquad \text{with} \qquad u_{\boldsymbol{k}}(\boldsymbol{r}+\boldsymbol{R}) = u_{\boldsymbol{k}}(\boldsymbol{r}), \tag{2.14}$$

where the wave function $\psi_{\boldsymbol{k}}(\boldsymbol{r})$ as well as the lattice periodic part of the wave function $u_{\boldsymbol{k}}(\boldsymbol{r})$ obtain the quantum number $\boldsymbol{k}$, the Bloch vector, as an index. Thus, the Bloch function obeys the desired property upon translation about the lattice vector $\boldsymbol{R}$:

$$\psi_{\boldsymbol{k}}(\boldsymbol{r}+\boldsymbol{R}) = e^{i\boldsymbol{k}\cdot\boldsymbol{R}}\psi_{\boldsymbol{k}}(\boldsymbol{r}). \tag{2.15}$$

To put Bloch's equation 2.14 in Felix Bloch's own words from 1936: *When I started to think about it, I felt that the main problem was to explain how the electrons could sneak by all the ions in a metal ... By straight Fourier analysis I found to my delight that the wave differed from the plane wave of free electrons only by a periodic modulation.*

2.1.2 Electronic Band Structure

Here, we briefly review important consequences of the Bloch theorem 2.14 for the solution of one-electron Schrödinger equation of type 2.7. First of all, Bloch functions belonging to different vectors $\boldsymbol{k}$ and $\boldsymbol{k}'$ are orthogonal to each other,

$$\left\langle \psi_{\boldsymbol{k}',\nu'}(\boldsymbol{r}) \,\middle|\, \psi_{\boldsymbol{k},\nu}(\boldsymbol{r}) \right\rangle = \delta_{\boldsymbol{k},\boldsymbol{k}'}\delta_{\nu,\nu'}, \tag{2.16}$$

where we have introduced the band index ν. Therefore, one can solve the Schrödinger equation *separately* for each Bloch vector $\boldsymbol{k}$, thus with the help of the translational symmetry, the Hamiltonian matrix is Block-diagonalized. Insertion of 2.14 into 2.7 leads to an eigenvalue equation for the periodic

part of the wave function:

$$\left[-\frac{1}{2}(\nabla + i\boldsymbol{k})^2 + v_s(\boldsymbol{r})\right] u_{\boldsymbol{k},\nu}(\boldsymbol{r}) = \varepsilon_{\boldsymbol{k},\nu} u_{\boldsymbol{k},\nu}(\boldsymbol{r}). \tag{2.17}$$

The eigenvalues $\varepsilon_\nu(\boldsymbol{k}) \equiv \varepsilon_{\boldsymbol{k},\nu}$ are termed the electronic band structure of the solid, where ν labels the individual bands and $\boldsymbol{k}$ is a vector within the first Brillouin zone. Using 2.6 it is easy to show that the band structure as well as the Bloch functions are periodic with respect to reciprocal lattice vectors $\boldsymbol{G}$:

$$\varepsilon_\nu(\boldsymbol{k} + \boldsymbol{G}) = \varepsilon_\nu(\boldsymbol{k}) \qquad \text{and} \qquad \psi_{\boldsymbol{k}+\boldsymbol{G},\nu}(\boldsymbol{r}) = \psi_{\boldsymbol{k},\nu}(\boldsymbol{r}). \tag{2.18}$$

Another important property which relies on the time-reversal symmetry of the Hamiltonian is the so-called *Kramer's theorem*. It can be shown that time-inversion symmetry requires that

$$\varepsilon_\nu(-\boldsymbol{k}) = \varepsilon_\nu(\boldsymbol{k}) \qquad \text{and} \qquad \psi^*_{-\boldsymbol{k},\nu}(\boldsymbol{r}) = \psi_{\boldsymbol{k},\nu}(\boldsymbol{r}). \tag{2.19}$$

2.1.3 Fourier Series for Local Functions

In this and the following subsections, we briefly state a number of important relations regarding the Fourier expansion of functions typically appearing in the context of periodic solids. Note that, Ω_0 denotes the volume of one unit cell, whereas Ω is the whole crystal volume. Thus $\Omega = N \cdot \Omega_0$, where N is the number of unit cells within the crystal for which we assume periodic boundary conditions (Born-van-Karmann boundary conditions). Hence the number of Bloch vectors $\boldsymbol{k}$ within the first Brillouin zone also equals $N = \frac{\Omega}{\Omega_0}$.

First, we consider a function $f(\boldsymbol{r})$ which has the lattice periodicity of the crystal, such as the electron density or the crystal potential

$$f(\boldsymbol{r} + \boldsymbol{R}) = f(\boldsymbol{r}), \tag{2.20}$$

where $\boldsymbol{R}$ denotes as usual any direct lattice vector. Then, the function f may be expanded in the Fourier series

$$f(\boldsymbol{r}) = \frac{1}{\Omega} \sum_{\boldsymbol{G}} f_{\boldsymbol{G}} e^{i\boldsymbol{G}\boldsymbol{r}}, \tag{2.21}$$

with the Fourier coefficients given by

$$f_{\boldsymbol{G}} = \int_\Omega \mathrm{d}^3 r f(\boldsymbol{r}) e^{-i\boldsymbol{G}\boldsymbol{r}}. \tag{2.22}$$

The summation runs over all reciprocal lattice vectors $\boldsymbol{G}$, and the integration is over the crystal volume Ω.

If the function f, however, does not have the periodicity of the lattice, such as an external perturbation, or indeed the Bloch wave function $\psi_{\boldsymbol{k}}(\boldsymbol{r})$, we have to include a sum over the a vector $\boldsymbol{q}$ from the first Brillouin zone, and write the Fourier expansion of f in the way

$$f(\boldsymbol{r}) = \frac{1}{\Omega}\sum_{\boldsymbol{q}}^{\mathrm{BZ}}\sum_{\boldsymbol{G}} f_{\boldsymbol{G}}(\boldsymbol{q})e^{i(\boldsymbol{q}+\boldsymbol{G})\boldsymbol{r}} \tag{2.23}$$

$$f_{\boldsymbol{G}}(\boldsymbol{q}) = \int_{\Omega} \mathrm{d}^3 r f(\boldsymbol{r})e^{-i(\boldsymbol{q}+\boldsymbol{G})\boldsymbol{r}}. \tag{2.24}$$

2.1.4 Fourier Series for Nonlocal Functions

Response functions for crystalline systems are in general non-local functions of $\boldsymbol{r}$ and $\boldsymbol{r}'$ that are invariant, if *both* space variables are translated by a direct lattice vector $\boldsymbol{R}$, thus

$$f(\boldsymbol{r}+\boldsymbol{R},\boldsymbol{r}'+\boldsymbol{R}) = f(\boldsymbol{r},\boldsymbol{r}'). \tag{2.25}$$

We use the following convention for the Fourier expansions of functions $f(\boldsymbol{r},\boldsymbol{r}')$ with the property (2.25)

$$f(\boldsymbol{r},\boldsymbol{r}') = \frac{1}{\Omega}\sum_{\boldsymbol{q}}^{\mathrm{BZ}}\sum_{\boldsymbol{G}\boldsymbol{G}'} e^{i(\boldsymbol{q}+\boldsymbol{G})\boldsymbol{r}} f_{\boldsymbol{G}\boldsymbol{G}'}(\boldsymbol{q})e^{-i(\boldsymbol{q}+\boldsymbol{G}')\boldsymbol{r}'} \tag{2.26}$$

$$f_{\boldsymbol{G}\boldsymbol{G}'}(\boldsymbol{q}) = \frac{1}{\Omega}\int_{\Omega}\mathrm{d}^3 r \int_{\Omega}\mathrm{d}^3 r' e^{-i(\boldsymbol{q}+\boldsymbol{G})\boldsymbol{r}} f(\boldsymbol{r},\boldsymbol{r}')e^{-i(\boldsymbol{q}+\boldsymbol{G}')\boldsymbol{r}'}. \tag{2.27}$$

The quantity $f_{\boldsymbol{G}\boldsymbol{G}'}(\boldsymbol{q})$ for a given $\boldsymbol{q}$ from the first Brillouin zone can be interpreted as a matrix where the matrix indices are reciprocal lattice vectors $\boldsymbol{G}$ and $\boldsymbol{G}'$.

2.1.5 Crystal Lattice Integrals and Summations

In this section, some useful integrals over the crystal volume or unit cell, and some relations involving summations over lattice vectors will be given.

$$\int_{\Omega}\mathrm{d}^3 r e^{i\boldsymbol{q}\boldsymbol{r}} = \Omega\,\delta_{\boldsymbol{q},\boldsymbol{0}} \tag{2.28}$$

$$\int_{\Omega_0}\mathrm{d}^3 r e^{i\boldsymbol{G}\boldsymbol{r}} = \Omega_0\,\delta_{\boldsymbol{G},\boldsymbol{0}}. \tag{2.29}$$

Here, Ω and Ω_0, respectively, denote the crystal and the unit cell volume, and $\boldsymbol{q}$ and $\boldsymbol{G}$ are vectors from the first Brillouin zone, and reciprocal lattice vectors, respectively. The summation over direct

lattice vectors $\boldsymbol{R}$ of the plane wave $e^{i\boldsymbol{q}\boldsymbol{R}}$ is given by

$$\sum_{\boldsymbol{R}} e^{i\boldsymbol{q}\boldsymbol{R}} = \frac{\Omega}{\Omega_0} \sum_{\boldsymbol{G}} \delta_{\boldsymbol{q},\boldsymbol{G}}, \tag{2.30}$$

where the factor Ω/Ω_0 is just the number of unit cells in the crystal. Note that the summation over $\boldsymbol{G}$ is only non-zero if $\boldsymbol{q}$ is equal to zero, provided that $\boldsymbol{q}$ is from the first Brillouin zone.

2.2 Independent-Electron Approximations

2.2.1 The Variational Principle

The variational principle, often also called the *Rayleigh-Ritz variational principle*, gives us a way of constructing upper bounds for the total energy of an electron system. We will use it to derive the Hartree and Hartree-Fock equations in Secs. 2.2.2 and 2.2.3, and later also make use to develop density functional theory in the next Chapter.

Let $\hat{H}$ be an Hermitian operator, for instance the Hamiltonian of the N-electron system, with the eigenvalues E_n and eigenstates $|\Phi_n\rangle$. Let us further denote the ground state energy and state as E_0 and $|\Phi_0\rangle$, respectively. Then, the Rayleigh-Ritz variational principle states that for any state $|\Psi\rangle$, which need not necessarily be normalized, the following relation holds

$$E[\Psi] = \frac{\left\langle \Psi \middle| \hat{H} \middle| \Psi \right\rangle}{\langle \Psi \mid \Psi \rangle} \geq E_0. \tag{2.31}$$

Equation 2.31 forms the foundation of the variational principle. Suppose $|\Phi_\eta\rangle$ is a *trial wave function* with some variable parameter η. If we are interested in the *ground state*, then the best approximation to the ground state will be characterized by a minimum of the $E[\Psi]$, thus

$$\frac{\partial E}{\partial \eta} = 0. \tag{2.32}$$

By successively more sophisticated trial wave functions with more variable parameters, we can get as close to E_0 as desired. $E[\Psi] = E_0$ exactly only if $|\Psi\rangle$ is the exact ground state wave function.

2.2.2 Hartree Approximation

As a first application of the variational principle, we consider the so-called Hartree approximation. To this end, we consider the Hamiltonian of an N-electron system already introduced in Eq. 1.3 and

rewrite it as a sum over the one-particle operator $\hat{h}$ and the two-particle operator $\hat{V}_{ee}$

$$\hat{H} = \sum_{i=1}^{N} \left(-\frac{1}{2}\Delta_i + v(\boldsymbol{r}_i) \right) + \frac{1}{2} \sum_{i,j \neq i} \frac{1}{|\boldsymbol{r}_i - \boldsymbol{r}_j|} = \sum_{i=1}^{N} \hat{h}(\boldsymbol{r}_i) + \frac{1}{2} \sum_{i,j \neq i} V(\boldsymbol{r_i}, \boldsymbol{r}_j). \tag{2.33}$$

In the Hartree approximation, the wave function $|\Psi\rangle$ is approximated by a simple product ansatz

$$\Psi(x_1, x_2, \cdots x_N) = \varphi_1(x_1)\varphi_2(x_2)\cdots\varphi_N(x_N). \tag{2.34}$$

Here, the N single-particle functions $\varphi_1, \varphi_2, \cdots \varphi_N$ are assumed to be normalized, which thereby results also in a normalized wave function Ψ. Also note that the coordinates x_i are meant to contain a spatial as well as a spin coordinate $x_i = (\boldsymbol{r}_i, \zeta_i)$. We can now apply the Rayleigh-Ritz variational principle and demand that the variation of $\left\langle \Psi \middle| \hat{H} \middle| \Psi \right\rangle$ under the constraint that all single-particle functions φ_i remain normalized vanishes

$$\delta_{\varphi_i} \left[\left\langle \Psi \middle| \hat{H} \middle| \Psi \right\rangle - \sum_{i=1}^{N} \varepsilon_i \int \mathrm{d}x_i \, \varphi_i^*(x_i)\varphi_i(x_i) \right] = 0. \tag{2.35}$$

Thus, we are varying the N single-particle functions φ_i to minimize the energy, where the Lagrange multipliers ε_i are introduced to satisfy the normalization of the wave function. Note that $\int \mathrm{d}x_i$ involves an integration over the spatial coordinate and a summation of spin coordinate. To evaluate 2.35, we first calculate the total energy $E = \left\langle \Psi \middle| \hat{H} \middle| \Psi \right\rangle$ inserting the product ansatz

$$\begin{aligned} \left\langle \Psi \middle| \hat{H} \middle| \Psi \right\rangle &= \int \mathrm{d}x_1 \cdots \mathrm{d}x_N \, \varphi_1^*(x_1) \cdots \varphi_N^*(x_N) \left[\sum_{i=1}^{N} \hat{h}(\boldsymbol{r}_i) + \frac{1}{2} \sum_{i,j \neq i} V(\boldsymbol{r_i}, \boldsymbol{r}_j) \right] \varphi_1(x_1) \cdots \varphi_N(x_N) \\ &= \sum_{i=1}^{N} \int \mathrm{d}x \, \varphi_i^*(x) \hat{h}(\boldsymbol{r}) \varphi_i(x) + \frac{1}{2} \sum_{i,j \neq i} \int \mathrm{d}x \mathrm{d}x' \varphi_i^*(x) \varphi_j^*(x') V(\boldsymbol{r}, \boldsymbol{r}') \varphi_i(x) \varphi_j(x'). \end{aligned} \tag{2.36}$$

For the variation, we choose to vary expression 2.36 with respect to φ_i^* which yields

$$\int \mathrm{d}x \left[\hat{h}(\boldsymbol{r})\varphi_i(x) + \sum_{j \neq i} \int \mathrm{d}x' \varphi_j^*(x') V(\boldsymbol{r}, \boldsymbol{r}') \varphi_i(x) \varphi_j(x') - \varepsilon_i \varphi_i(x) \right] = 0. \tag{2.37}$$

Here, we have made use of the fact that $V(\boldsymbol{r}, \boldsymbol{r}') = V(\boldsymbol{r}', \boldsymbol{r})$ and by changing the dummy integration variables have combined terms. By noting that Eq. 2.37 must hold for arbitrary variations, we see

that the integrand in square brackets must vanish which leads us to the *Hartree Equations*

$$\left[\hat{h}(\boldsymbol{r}) + \sum_{j\neq i} \int \mathrm{d}x' \varphi_j^*(x') V(\boldsymbol{r},\boldsymbol{r}') \varphi_j(x')\right] \varphi_i(x) = \varepsilon_i \varphi_i(x). \tag{2.38}$$

Several observations can be made about these Hartree equations 2.38. First, instead of having of *one* Schrödinger equation for the N-electron wave function, we now have N Schrödinger equations for the N *one*-electron orbitals φ_i. For a given orbital φ_i, the second term in square brackets, the Hartree-potential, depends on all other orbitals φ_j. Thus, the way to solve 2.38 is to start with a guess for the set of orbitals φ_i, and then use 2.38 to calculate a new set. This process is continued until the φ_i that are put into 2.38 are the same as (or numerically very close to) the φ_i that result from 2.38. This is called *self-consistent solution*, a term that we will come across also in the framework of density functional theory. Last but not least, the interpretation of the Hartree potential $v_H(\boldsymbol{r})$ has an intuitive interpretation:

$$v_{H,i}(\boldsymbol{r}) = \sum_{j\neq i} \int \mathrm{d}x' \varphi_j^*(x') V(\boldsymbol{r},\boldsymbol{r}') \varphi_j(x') = \int \mathrm{d}^3 r' \frac{\sum_{j\neq i} |\varphi_j(\boldsymbol{r}')|^2}{|\boldsymbol{r}-\boldsymbol{r}'|} \overset{N\gg 1}{\approx} \int \mathrm{d}^3 r' \frac{n(\boldsymbol{r}')}{|\boldsymbol{r}-\boldsymbol{r}'|} = v_H(\boldsymbol{r}). \tag{2.39}$$

Here, we have used the fact that the electron-electron interaction $V(\boldsymbol{r},\boldsymbol{r}')$ does not depend on the spin coordinates. In the last step, we have noted that for the case of a large electron number N, the $i=j$ term may be included and the sum over all orbitals is equal to the electron density $\sum_{j\neq i} |\varphi_j(\boldsymbol{r}')|^2 \approx \sum_{j=1}^{N} |\varphi_j(\boldsymbol{r}')|^2 = n(\boldsymbol{r}')$. This shows that the Hartree potential $v_H(\boldsymbol{r})$ can be interpreted as the classical electrostatic potential due to the total electron charge density $n(\boldsymbol{r}')$. It is clear in including the $i=j$ term in the summation, one introduces a spurious interaction of the electron in orbital φ_i with itself, the so-called *self-interaction*.

2.2.3 Hartree-Fock Approximation

One problem with the Hartree approximation is that the underlying wave function, as defined by the product ansatz 2.34, does not satisfy the Pauli principle, that is the wave function is not anti-symmetric with respect to the interchange of two particles. A natural way to fulfil the anti-symmetry of the wave function is to write $|\Psi\rangle$ as a Slater determinant in the following way

$$\Psi(x_1, x_2, \cdots x_N) = \frac{1}{\sqrt{N!}} \begin{vmatrix} \varphi_1(x_1) & \varphi_2(x_1) & \cdots & \varphi_N(x_1) \\ \varphi_1(x_2) & \varphi_2(x_2) & \cdots & \varphi_N(x_2) \\ \vdots & \vdots & & \vdots \\ \varphi_1(x_N) & \varphi_2(x_N) & \cdots & \varphi_N(x_N) \end{vmatrix}. \tag{2.40}$$

Applying the same variational procedure as before by using the Slater determinant 2.40 as ansatz for the wave function with normalized orbitals φ_i leads to the Hartree-Fock equations. The derivation is a bit more cumbersome [22] than before for the Hartree-equations, and we will only show the results here. The so-called Hartree-Fock equations are given by:

$$\hat{h}(\boldsymbol{r})\varphi_i(x) + \sum_{j=1}^{N}\left[\int \mathrm{d}x'\varphi_j^*(x')V(\boldsymbol{r},\boldsymbol{r}')\varphi_i(x)\varphi_j(x') - \int \mathrm{d}x'\varphi_j^*(x')V(\boldsymbol{r},\boldsymbol{r}')\varphi_j(x)\varphi_i(x')\right] = \varepsilon_i\varphi_i(x). \tag{2.41}$$

These are again N single-particle Schrödinger equations for $i = 1, 2\cdots N$. Compared to the Hartree equations 2.38, an additional term appears which is the so-called *Fock exchange* potential which is attractive (minus sign) and thereby lowers the energy compared to the Hartree solution. It should also be noted that the summation can now be extended over all $j = 1, 2\cdots N$ including the $j = i$ term since the spurious self-interaction term in the first term (Hartree potential) is exactly compensated by the second term (exchange potential). The total energy $E = \left\langle \Psi \middle| \hat{H} \middle| \Psi \right\rangle$ in the Hartree-Fock approximation turns out to be

$$\begin{aligned} E = \left\langle \Psi \middle| \hat{H} \middle| \Psi \right\rangle &= \sum_{i=1}^{N}\int \mathrm{d}x\,\varphi_i^*(x)\hat{h}(\boldsymbol{r})\varphi_i(x) \\ &+ \frac{1}{2}\sum_{i,j}\int \mathrm{d}x\mathrm{d}x'\left[\varphi_i^*(x)\varphi_j^*(x')V(\boldsymbol{r},\boldsymbol{r}')\varphi_i(x)\varphi_j(x') - \varphi_i^*(x)\varphi_j^*(x')V(\boldsymbol{r},\boldsymbol{r}')\varphi_j(x)\varphi_i(x')\right] \end{aligned} \tag{2.42}$$

To make the structure of the Hartree-Fock equations 2.41 clearer, we can rewrite them in the following form

$$\left[\hat{h}(\boldsymbol{r}) + \underbrace{\int \mathrm{d}^3r'\frac{n(\boldsymbol{r}')}{|\boldsymbol{r}-\boldsymbol{r}'|}}_{=v_H(\boldsymbol{r})} \underbrace{- \sum_{j=1}^{N}\int \mathrm{d}x'\frac{\varphi_j^*(x')V(\boldsymbol{r},\boldsymbol{r}')\varphi_j(x)\varphi_i(x')}{\varphi_i(x)}}_{=v_F^i(x)}\right]\varphi_i(x) = \varepsilon_i\varphi_i(x), \tag{2.43}$$

where we have introduced in addition to the already known Hartree potential, $v_H(\boldsymbol{r})$, also the orbital-dependent Fock exchange potential $v_F^i(x)$. Similarly to the Hartree equations, also the Hartree-Fock equations 2.43 need to be solved self-consistently.

In order to analyse the Fock exchange potential further, we now explicitly re-introduce spatial and spin coordinates according to the following scheme

$$i = (\boldsymbol{k},\alpha), \qquad j = (\boldsymbol{k}',\alpha'), \qquad x = (\boldsymbol{r},\zeta), \qquad x' = (\boldsymbol{r}',\zeta'), \qquad \int \mathrm{d}x' = \sum_{\zeta'}\int \mathrm{d}^3r' \tag{2.44}$$

Thus the quantum number i is split into a quantum number for the spatial part, the Bloch vector $\boldsymbol{k}$, and the spin quantum number α, and the coordinate x contains the spatial coordinate $\boldsymbol{r}$ and the spin coordinate ζ. Since the Hartree-Fock Hamiltonian does not have an explicit spin-dependence, we can also assume the following product ansatz for the single-particle orbitals

$$\varphi_i(x) = \phi_{\boldsymbol{k}}(\boldsymbol{r})\chi_\alpha(\zeta), \tag{2.45}$$

where $\phi_{\boldsymbol{k}}(\boldsymbol{r})$ denotes the spatial and $\chi_\alpha(\zeta)$ the spin part of the orbital, respectively. Using 2.44 and 2.45 in the Fock exchange potential $v_F^i(x)$ as defined in 2.43, we find

$$\begin{aligned}
v_F^i(x) &= -\sum_{j=1}^{N} \int \mathrm{d}x' \frac{\varphi_j^*(x')V(\boldsymbol{r},\boldsymbol{r}')\varphi_j(x)\varphi_i(x')}{\varphi_i(x)} \\
v_F^{\boldsymbol{k},\alpha}(\boldsymbol{r},\zeta) &= -\sum_{\boldsymbol{k}'}^{occ}\sum_{\alpha'}\sum_{\zeta'} \int \mathrm{d}^3r' \frac{\phi_{\boldsymbol{k}'}^*(\boldsymbol{r}')\chi_{\alpha'}^*(\zeta')V(\boldsymbol{r},\boldsymbol{r}')\phi_{\boldsymbol{k}'}(\boldsymbol{r})\chi_{\alpha'}(\zeta)\phi_{\boldsymbol{k}}(\boldsymbol{r}')\chi_\alpha(\zeta')}{\phi_{\boldsymbol{k}}(\boldsymbol{r})\chi_\alpha(\zeta)} \\
&= -\frac{1}{\chi_\alpha(\zeta)}\sum_{\alpha'}\chi_{\alpha'}(\zeta)\underbrace{\sum_{\zeta'}\chi_{\alpha'}^*(\zeta')\chi_\alpha(\zeta')}_{\delta_{\alpha,\alpha'}}\sum_{\boldsymbol{k}'}^{occ}\int \mathrm{d}^3r' \frac{\phi_{\boldsymbol{k}'}^*(\boldsymbol{r}')V(\boldsymbol{r},\boldsymbol{r}')\phi_{\boldsymbol{k}'}(\boldsymbol{r})\phi_{\boldsymbol{k}}(\boldsymbol{r}')}{\phi_{\boldsymbol{k}}(\boldsymbol{r})}.
\end{aligned}$$

Due to the appearance of the Kronecker-$\delta_{\alpha,\alpha'}$, the spin indices α and α' need to be equal, thus the exchange potential is only acting on electrons with parallel spin. This is of course due to the fact that it expresses the Pauli-exclusion principle that does not allow electrons of parallel spin to occupy the same orbital. We can thus write for the Fock-exchange potential

$$v_F^{\boldsymbol{k},\uparrow\uparrow}(\boldsymbol{r}) = -\sum_{\boldsymbol{k}'}^{occ}\int \mathrm{d}^3r' \frac{1}{|\boldsymbol{r}-\boldsymbol{r}'|}\frac{\phi_{\boldsymbol{k}'}^*(\boldsymbol{r}')\phi_{\boldsymbol{k}}(\boldsymbol{r}')\phi_{\boldsymbol{k}'}(\boldsymbol{r})}{\phi_{\boldsymbol{k}}(\boldsymbol{r})} \tag{2.46}$$

This potential can be thought of arising from the following charge density

$$\rho_F^{\boldsymbol{k},\uparrow\uparrow}(\boldsymbol{r},\boldsymbol{r}') = \sum_{\boldsymbol{k}'}^{occ}\frac{\phi_{\boldsymbol{k}'}^*(\boldsymbol{r}')\phi_{\boldsymbol{k}}(\boldsymbol{r}')\phi_{\boldsymbol{k}'}(\boldsymbol{r})}{\phi_{\boldsymbol{k}}(\boldsymbol{r})} \tag{2.47}$$

However, this charge density associated with the exchange potential is *non-local* since it depends on $\boldsymbol{r}$ and $\boldsymbol{r}'$ and it is also a function of $\boldsymbol{k}$. This demonstrates that, in contrast to the Hartree potential, the Fock exchange potential is a purely quantum-mechanical effect arising from the Fermion statistics and has no classical analogue.

Before we conclude this section about the Hartree-Fock method, we return to Equation 2.43 and ask ourselves, if there is any physical interpretation of the Lagrangian multipliers ε_i. Indeed, according

to *Koopmans' theorem* the ε_i can be interpreted as the negative of the energy required to remove an electron in the state i from the system. The proof of Koopmans' theorem is quite simple. First we see from 2.41 that by multiplying from the left with $\int \mathrm{d}x\varphi_k^*(x)$ we get for the orbital $i = k$

$$\begin{aligned} \varepsilon_k &= \int \mathrm{d}x\varphi_k^*(x)\hat{h}(\boldsymbol{r})\varphi_k(x) \\ &+ \sum_{j=1}^{N} \int \mathrm{d}x\mathrm{d}x' \left[\varphi_k^*(x)\varphi_j^*(x')V(\boldsymbol{r},\boldsymbol{r}')\varphi_k(x)\varphi_j(x') - \varphi_k^*(x)\varphi_j^*(x')V(\boldsymbol{r},\boldsymbol{r}')\varphi_j(x)\varphi_k(x')\right] \end{aligned} \tag{2.48}$$

The comparison of 2.48 with a total energy expression 2.42 for a system where the electron in state k has been removed, thus the terms $i = k$ and $j = k$ omitted in the sums appearing in 2.42, shows that indeed

$$\varepsilon_k = -\left(E_{\text{without } k} - E\right), \tag{2.49}$$

where E denotes the energy of the N electron system, and $E_{\text{without } k}$ is the energy of the $N-1$ electron system where one electron from state k has been removed.

2.3 Uniform Electron Gas

The uniform electron gas, also known as homogeneous electron gas or jellium model, is a quantum mechanical model of interacting electrons in a model solid where the positive charges (i.e. the atomic nuclei) are assumed to be uniformly distributed in space forming a "jellium" of a positively charged background. As a consequence the electron density as well is a uniform quantity in space. The jellium model allows one to focus on the effects in solids that occur due to the quantum nature of electrons and their mutual repulsive interactions (due to like charge) without explicit introduction of the atomic lattice and structure making up a real material. The uniform electron gas is also at the heart of the local density approximation which forms the basis of exchange-correlation functionals to be used in density functional theory for systems with an homogeneous electron distribution.

At zero temperature, the properties of jellium depend solely upon the constant electronic density

$$n = \frac{N}{\Omega}, \tag{2.50}$$

where N is the number of electrons in the crystal volume Ω. Equivalently one can express the electron density in terms of the Fermi wave vector

$$k_F = \left(3\pi^2 n\right)^{\frac{1}{3}}, \tag{2.51}$$

or the Seitz radius r_s which is the radius of a sphere which on average contains one electron

$$\frac{4}{3}\pi r_s^3 = \frac{\Omega}{N} = \frac{1}{n} \quad \Rightarrow \quad r_s = \left(\frac{3}{4\pi}\right)^{\frac{1}{3}} n^{-\frac{1}{3}} = \left(\frac{9\pi}{4}\right)^{\frac{1}{3}} \frac{1}{k_F}. \tag{2.52}$$

2.3.1 Hartree-Fock Equations for the Jellium

For the uniform electron gas, the Hartree-Fock equations can be solved analytically. We will show that – as for a system of non-interacting electrons – the eigenfunctions turn out to be plane waves

$$\phi_{\boldsymbol{k}}(\boldsymbol{r}) = \frac{1}{\sqrt{\Omega}} e^{i\boldsymbol{k}\cdot\boldsymbol{r}} \tag{2.53}$$

Insertion of 2.53 into 2.43 and using $\hat{h}(\boldsymbol{r}) = -\frac{1}{2}\Delta - n\int \mathrm{d}^3 r' \frac{1}{|\boldsymbol{r}-\boldsymbol{r}'|}$ for the kinetic energy and attractive potential of the positive jellium background leads to

$$\begin{aligned}
\left[\hat{h}(\boldsymbol{r}) + n\int \mathrm{d}^3 r' \frac{1}{|\boldsymbol{r}-\boldsymbol{r}'|} - \sum_{\boldsymbol{k}'}^{occ} \int \mathrm{d}^3 r' \frac{1}{|\boldsymbol{r}-\boldsymbol{r}'|} \frac{\phi^*_{\boldsymbol{k}'}(\boldsymbol{r}')\phi_{\boldsymbol{k}}(\boldsymbol{r}')\phi_{\boldsymbol{k}'}(\boldsymbol{r})}{\phi_{\boldsymbol{k}}(\boldsymbol{r})}\right]\phi_{\boldsymbol{k}}(\boldsymbol{r}) &= \varepsilon_{\boldsymbol{k}}\phi_{\boldsymbol{k}}(\boldsymbol{r}) \\
\left[\frac{k^2}{2} - \frac{1}{\Omega}\sum_{\boldsymbol{k}'}^{occ} \int \mathrm{d}^3 r' \frac{1}{|\boldsymbol{r}-\boldsymbol{r}'|} e^{i(\boldsymbol{k}'-\boldsymbol{k})(\boldsymbol{r}-\boldsymbol{r}')}\right] e^{i\boldsymbol{k}\cdot\boldsymbol{r}} &= \varepsilon_{\boldsymbol{k}} e^{i\boldsymbol{k}\cdot\boldsymbol{r}}.
\end{aligned}$$

By noting that due to the uniformity of the electron gas, the result will not depend on a chosen point $\boldsymbol{r}$, but only on the relative coordinate $\boldsymbol{u} = \boldsymbol{r}' - \boldsymbol{r}$, we find for the band energy $\varepsilon_{\boldsymbol{k}}^{\mathrm{HF}}$ in the Hartree-Fock approximation

$$\varepsilon_{\boldsymbol{k}}^{\mathrm{HF}} = \underbrace{\frac{k^2}{2}}_{\varepsilon_{\boldsymbol{k}}^{\mathrm{kin}}} + \underbrace{\frac{(-1)}{\Omega}\sum_{\boldsymbol{k}'}^{occ} \int \frac{\mathrm{d}^3 u}{u} e^{-i(\boldsymbol{k}'-\boldsymbol{k})\boldsymbol{u}}}_{\varepsilon_{\boldsymbol{k}}^{x}}, \tag{2.54}$$

where the first term arises from the kinetic energy and the second term is due to the Fock exchange.

2.3.2 Kinetic Energy

We first evaluate the kinetic energy per particle $t = \frac{T}{N}$ in the usual manner by replacing $\sum_{\boldsymbol{k}}^{occ} \to \frac{\Omega}{(2\pi)^3}\int \mathrm{d}^3 k$ where the factor of 2 arises from spin degeneracy

$$t = \frac{1}{N} 2 \sum_{\boldsymbol{k}}^{occ} \frac{k^2}{2} = \frac{2}{N}\frac{\Omega}{(2\pi)^3} \int\limits_{k\le k_F} \mathrm{d}^3 k \frac{k^2}{2} = \frac{2\cdot 3\pi^2 \cdot 4\pi}{8\pi^3 k_F^3 \cdot 2}\frac{k_F^5}{5} = \frac{3}{5}\frac{k_F^2}{2}. \tag{2.55}$$

Here we have used the relation $3\pi^2 n = k_F^3$ and have obtained the well-known result that the kinetic energy per particle is $\frac{3}{5}$ of the Fermi energy, i.e., the kinetic energy at the Fermi surface. Alternatively, we can also express t in terms of n or r_s,

$$t(k_F) = \frac{3}{5}\frac{k_F^2}{2} \propto k_F^2, \qquad t(n) = \frac{3}{10}(3\pi^2 n)^{\frac{2}{3}} \propto n^{\frac{2}{3}}, \qquad t(r_s) = \frac{3}{10}\frac{(9\pi/4)^{\frac{2}{3}}}{r_s^2} \propto \frac{1}{r_s^2}. \tag{2.56}$$

2.3.3 Exchange Energy

Next we evaluate the exchange energy per particle $e_x = \frac{E_x}{N}$. To this end, we first evaluate $\varepsilon_{\boldsymbol{k}}^x$ defined in 2.54 and insert the Fourier series of

$$\frac{1}{u} = \frac{1}{\Omega}\sum_{\boldsymbol{q}} \frac{4\pi}{q^2} e^{i\boldsymbol{q}\boldsymbol{u}}. \tag{2.57}$$

This leads to

$$\begin{aligned}
\varepsilon_{\boldsymbol{k}}^x &= -\frac{1}{\Omega}\sum_{\boldsymbol{k}'}^{occ} \int \frac{\mathrm{d}^3 u}{u} e^{-i(\boldsymbol{k}'-\boldsymbol{k})\boldsymbol{u}} \\
&= -\frac{1}{\Omega^2}\sum_{\boldsymbol{k}'}^{occ}\sum_{\boldsymbol{q}} \frac{4\pi}{q^2} \underbrace{\int \mathrm{d}^3 u\, e^{i(\boldsymbol{q}-\boldsymbol{k}'+\boldsymbol{k})\boldsymbol{u}}}_{=\Omega\cdot\delta_{\boldsymbol{q},\boldsymbol{k}-\boldsymbol{k}'}} = -\frac{1}{\Omega}\sum_{\boldsymbol{k}'}^{occ} \frac{4\pi}{|\boldsymbol{k}-\boldsymbol{k}'|^2} \\
&= -\frac{1}{(2\pi)^3}\int_{k'\le k_F} \mathrm{d}^3 k' \frac{4\pi}{|\boldsymbol{k}-\boldsymbol{k}'|^2} = -\frac{1}{(2\pi)^2}\int_{k'=0}^{k_F} \mathrm{d}k'\, k'^2 \int_{\xi=-1}^{+1} \mathrm{d}\xi \frac{4\pi}{k^2+k'^2-2kk'\xi} = \cdots \\
&= -\frac{k_F}{2\pi}\left[2 + \frac{k_F^2-k^2}{k\cdot k_F}\ln\left|\frac{k+k_F}{k-k_F}\right|\right].
\end{aligned} \tag{2.58}$$

The final result shows that $\varepsilon_{\boldsymbol{k}}^x$ is actually only a function of the magnitude of $\boldsymbol{k}$, as expected from the isotropy of the jellium model, thus $\varepsilon_{|\boldsymbol{k}|}^x$, and all occupied states are within a Fermi sphere of radius k_F. Next, we can compute the exchange energy per electron as $e_x = \frac{1}{N}\sum_{\boldsymbol{k}}^{occ} \varepsilon_{|\boldsymbol{k}|}^x$. Note that here, in contrast to the kinetic energy, in the sum $\sum_{\boldsymbol{k}}^{occ}$ only spin-parallel electrons have to be considered and hence no factor of 2 needs to be added. The resulting integral can be evaluated analytically and one finds

$$e_x(k_F) = -\frac{3}{4\pi}k_F \propto -k_F, \qquad e_x(n) = -\frac{3}{4\pi}(3\pi^2 n)^{\frac{1}{3}} \propto -n^{\frac{1}{3}}, \qquad e_x(r_s) = -\frac{3}{4\pi}\frac{(9\pi/4)^{\frac{1}{3}}}{r_s} \propto -\frac{1}{r_s}. \tag{2.59}$$

Note that these results will be used later on within the local density approximation (LDA) also for the inhomogeneous electrons gas by allowing for a spatially dependent electron gas parameters, e.g.,

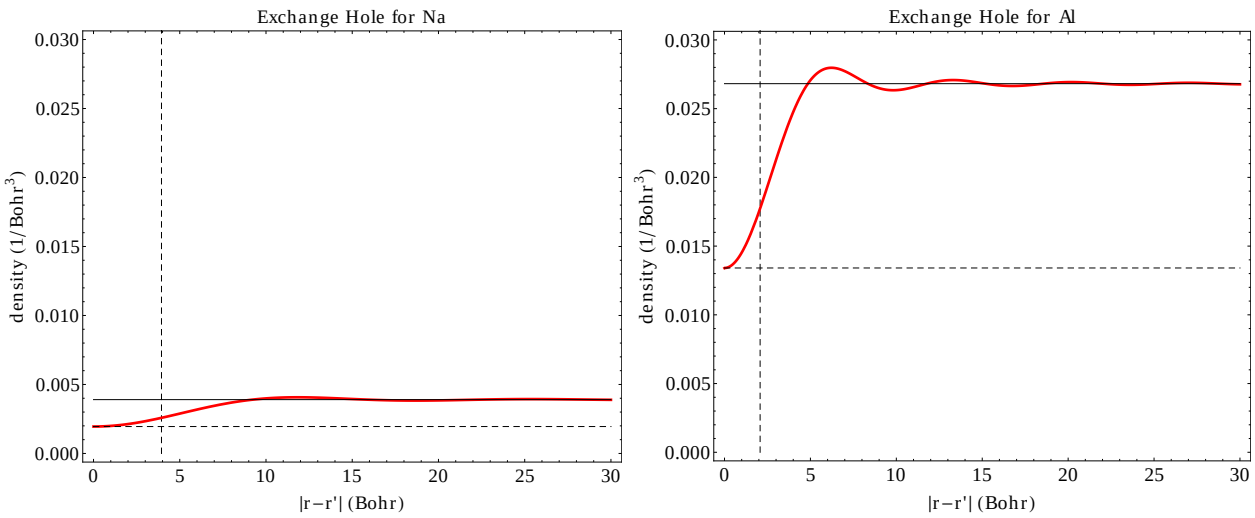

Figure 2.1: Illustration of the exchange hole $n - \overline{\rho_x}(u)$ for Na ($k_F \approx 0.487$ Bohr^{-1}) (left) and for Al ($k_F \approx 0.926$ Bohr^{-1}) (right). Note that the corresponding Wigner-Seitz radii (in Bohr unit) are $r_S \approx 3.94$ and $r_S \approx 2.07$ for Na and Al, respectively, as indicated by the vertical dashed line.

$n = n(\boldsymbol{r})$ or equivalently $r_s = r_s(\boldsymbol{r})$.

In order to interpret the physical meaning of the exchange energy further, we also evaluate the non-local exchange charge density defined in 2.47 now for the uniform electron gas

$$\begin{aligned} \rho_F^{\boldsymbol{k},\uparrow\uparrow}(\boldsymbol{r},\boldsymbol{r}') &= \frac{1}{\Omega}\sum_{\boldsymbol{k}'}^{occ} e^{i(\boldsymbol{k}'-\boldsymbol{k})(\boldsymbol{r}-\boldsymbol{r}')} = \cdots \\ \rho_F^{\boldsymbol{k},\uparrow\uparrow}(\boldsymbol{u}) &= \frac{2}{(2\pi)^2} e^{-i\boldsymbol{k}\cdot\boldsymbol{u}} \frac{\sin(k_F u) - k_F u\cos(k_F u)}{u^3}, \end{aligned} \tag{2.60}$$

where $\boldsymbol{u} = \boldsymbol{r} - \boldsymbol{r}'$ is the relative coordinate of the two interacting electrons. Note that this charge density is not spherical symmetric, depends on $\boldsymbol{k}$ and is complex-valued. Therefore, it is common to consider a charge density which is an average over all occupied states defined as

$$\overline{\rho_x}(u) = \frac{2}{N}\sum_{\boldsymbol{k}}^{occ} \rho_F^{\boldsymbol{k},\uparrow\uparrow}(\boldsymbol{u}) = \cdots = \frac{k_F^3}{2\pi^2}\frac{\sin(k_F u) - k_F u\cos(k_F u)}{(k_F u)^3}. \tag{2.61}$$

Subtracting this exchange density $\overline{\rho_x}(u)$ from the overall electron density $n = \frac{k_F^3}{3\pi^2}$ we see (Fig. 2.1) that the charge density around a given electron at $\boldsymbol{r}$ is depleted. For $u = 0$, that is for $\boldsymbol{r} = \boldsymbol{r}'$, the density is reduced by exactly a factor $\frac{1}{2}$ which is a direct consequence of the Pauli exclusion principle which does not allow electrons of the same spin to be present at the same point in space, and is thus a purely quantum mechanical phenomenon with no classical analogue. Intuitively, each electron is

thus surrounded by a sphere of radius $\propto r_s$ (vertical dashed line in Fig. 2.1), where no spin-parallel electron is present. Since this depletion arises from the exchange-term in the Hartree-Fock equations, this sphere is called *exchange hole*. Also note that there are oscillations around the overall density with a wave length set by the Fermi wave vector k_F which are called *Friedel oscillations*.

2.3.4 Correlation Energy

Summing up the results of the previous two sections, within the Hartree-Fock approximation the energy $e_{\mathrm{HF}} = E_{\mathrm{HF}}/N$ per electron in the uniform electron gas is given by (using atomic units, i.e., Hartree for the energy and Bohr for r_s)

$$e_{\mathrm{HF}}(r_s) = t(r_s) + e_x(r_s) = \frac{3}{10}\frac{(9\pi/4)^{\frac{2}{3}}}{r_s^2} - \frac{3}{4\pi}\frac{(9\pi/4)^{\frac{1}{3}}}{r_s} \approx \frac{1.10495}{r_s^2} - \frac{0.458165}{r_s} \tag{2.62}$$

We remember that the Hartree-Fock approximation has been obtained by applying the variational principle to a wave function in the form of a *single* Slater determinant. If one attempts to further improve the description of the wave function, and thereby find an even better approximation for the energy, one can use a linear combination of N-electron Slater determinants which include excitations from occupied states to unoccupied states. All effects that go beyond the Hartree-Fock description are termed *correlations* and lead to a lowering of the total energy. Even for the uniform electron gas, the computation of the correlation energy can no longer be accomplished in an analytic form except for the hight density, $r_s \to 0$, and the low-density, $r_s \to \infty$, limits. For intermediate r_s, typically numerical results are obtained from quantum Monte-Carlo simulations. The derivations of the expressions for the limiting cases and the detailed description of the quantum Monte-Carlo method is beyond the scope this lecture, and we here only give the results since they will prove important later on in the context of the local density approximation (LDA) within the framework of DFT.

The high-density limit $r_s \to 0$

Inspection of 2.62 shows that in the limit $r_s \to 0$, the kinetic energy dominates over the exchanges energy since the former grows faster than the latter. Thus, for high densities, the electron-electron interaction can be regarded as a small *perturbation*. In other words, the high density limit can also be called the *weak coupling limit*. This may be somewhat counter-intuitive since in the limit $r_s \to 0$, also the distance between electrons approaches zero, however, the kinetic energy grows faster than the Coulomb interactions. Therefore, in the $r_s \to 0$ limit expressions for the correlation energy can be derived with the help of many-body perturbation theory with the following result expressed as an

perturbation expansion in terms Wigner-Seitz radius r_s:

$$e_c(r_s \to 0) = c_0 \ln r_s - c_1 + c_2 r_s \ln r_s + \cdots \tag{2.63}$$

The coefficients c_0 and c_1 have already been obtained by Gell-Mann and Brückner [23] and Onsager et al. [24], respectively, while an accurate value of c_2 is due to Perdew [25] (values in Hartree)

$$c_0 = \frac{1}{\pi^2}(1 - \ln 2) \approx 0.031091, \qquad c_1 \approx 0.046644, \qquad c_2 \approx 0.006644. \tag{2.64}$$

The low-density limit $r_s \to \infty$

Contrary, in the limit $r_s \to \infty$ the kinetic energy contribution vanishes faster than the energy contributions arising from Coulomb interactions, thus the low-density limit can also be termed the *strong coupling limit*. In the low-density limit the uniform electron gas is unstable against the formation of the so-called Wigner lattice which can be thought of as a crystallization of electrons on a close-packed lattice. Because the energies of the uniform phase and the Wigner lattice are almost degenerate, the energy in this limit follows from electro-static arguments and by taking into account zero-point vibrations of the electrons around their lattice points [1, 26]

$$e_c(r_s \to \infty) = -\frac{d_0}{r_s} + \frac{d_1}{r_s^{3/2}} \cdots \tag{2.65}$$

An interpolating expression for general r_s values

For general values of r_s no analytic expressions can be derived. However, Perdew and Wang [25] have suggested an analytic expression which encompasses both limits

$$e_c(r_s) = -2c_0(1 + \alpha_1 r_s) \ln \left[1 + \frac{1}{2c_0 \left(\beta_1 r_s^{1/2} + \beta_2 r_s + \beta_3 r_s^{3/2} + \beta_4 r_s^2 \right)} \right]. \tag{2.66}$$

In order to have the correct limits, β_1 and β_2 are already determined by the high-density expansion $r_s \to 0$ as follows:

$$\beta_1 = \frac{1}{2c_0} \exp\left(-\frac{c_1}{2c_0} \right), \qquad \beta_2 = 2c_0\beta_1^2. \tag{2.67}$$

The coefficients α_1, β_3 and β_4, on the other hand, are found by fitting the the expression 2.66 to accurate correlations energies from Quantum Monte-Carlo simulations [27, 28]. Thereby, Perdew and Wang found the following values [25]

$$\alpha_1 = 0.21370, \qquad \beta_3 = 1.6382, \qquad \beta_4 = 0.49294. \tag{2.68}$$

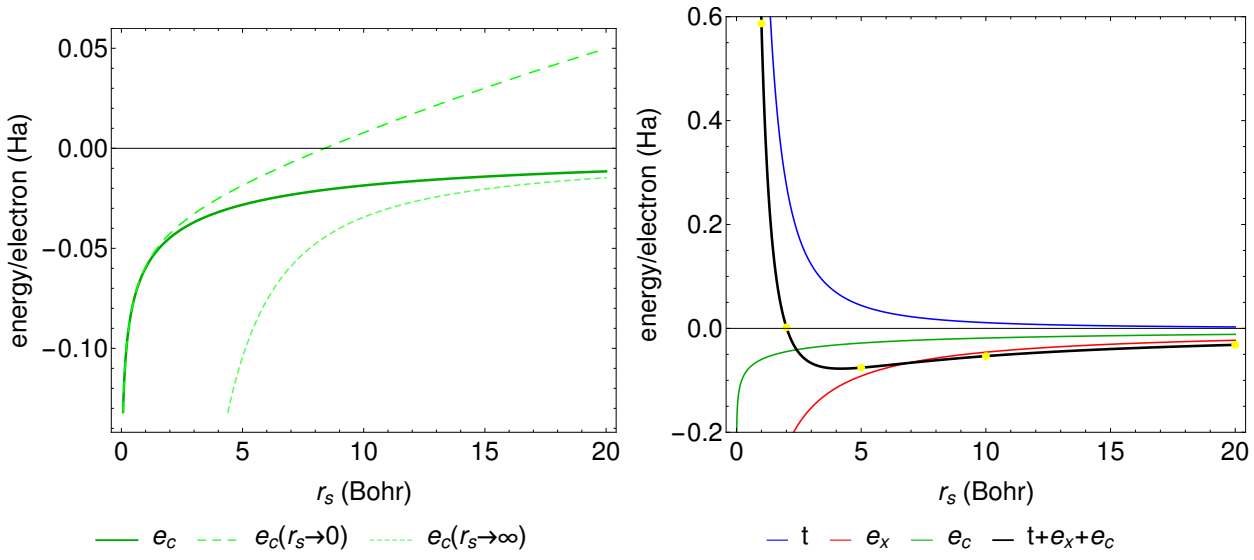

Figure 2.2: Left panel: Correlation energy per electron for the uniform electron gas according to Eq. 2.66 (sold line) and the two limiting expression for $r_s \to 0$ (long dashed) and $r_s \to \infty$ (short dashed). Right panel: Kinetic energy (t), exchange energy (e_x), correlation energy (e_c) as well as the sum of all contributions for the uniform electron gas compared to numerical results (yellow dots) from Quantum Monte-Carlo simulations [27].

The correlation energy 2.66 together with the limiting expressions for $r_s \to 0$ and $r_s \to \infty$ is depicted in the left panel of Fig. 2.2. The right panel of the figure shows the kinetic energy (t), the exchange energy (e_x), the correlation energy (e_c) as well as the sum of all contributions for the uniform electron gas compared to numerical results (yellow dots) from Quantum Monte-Carlo simulations [27]. Note that Fig. 2.2 has been obtained with the Mathematica Notebook `jellium.nb`.

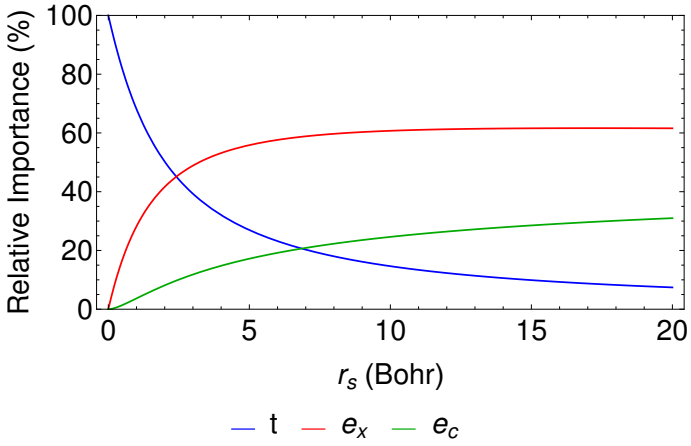

Figure 2.3: Relative contributions of kinetic energy (t), exchange energy (e_x) and correlation energy (e_c) to the total energy of the uniform electron gas as a function of r_s.

Chapter 3

Density Functional Theory

In the very first section of these lecture notes 1.1, we have already introduced the many-electron Hamiltonian, Eq. 1.3, in the following form

$$\hat{H} = \hat{T} + \hat{V}_{\text{ext}} + \hat{V}_{ee} = -\frac{1}{2}\sum_{i=1}^{N}\Delta_i + \sum_{i=1}^{N} v(\boldsymbol{r}_i) + \frac{1}{2}\sum_{i,j\neq i}\frac{1}{|\boldsymbol{r}_i - \boldsymbol{r}_j|}. \tag{3.1}$$

We have also already introduced the electron density in Eq. 1.6 which can be obtained from the N-electron wave function by integrating over all but one spatial coordinate and summing over all but one spin coordinate:

$$n_\sigma(\boldsymbol{r}) = N \sum_{\sigma_2\cdots\sigma_N} \int \mathrm{d}^3 r_2 \cdots \int \mathrm{d}^3 r_N \, |\psi(\boldsymbol{r}\sigma, \boldsymbol{r}_2\sigma_2, \cdots, \boldsymbol{r}_N\sigma_N)|^2 . \tag{3.2}$$

In this Chapter, we will show that ground state energy of a system of interacting electrons can be expressed as a *functional* of the electron density $n_\sigma(\boldsymbol{r})$. We will first review the foundations of density functional theory (DFT) and then derive the Kohn-Sham equations. In the second half of this chapter, we will focus on the so-called exchange-correlation functional and derive some of its exact properties before we discuss the most widely used approximations for it. Finally, we will also introduce Janak's theorem which allows us to interpret the Kohn-Sham energies.

3.1 Density as Basic Variable

The basic lemma of HOHENBERG and KOHN states that the ground state density $n(\boldsymbol{r})$ of a bound system of interacting electrons in some external potential $v(\boldsymbol{r})$ determines this potential uniquely (up to an additive constant) [4]. The proof is very simple: Let $n(\boldsymbol{r})$ be the non-degenerate ground-state density of N electrons in the external potential $v_1(\boldsymbol{r})$, corresponding to the ground state characterized by the many-electron wave function Ψ_1 and its total energy E_1. Then, we can write

$$\begin{aligned} E_1 &= \langle \Psi_1 | \hat{H}_1 | \Psi_1 \rangle \\ &= \int \mathrm{d}^3 r \, v_1(\boldsymbol{r}) n(\boldsymbol{r}) + \langle \Psi_1 | \hat{T} + \hat{V}_{ee} | \Psi_1 \rangle, \end{aligned} \tag{3.3}$$

where $\hat{H}_1$ is the total Hamiltonian corresponding to the external potential $v_1(\boldsymbol{r})$, and $\hat{T}$ and $\hat{V}_{ee}$ are the kinetic and electron-electron interaction energy operators, respectively, as defined in 3.1. Note that first term arises because the expectation value of the *local and spin-independent* external potential can be simplified as follows

$$\begin{aligned} \left\langle \Psi \left| \hat{V}_{\text{ext}} \right| \Psi \right\rangle &= \left\langle \Psi \left| \sum_{i=1}^{N} v(\boldsymbol{r}_i) \right| \Psi \right\rangle \\ &= \sum_{\sigma_1 \cdots \sigma_N} \int \mathrm{d}^3 r_1 \cdots \int \mathrm{d}^3 r_N \Psi^*(\boldsymbol{r}_1 \sigma_1, \cdots, \boldsymbol{r}_N \sigma_N) \sum_{i=1}^{N} v(\boldsymbol{r}_i) \Psi(\boldsymbol{r}_1 \sigma_1, \cdots, \boldsymbol{r}_N \sigma_N) \\ &= \sum_{i=1}^{N} \sum_{\sigma} \int \mathrm{d}^3 r \, v(\boldsymbol{r}) \underbrace{\sum_{\sigma_2 \cdots \sigma_N} \int \mathrm{d}^3 r_2 \cdots \int \mathrm{d}^3 r_N \, |\Psi(\boldsymbol{r}\sigma, \boldsymbol{r}_2 \sigma_2, \cdots, \boldsymbol{r}_N \sigma_N)|^2}_{= \frac{1}{N} n_\sigma(\boldsymbol{r})} \\ &= N \cdot \frac{1}{N} \int \mathrm{d}^3 r \, v(\boldsymbol{r}) n(\boldsymbol{r}) = \int \mathrm{d}^3 r \, v(\boldsymbol{r}) n(\boldsymbol{r}), \end{aligned} \tag{3.4}$$

where

$$n(\boldsymbol{r}) = \sum_{\sigma} n_\sigma(\boldsymbol{r}) = n_\uparrow(\boldsymbol{r}) + n_\downarrow(\boldsymbol{r}). \tag{3.5}$$

Now suppose that there exists a second external potential $v_2(\boldsymbol{r})$, which differs from $v_1(\boldsymbol{r})$ not just by a constant, leading to the *same* density $n(\boldsymbol{r})$. If we denote its ground state wave function and energy with Ψ_2 and E_2, respectively, we obtain in complete analogy to 3.3

$$E_2 = \int \mathrm{d}^3 r \, v_2(\boldsymbol{r}) n(\boldsymbol{r}) + \langle \Psi_2 | \hat{T} + \hat{V}_{ee} | \Psi_2 \rangle. \tag{3.6}$$

The Rayleigh-Ritz minimal principle discussed in Sec. 2.2.1 applied to the ground state Ψ_1 with energy

E_1 gives the following inequality

$$E_1 < \langle \Psi_2 | \hat{H}_1 | \Psi_2 \rangle = \int \mathrm{d}^3 r \, v_1(\boldsymbol{r}) n(\boldsymbol{r}) + \langle \Psi_2 | \hat{T} + \hat{V}_{ee} | \Psi_2 \rangle = E_2 + \int [v_1(\boldsymbol{r}) - v_2(\boldsymbol{r})] n(\boldsymbol{r}) \mathrm{d}^3 r. \tag{3.7}$$

On the other hand, the analogous argument for the ground state of Ψ_2 leads to the expression

$$E_2 < \langle \Psi_1 | \hat{H}_2 | \Psi_1 \rangle = E_1 + \int [v_2(\boldsymbol{r}) - v_1(\boldsymbol{r})] n(\boldsymbol{r}) \mathrm{d}^3 r. \tag{3.8}$$

Adding Eqs. (3.7) and (3.8) leads to the contradiction

$$E_1 + E_2 < E_1 + E_2. \tag{3.9}$$

Thus, our initial assumption of the existence of a second external potential $v_2(\boldsymbol{r})$ leading to the identical density $n(\boldsymbol{r})$ must be wrong, and the Hohenberg-Kohn lemma is proven. We note that the proof presented above is based on the assumption of the non-degeneracy of the ground state. This requirement, however, can be lifted as shown by Kohn [29]. Moreover, we have assumed that *any* well-behaved positive function $n(\boldsymbol{r})$, which integrates to the number of electrons N, is a possible ground-state density corresponding to *some* $v(\boldsymbol{r})$ (v-representability). Levy [30] and Lieb have shown that there are indeed examples of well-behaved densities that are not v-representable, but these cases do not appear to limit the practical application of DFT. Thus, the important message of this section is, that the total electron density $n(\boldsymbol{r})$ of a system of interacting electrons determines both, the number of electrons N and the external potential $v(\boldsymbol{r})$. Moreover, the many-body wave function Ψ is also a functional of the electron density $n(\boldsymbol{r})$ [4]. Consequently, the density gives us the full Hamiltonian $\hat{H}$ for the electronic system, and $n(\boldsymbol{r})$ implicitly contains all properties derivable from $\hat{H}$ through solution of the Schrödinger equation.

3.2 Hohenberg-Kohn Theorem

The ground state energy E of a system of interacting electrons can be obtained from the solution of the many-body Schrödinger equation $\hat{H}\Psi = E\Psi$. Another approach is provided by the Rayleigh-Ritz minimal principle

$$E = \min_{\Psi} \left\langle \Psi \middle| \hat{H} \middle| \Psi \right\rangle, \tag{3.10}$$

where Ψ is a normalized trial function for the N electron system. Equivalently, the minimal principle can be formulated in terms of trial densities $n(\boldsymbol{r})$, rather than trial wave functions Ψ, as was first shown by Hohenberg and Kohn [4], and later in the form of the *constrained search method* by Levy [30]. By integrating the trial wave function Ψ over all space variables except the first, one obtains the

corresponding density $n(\boldsymbol{r})$. Thus, the minimization of Eq. (3.10) may be achieved in two steps: First, fix a trial density $n(\boldsymbol{r})$, where we denote all wave functions resulting in this density by $\Psi \to n$. We define an energy *functional* of the density $n(\boldsymbol{r})$ in the way

$$E[n(\boldsymbol{r})] = \min_{\Psi \to n} \left\langle \Psi \middle| \hat{H} \middle| \Psi \right\rangle = \min_{\Psi \to n} \left\langle \Psi \middle| \hat{T} + \hat{V}_{ee} \middle| \Psi \right\rangle + \int \mathrm{d}^3 r \, v(\boldsymbol{r}) n(\boldsymbol{r}) = F[n(\boldsymbol{r})] + \int \mathrm{d}^3 r \, v(\boldsymbol{r}) n(\boldsymbol{r}), \tag{3.11}$$

where we have introduced the *universal* functional $F[n(\boldsymbol{r})]$ which is independent of the external potential $v(\boldsymbol{r})$ and given by

$$F[n(\boldsymbol{r})] = \min_{\Psi \to n} \left\langle \Psi \middle| \hat{T} + \hat{V}_{ee} \middle| \Psi \right\rangle. \tag{3.12}$$

In a second step, minimize Eq. (3.11) over all densities $n(\boldsymbol{r})$ resulting in the ground state energy E

$$E = \min_{n(\boldsymbol{r})} E[n(\boldsymbol{r})] = \min_{n(\boldsymbol{r})} \left\{ F[n(\boldsymbol{r})] + \int \mathrm{d}^3 r \, v(\boldsymbol{r}) n(\boldsymbol{r}) \right\}. \tag{3.13}$$

This is the Hohenberg-Kohn minimum principle [4] stating that the total energy is a functional of the density, and that the ground state density $n(\boldsymbol{r})$ minimizes this functional resulting in the ground state energy $E = E[n(\boldsymbol{r})]$.

Searching for the minimum of Eq. 3.13 under the constraint of a fixed electron number $N = \int \mathrm{d}^3 r \, n(\boldsymbol{r})$ with the help of the Lagrangian multiplier N leads to

$$\delta \left\{ F[n(\boldsymbol{r})] + \int \mathrm{d}^3 r \, v(\boldsymbol{r}) n(\boldsymbol{r}) - \mu \int \mathrm{d}^3 r \, n(\boldsymbol{r}) \right\} = 0 \qquad \Rightarrow \qquad \frac{\delta F[n(\boldsymbol{r})]}{\delta n(\boldsymbol{r})} + v(\boldsymbol{r}) = \mu. \tag{3.14}$$

This equation shows that the potential $v(\boldsymbol{r})$ is uniquely determines by the ground state density (up to the constant μ, the Lagrangian parameter).

3.3 Excursion to Functional Derivatives

At this point, we want to make a small excursion to functional derivatives such as $\frac{\delta F[n(\boldsymbol{r})]}{\delta n(\boldsymbol{r})}$ and remind the reader about their meaning and how they can be calculated. Consider a simple example for a density functional that we will alter encounter as the exchange functional within the local density approximation:

$$E_x[n(\boldsymbol{r})] = A_x \int \mathrm{d}^3 r \, [n(\boldsymbol{r})]^{\frac{4}{3}}. \tag{3.15}$$

What do we mean by the *functional* derivative $\frac{\delta E_x[n(\boldsymbol{r})]}{\delta n(\boldsymbol{r})}$ or the variation $\delta E_x[n(\boldsymbol{r})]$. To see this, we make the analogy to a *function* f of several variables and consider its total derivative $\mathrm{d}f$:

$$f = f(x_1, x_2, \cdots, x_N) \qquad \Rightarrow \qquad \mathrm{d}f = \sum_{i=1}^{N} \frac{\partial f}{\partial x_i} \mathrm{d}x_i. \tag{3.16}$$

Now consider a functional $F[n(\boldsymbol{r})]$. The functional derivative tells us how the functional changes under a small variation $\delta n(\boldsymbol{r})$ of the function $n(\boldsymbol{r})$:

$$F = F[n(\boldsymbol{r})] \qquad \Rightarrow \qquad \delta F = \int \mathrm{d}^3 r \, \frac{\delta F}{\delta n(\boldsymbol{r})} \delta n(\boldsymbol{r}) = \int \mathrm{d}^3 r \, \left\{ F[n(\boldsymbol{r}) + \delta n(\boldsymbol{r})] - F[n(\boldsymbol{r})] \right\} \delta n(\boldsymbol{r}). \tag{3.17}$$

Thus, for our example 3.15, we have[1]

$$\begin{aligned} \delta E_x[n(\boldsymbol{r})] &= A_x \int \mathrm{d}^3 r \, \left\{ [n(\boldsymbol{r}) + \delta n(\boldsymbol{r})]^{\frac{4}{3}} - [n(\boldsymbol{r})]^{\frac{4}{3}} \right\} \delta n(\boldsymbol{r}) \\ &= \int \mathrm{d}^3 r \, \underbrace{A_x \frac{4}{3} [n(\boldsymbol{r})]^{\frac{1}{3}}}_{= \frac{\delta E_x[n(\boldsymbol{r})]}{\delta n(\boldsymbol{r})}} \delta n(\boldsymbol{r}). \end{aligned}$$

As another example for a density functional consider the Hartree energy $U[n(\boldsymbol{r})]$ given by the following electrostatic integral

$$U[n(\boldsymbol{r})] = \frac{1}{2} \int \mathrm{d}^3 r \int \mathrm{d}^3 r' \, \frac{n(\boldsymbol{r}) n(\boldsymbol{r}')}{|\boldsymbol{r} - \boldsymbol{r}'|}. \tag{3.18}$$

Now, let us compute the functional derivative

$$\begin{aligned} \delta U[n(\boldsymbol{r})] &= \frac{1}{2} \int \mathrm{d}^3 r \int \mathrm{d}^3 r' \left\{ \frac{[n(\boldsymbol{r}) + \delta n(\boldsymbol{r})] n(\boldsymbol{r}')}{|\boldsymbol{r} - \boldsymbol{r}'|} - \frac{n(\boldsymbol{r}) n(\boldsymbol{r}')}{|\boldsymbol{r} - \boldsymbol{r}'|} \right\} \\ &= 2 \frac{1}{2} \int \mathrm{d}^3 r \underbrace{\left[\int \mathrm{d}^3 r' \frac{n(\boldsymbol{r}')}{|\boldsymbol{r} - \boldsymbol{r}'|} \right]}_{= v_H([n], \boldsymbol{r})} \delta n(\boldsymbol{r}). \end{aligned}$$

Thus, we see that the functional derivative of the Hartree energy $U[n(\boldsymbol{r})]$ leads to the Hartree potential $v_H([n], \boldsymbol{r})$ which, in mathematical terms, is a functional of the density $n(\boldsymbol{r})$ and a function of $\boldsymbol{r}$.

[1] $(n + \delta n)^a = n^a + a n^{a-1} \delta n + \mathcal{O}(\delta n^2)$

3.4 Kohn-Sham Equations

While the Hohenberg-Kohn theorem in the form of the minimization condition 3.14 in principle allows to determine the ground state density – provided the functional form of the universal functional $F[n(\boldsymbol{r})]$ is known – in practice a different approach has been proposed by Kohn and Sham to obtain the ground state density [5]. They have suggested to consider an auxiliary (a fictitious) system of N *non-interacting* electrons. Thus compared to the true physical Hamiltonian defined in Eq. 3.1, the electron-electron interaction $\hat{V}_{ee} \equiv 0$

$$\hat{H}_s = \hat{T} + \hat{V}_{s,\text{ext}} = -\frac{1}{2}\sum_{i=1}^{N} \Delta_i + \sum_{i=1}^{N} v_s(\boldsymbol{r}_i) = \sum_{i=1}^{N} \hat{h}_s(\boldsymbol{r}_i). \tag{3.19}$$

Thus, the Hamiltonian can be written as the sum over single-particle Hamiltonians $\hat{h}_s$, where we have introduced the subscript s to indicate that we are considering our auxiliary system of non-interacting particles. It is important to note that we allow the external potential $v_s(\boldsymbol{r}_i)$ to be different from the interacting case with the potential $v(\boldsymbol{r}_i)$. In fact, the idea of Kohn and Sham was to choose the potential $v_s(\boldsymbol{r}_i)$ in such a way that the resulting electron density $n(\boldsymbol{r})$ equals the true, physical density! Thus, we do not need to introduce any subscript on the density of the auxiliary system since, by construction, it yields the same density. Because the Hamiltonian 3.19 is just a sum of single-particle contributions without any coupling, the resulting N-electron wave functions can be *exactly* written as a single Slater determinant which we denote by $|\Phi\rangle$ obeying the following eigenvalue equation

$$\hat{H}_s \left|\Phi\right\rangle = E \left|\Phi\right\rangle. \tag{3.20}$$

To calculate the total energy, we apply the same two-step constrained-search minimum principle which we have already used earlier in Sec. 3.2 with the difference that the minimization only has to consider single Slater determinants and that the electron-electron interaction is set to zero.

$$E[n(\boldsymbol{r})] = \min_{\Phi\to n} \left\langle \Phi \middle| \hat{H}_s \middle| \Phi \right\rangle = \underbrace{\min_{\Phi\to n} \left\langle \Phi \middle| \hat{T} \middle| \Phi \right\rangle}_{T_s[n(\boldsymbol{r})]} + \int \mathrm{d}^3r\, v_s(\boldsymbol{r}) n(\boldsymbol{r}) = T_s[n(\boldsymbol{r})] + \int \mathrm{d}^3r\, v_s(\boldsymbol{r}) n(\boldsymbol{r}). \tag{3.21}$$

Here, we have introduced the functional $T_s[n(\boldsymbol{r})]$ which describes the kinetic energy for a system of non-interacting electrons. The ground state energy can now be obtained by minimizing over all densities corresponding to a fixed electron number N, thus

$$\delta\left\{T_s[n(\boldsymbol{r})] + \int \mathrm{d}^3r\, v_s(\boldsymbol{r}) n(\boldsymbol{r}) - \mu_s \int \mathrm{d}^3r\, n(\boldsymbol{r})\right\} = 0 \qquad \Rightarrow \qquad \frac{\delta T_s[n(\boldsymbol{r})]}{\delta n(\boldsymbol{r})} + v_s(\boldsymbol{r}) = \mu_s. \tag{3.22}$$

We can now equate 3.14 and 3.22 since any possible difference in the value of the constants μ and μ_s (the Lagrangian multipliers) can be adsorbed in the potential $v_s(\boldsymbol{r})$

$$\frac{\delta F[n(\boldsymbol{r})]}{\delta n(\boldsymbol{r})} + v(\boldsymbol{r}) = \frac{\delta T_s[n(\boldsymbol{r})]}{\delta n(\boldsymbol{r})} + v_s(\boldsymbol{r}). \tag{3.23}$$

Implicitly this equation assumes that the electron density $n(\boldsymbol{r})$ is both, interacting and non-interacting v-representable, in other words, that the electron density is of such a form that it results from the solution of the Hamiltonians $\hat{H}$ and $\hat{H}_s$ containing the external potentials $v(\boldsymbol{r})$ and $v_s(\boldsymbol{r})$, respectively. In practical applications, this requirement turns out to be no restriction.

In order to proceed, Kohn and Sham further suggested to write the universal functional $F[n(\boldsymbol{r})]$ in the following form by splitting off terms that are known and putting yet unknown terms into a new functional, the *exchange-correlation functional* $E_{xc}[n(\boldsymbol{r})]$:

$$F[n(\boldsymbol{r})] = T_s[n(\boldsymbol{r})] + U[n(\boldsymbol{r})] + E_{xc}[n(\boldsymbol{r})]. \tag{3.24}$$

Here, $U[n(\boldsymbol{r})]$ is the Hartree energy already introduced in Eq. 3.18 and describes the classical electrostatic self-repulsion of the charge density $n(\boldsymbol{r})$. Note that 3.24 can be viewed as the definition of the exchange-correlation functional within DFT. Inserting of 3.24 into 3.23 then directly leads to an expression for the yet unknown potential $v_s(\boldsymbol{r})$, the so-called Kohn-Sham potential

$$v_s(\boldsymbol{r}) = v(\boldsymbol{r}) + \frac{\delta U[n(\boldsymbol{r})]}{\delta n(\boldsymbol{r})} + \frac{\delta E_{xc}[n(\boldsymbol{r})]}{\delta n(\boldsymbol{r})} = v(\boldsymbol{r}) + v_H([n], \boldsymbol{r}) + v_{xc}([n], \boldsymbol{r}). \tag{3.25}$$

Using the Kohn-Sham potential defined above 1.10, the desired ground state electron density can be constructed from the single-particle orbitals $\varphi_i(\boldsymbol{r})$, the Kohn-Sham orbitals, which are the eigenstates of the Kohn-Sham equations

$$\left[-\frac{1}{2}\Delta + v_s(\boldsymbol{r})\right] \varphi_i(\boldsymbol{r}) = \varepsilon_i \varphi_i(\boldsymbol{r}), \tag{3.26}$$

by summing over all occupied Kohn-Sham orbital densities

$$n(\boldsymbol{r}) = \sum_{i=1}^{N} |\varphi_i(\boldsymbol{r})|^2. \tag{3.27}$$

Finally, the total ground state energy can be obtained from the following expression

$$E[n] = T_s[n] + U[n] + E_{xc}[n] + \int \mathrm{d}^3 r\, v(\boldsymbol{r}) n(\boldsymbol{r}) \qquad \text{with} \qquad T_s[n] = \sum_{i=1}^{N} \langle \varphi_i | -\frac{1}{2}\Delta | \varphi_i \rangle \,. \tag{3.28}$$

There are several things that should not be noted regarding the Kohn-Sham scheme defined by the

three Eqs. 3.25, 3.26 and 3.27. First, the Kohn-Sham method introduces the *orbitals* of the auxiliary non-interacting system in order to construct the density. Second, the simple form of 3.27 is due to the non-interacting character of the Hamiltoian which allows one to write the wave function of the the auxiliary system as single Slater determinant. Third, the Eqs. 3.25, 3.26 and 3.27 need to be solved in a *self-consistent* manner because two terms of the effective potential, that is the Hartree potential $v_H([n], \boldsymbol{r})$ as well as the exchange-correlation potential $v_{xc}([n], \boldsymbol{r})$, depend on the electron density. In practice, this means the Kohn-Sham equations are solved iteratively: one starts with an electron density $n_1(\boldsymbol{r})$ from which the effective potential $v_s(\boldsymbol{r})$ is calculated. Second, the Kohn-Sham equations 3.26 are solved leading to the Kohn-Sham orbitals $\varphi_i(\boldsymbol{r})$ and Kohn-Sham energies ε_i. Third, a new electron density $\tilde{n}_2(\boldsymbol{r})$ is obtained from these orbitals following Eq. 3.27. The iterative loop, the self-consistent loop, is closed by computing a new effective potential $v_s(\boldsymbol{r})$ from the new density. In practice, some sort of mixing of old and new densities is used in order to damp oscillation in the convergence, such as $n_2 = \alpha\tilde{n}_2 + (1-\alpha)n_1$, where α is a mixing parameter.

In summary, by splitting the univeral functional $F[n]$ as in 3.24, the Kohn-Sham method treats the kinetic energy T_s exactly, while the exchange-correlation energy E_{xc} needs to be approximated in some way. This turns out to be extremely successful in practical applications, because (i) T_s is usually a large part of the total energy while E_{xc} is usually smaller (see also Fig. 2.3). (ii) The kinetic energy T_s is responsible for density oscillations (e.g. shell structure in atoms) which is difficult to reproduce in schemes where a desnity dfunctional for the kinetic energy is used such as in the Thomas-Fermi method. (iii) It turns out that E_{xc} is better suited for local (or semi-local) approximations than T_s. A drawback of the Kohn-Sham scheme is that it introduces auxiliary orbitals into a density functional theory.

3.5 Exchange and Correlation

The usefulness of the Kohn-Sham scheme defined by the Eqs. 3.25, 3.26 and 3.27 for practical applications entirely depends on the availability of accurate and numerically tractable approximations for the exchange correlation energy. In this section, we will first derive a number of exact properties of the exchange-correlation functional, before we review the most-widely used approximations, namely the local density approximation (LDA) and the generalized gradient approximation (GGA). We will also outline more recent developments organized in a hierarchy of approximations called "Jacob's Ladder of DFT" and briefly mention how fully non-local correlations, which are important of the treatment of van-der-Waals interaction, can be incorporated into the exchange-correlation functional.

3.5.1 Exact Properties of E_{xc}

We begin by splitting the exchange-correlation energy into an *exchange* part and into a *correlation* part

$$E_{xc}[n] = E_x[n] + E_c[n]. \tag{3.29}$$

We complete the above equation by defining what we mean by exchange energy in the context of density functional theory where we use the following definition:

$$E_x[n] = \left\langle \Phi_n^{\min} \middle| \hat{V}_{ee} \middle| \Phi_n^{\min} \right\rangle - U[n]. \tag{3.30}$$

Here, we have introduced the short-hand notation $\left|\Phi_n^{\min}\right\rangle$ for the single Slater determinant which leads to the density n and minimizes the kinetic energy as introduced in Eq. 3.21, and $U[n]$ is the Hartree energy. It is noteworthy that the exchange energy defined above in Eq. 3.30 differs from the exchange energy introduced in the framework of Hartree-Fock theory, because the former is computed from Kohn-Sham orbitals while the latter is obtained from Hartree-Fock orbitals.

With the definition 3.30, we can now analyze the correlation energy further

$$\begin{aligned} E_c[n] &= E_{xc}[n] - E_x[n] \\ &= F[n] - T_s[n] - U[n] - \left\langle \Phi_n^{\min} \middle| \hat{V}_{ee} \middle| \Phi_n^{\min} \right\rangle + U[n] \\ &= \left\langle \Psi_n^{\min} \middle| \hat{T} + \hat{V}_{ee} \middle| \Psi_n^{\min} \right\rangle - \left\langle \Phi_n^{\min} \middle| \hat{T} + \hat{V}_{ee} \middle| \Phi_n^{\min} \right\rangle. \end{aligned} \tag{3.31}$$

Here, $\left|\Phi_n^{\min}\right\rangle$ is the single Slater determiant leading to the density n which minimizes $\hat{T}$ as above, and $\left|\Psi_n^{\min}\right\rangle$ is the interacting wave function leading to the density n which minimizes $\hat{T} + \hat{V}_{ee}$ as used in in the definition of the universal functional in Eq. 3.12. Therefore, the first expectation value in 3.31 must necessarily by smaller then the second one, and we conclude that

$$E_c[n] < 0, \tag{3.32}$$

as expected since correlation lower the total energy. We can also use 3.31 to separate the correlation energy into a kinetic and a potential part in the following way

$$\begin{aligned} E_c[n] &= E_c^{\text{kin}}[n] + E_c^{\text{pot}}[n] \\ &= \underbrace{\left\langle \Psi_n^{\min} \middle| \hat{T} \middle| \Psi_n^{\min} \right\rangle - \left\langle \Phi_n^{\min} \middle| \hat{T} \middle| \Phi_n^{\min} \right\rangle}_{E_c^{\text{kin}}[n]>0} + \underbrace{\left\langle \Psi_n^{\min} \middle| \hat{V}_{ee} \middle| \Psi_n^{\min} \right\rangle - \left\langle \Phi_n^{\min} \middle| \hat{V}_{ee} \middle| \Phi_n^{\min} \right\rangle}_{E_c^{\text{pot}}[n]<0}. \end{aligned} \tag{3.33}$$

From what was said above, the kinetic contribution must be a positive contribution, while the potential contribution will a negative quantity.

We can also investigate what will happen to the exchange and correlation energy in the limit of only one electron, that is $N = 1$. Since in the one-electron limit, there is no electron-electron interaction, $\hat{V}_{ee} = 0$, we have from Eq. 3.30

$$E_x[n] = -U[n] \qquad (N = 1), \tag{3.34}$$

and from 3.31

$$E_c[n] = 0 \qquad (N = 1). \tag{3.35}$$

The exchange energy exactly cancels the unphysical self-interaction present in the Hartree energy, and the correlation-energy exactly vanishes. Thus, starting from the exact definition of $E_x[n]$ and $E_c[n]$, the Kohn-Sham equations will lead to a proper description also in the one-electron limit, a property that will get lost to some extent once approximations to $E_{xc}[n]$ are undertaken.

3.5.2 Coupling Constant Integration

We have seen in Sec. 3.4 that the Kohn-Sham scheme considers an auxiliary system in which the electrons are assumed to be non-interacting but which is constructed in such a way that it leads to the same ground state electron density as the physical system of interacting electrons. We will now consider a smooth, an *adiabatic*, connection between the non-interacting and the interacting system. To this end, we consider an N-electron Hamiltonian in which we scale the electron-electron interaction with the *coupling constant* λ

$$\hat{H}_\lambda = \hat{T} + \lambda \cdot \hat{V}_{ee} + \hat{V}_{\text{ext},\lambda} \qquad \text{where} \qquad \lambda \in [0, 1]. \tag{3.36}$$

It is important to note that for each value of λ, the external potential is adjusted in such a way that the resulting ground state density is identical to the ground state density of the fully interacting system. Thus, for $\lambda = 1$, the external potential is only due to the atomic nuclei while for $\lambda = 0$, the external potential $\hat{V}_{\text{ext},\lambda=0}$ equals the Kohn-Sham potential. In complete analogy to the definition of the universal functional $F[n]$ in Eq. 3.12, we now define a functional $F_\lambda[n]$ for each value of λ in the following way

$$F_\lambda[n] = \min_{\Psi_\lambda \to n} \left\langle \Psi_\lambda \middle| \hat{T} + \lambda \cdot \hat{V}_{ee} \middle| \Psi_\lambda \right\rangle \equiv \left\langle \Psi_n^{\min,\lambda} \middle| \hat{T} + \lambda \cdot \hat{V}_{ee} \middle| \Psi_n^{\min,\lambda} \right\rangle. \tag{3.37}$$

Here we have introduced the short-hand notation $\Psi_n^{\min,\lambda}$ for the wave function which minimizes $\hat{T} + \lambda \cdot \hat{V}_{ee}$ and yields the density n. Once again, the density n is kept constant over the entire adiabatic connection by adjusting the external potential.

We will now make use of this adiabatic connection in order to rewrite the exchange-correlation functional in a form that is better suited for deriving approximations and also allows an easier physical

interpretation. We start with the expression 3.31 for the correlation energy and combine it with the definition of the exchange energy 3.30 to arrive at

$$\begin{aligned} E_{xc}[n] &= \left\langle \Psi_n^{\min} \middle| \hat{T} + \hat{V}_{ee} \middle| \Psi_n^{\min} \right\rangle - \left\langle \Phi_n^{\min} \middle| \hat{T} + 0 \cdot \hat{V}_{ee} \middle| \Phi_n^{\min} \right\rangle - U[n] \\ &= \left\langle \Psi_n^{\min,\lambda} \middle| \hat{T} + \lambda \hat{V}_{ee} \middle| \Psi_n^{\min,\lambda} \right\rangle \Big|_{\lambda=1} - \left\langle \Psi_n^{\min,\lambda} \middle| \hat{T} + \lambda \hat{V}_{ee} \middle| \Psi_n^{\min,\lambda} \right\rangle \Big|_{\lambda=0} - U[n] \\ &= \int_0^1 \mathrm{d}\lambda \frac{\mathrm{d}}{\mathrm{d}\lambda} \left\langle \Psi_n^{\min,\lambda} \middle| \hat{T} + \lambda \hat{V}_{ee} \middle| \Psi_n^{\min,\lambda} \right\rangle - U[n]. \end{aligned} \tag{3.38}$$

We can simplify this expression further by recalling the Hellmann-Feynman theorem, Eq. 1.14, for expectation values of a Hamiltonian which depend on a parameter. Thus, we have

$$E_{xc}[n] = \int_0^1 \mathrm{d}\lambda \left\langle \Psi_n^{\min,\lambda} \middle| \hat{V}_{ee} \middle| \Psi_n^{\min,\lambda} \right\rangle - U[n]. \tag{3.39}$$

This is the adiabatic connection formula for the exchange-correlation functional which involves an integration over the coupling constant.

We will now evaluate the matrix element of the electron-electron interaction $\langle \hat{V}_{ee} \rangle$ further. Similar to the derivation of Eq. 3.4 for the *local* external potential which led us to the appearance of the electron density $n(\boldsymbol{r})$, the evaluation of the matrix element for the non-local, two-point operator $\hat{V}_{ee}$, will lead us to the two-electron density matrix $\rho_2(\boldsymbol{r}', \boldsymbol{r})$ which is defined in the following way [1]

$$\rho_2(\boldsymbol{r}', \boldsymbol{r}) = N(N-1) \sum_{\sigma_1 \cdots \sigma_N} \int \mathrm{d}^3 r_3 \cdots \mathrm{d}^3 r_N \left| \Psi(\boldsymbol{r}'\sigma_1, \boldsymbol{r}\sigma_2, \boldsymbol{r}_3\sigma_3, \cdots, \boldsymbol{r}_N\sigma_N) \right|^2. \tag{3.40}$$

What is the interpretation of this quantity? Remember that $n_\sigma(\boldsymbol{r})\mathrm{d}^3 r$ is the average number of electrons of spin σ in volume element $\mathrm{d}^3 r$. Similarly, we interpret $\rho_2(\boldsymbol{r}', \boldsymbol{r})\mathrm{d}^3 r' \mathrm{d}^3 r$ as the joint probability of finding an electron in volume element $\mathrm{d}^3 r'$ at $\boldsymbol{r}'$, *and* an electron in $\mathrm{d}^3 r$ at $\boldsymbol{r}$. We now evaluate

$$\begin{aligned} \left\langle \Psi \middle| \hat{V}_{ee} \middle| \Psi \right\rangle &= \left\langle \Psi \middle| \frac{1}{2} \sum_{i,j \neq i} \frac{1}{|\boldsymbol{r}_i - \boldsymbol{r}_j|} \middle| \Psi \right\rangle \\ &= \sum_{\sigma_1 \cdots \sigma_N} \int \mathrm{d}^3 r_1 \cdots \int \mathrm{d}^3 r_N \left| \Psi(\sigma_1 \boldsymbol{r}_1, \cdots, \sigma_i \boldsymbol{r}_i, \cdots, \sigma_j \boldsymbol{r}_j, \cdots, \sigma_N \boldsymbol{r}_N) \right|^2 \frac{1}{2} \sum_{i,j \neq i} \frac{1}{|\boldsymbol{r}_i - \boldsymbol{r}_j|} \\ &= \frac{1}{2} N(N-1) \int \mathrm{d}^3 r \int \mathrm{d}^3 r' \frac{1}{|\boldsymbol{r} - \boldsymbol{r}'|} \sum_{\sigma_1 \cdots \sigma_N} \int \mathrm{d}^3 r_3 \cdots \mathrm{d}^3 r_N \left| \Psi(\boldsymbol{r}'\sigma_1, \boldsymbol{r}\sigma_2, \boldsymbol{r}_3\sigma_3, \cdots, \boldsymbol{r}_N\sigma_N) \right|^2 \\ &= \frac{1}{2} \int \mathrm{d}^3 r \int \mathrm{d}^3 r' \frac{\rho_2(\boldsymbol{r}', \boldsymbol{r})}{|\boldsymbol{r} - \boldsymbol{r}'|}. \end{aligned} \tag{3.41}$$

We now use this result in the expression in the adiabatic connection formula for the exchange-

correlation functional 3.39, where we introduce the *coupling-constant averaged* density matrix

$$\overline{\rho}_2(\boldsymbol{r}', \boldsymbol{r}) = \int_0^1 \mathrm{d}\lambda\, \rho_2^\lambda(\boldsymbol{r}', \boldsymbol{r}), \tag{3.42}$$

and obtain

$$\begin{aligned} E_{xc}[n] &= \frac{1}{2}\int \mathrm{d}^3 r \int \mathrm{d}^3 r' \frac{\overline{\rho}_2(\boldsymbol{r}', \boldsymbol{r}) - n(\boldsymbol{r})n(\boldsymbol{r}')}{|\boldsymbol{r} - \boldsymbol{r}'|} \\ &= \frac{1}{2}\int \mathrm{d}^3 r \int \mathrm{d}^3 r' \frac{n(\boldsymbol{r})\overline{n}_{xc}(\boldsymbol{r}, \boldsymbol{r}')}{|\boldsymbol{r} - \boldsymbol{r}'|}. \end{aligned} \tag{3.43}$$

In the last step, we have brought in the coupling-constant-averaged *exchange-correlation hole* defined as

$$\overline{n}_{xc}(\boldsymbol{r}, \boldsymbol{r}') = \frac{\overline{\rho}_2(\boldsymbol{r}', \boldsymbol{r})}{n(\boldsymbol{r})} - n(\boldsymbol{r}'). \tag{3.44}$$

The exchange-correlation hole $\overline{n}_{xc}(\boldsymbol{r}, \boldsymbol{r}')$ describes the effect of the interelectronic repulsions, i.e., the fact that an electron present at point $\boldsymbol{r}$ reduces the probability of finding one at $\boldsymbol{r}'$. Eq. 3.43 demonstrates that the exchange-correlation energy is then the electrostatic interaction energy between each electron and the coupling-constant-averaged hole which surrounds it. The exchange-correlation hole is created by three effects [1]. (i) Self-interaction correction, which guarantees that an electron cannot interact with itself and therefore cancels the self-interaction present in the Hartree energy. (ii) The Pauli exclusion principle, which tends to keep two electrons with parallel spins apart in space. (iii) Coulomb repulsion, which tends to keep any two electrons apart in space. Effects (i) and (ii) are responsible for the exchange energy, which is present even at $\lambda = 0$, while effect (iii) is responsible for the correlation energy, and arises only for $\lambda \neq 0$. One can show [1] that the exchange-correlation hole, respectively the exchange hole $n_x(\boldsymbol{r}, \boldsymbol{r}')$ and the correlation hole $n_c^\lambda(\boldsymbol{r}, \boldsymbol{r}')$, satisfy the following *sum rules*:

$$\int \mathrm{d}^3 r'\, n_{xc}^\lambda(\boldsymbol{r}, \boldsymbol{r}') = -1, \qquad \int \mathrm{d}^3 r'\, n_x(\boldsymbol{r}, \boldsymbol{r}') = -1, \qquad \int \mathrm{d}^3 r'\, n_c^\lambda(\boldsymbol{r}, \boldsymbol{r}') = 0. \tag{3.45}$$

The first of the above sum rules says that, if an electron is definitely at $\boldsymbol{r}$, then it is missing from the rest of the system. The same sum rule also applies to the exchange-hole alone which means that Coulomb repulsion changes the shape of the hole but not its integral. It can be shown that Coulomb correlations make the hole deeper but more short-ranged.

Before we conclude this section, we mention one more important consequence of Eq. 3.43. Because the Coulomb interaction $\frac{1}{|\boldsymbol{r}-\boldsymbol{r}'|}$ is isotropic in space, the exchange-correlation energy only depends on

the *spherical average* of the exchange-correlation hole around $\boldsymbol{r}$

$$E_{xc}[n] = \frac{1}{2}\int \mathrm{d}^3 r\, n(\boldsymbol{r}) \int_0^\infty \mathrm{d}u\, u \int \mathrm{d}\Omega_{\boldsymbol{u}} \overline{n}_{xc}(\boldsymbol{r}, \boldsymbol{r}+\boldsymbol{u}) = \frac{1}{2}\int \mathrm{d}^3 r\, n(\boldsymbol{r}) \int_0^\infty \mathrm{d}u\, u\, \overline{n}_{xc}(\boldsymbol{r}, u), \tag{3.46}$$

where we have introduced the $\boldsymbol{u} = \boldsymbol{r}' - \boldsymbol{r}$. This means that approximations for $E_{xc}[n]$ can give an exact value even if the description of the nonspherical parts of the exchange-correlation hole is quite inaccurate. This is illustrated for the exchange hole in a nitrogen atom in Fig. 3.1. For a discussion and illustration of the exchange-hole (also called Fermi-hole), the correlation hole (also called Coulomb hole) in the H_2 molecule at various values of the internuclear distance see Ref. [31].

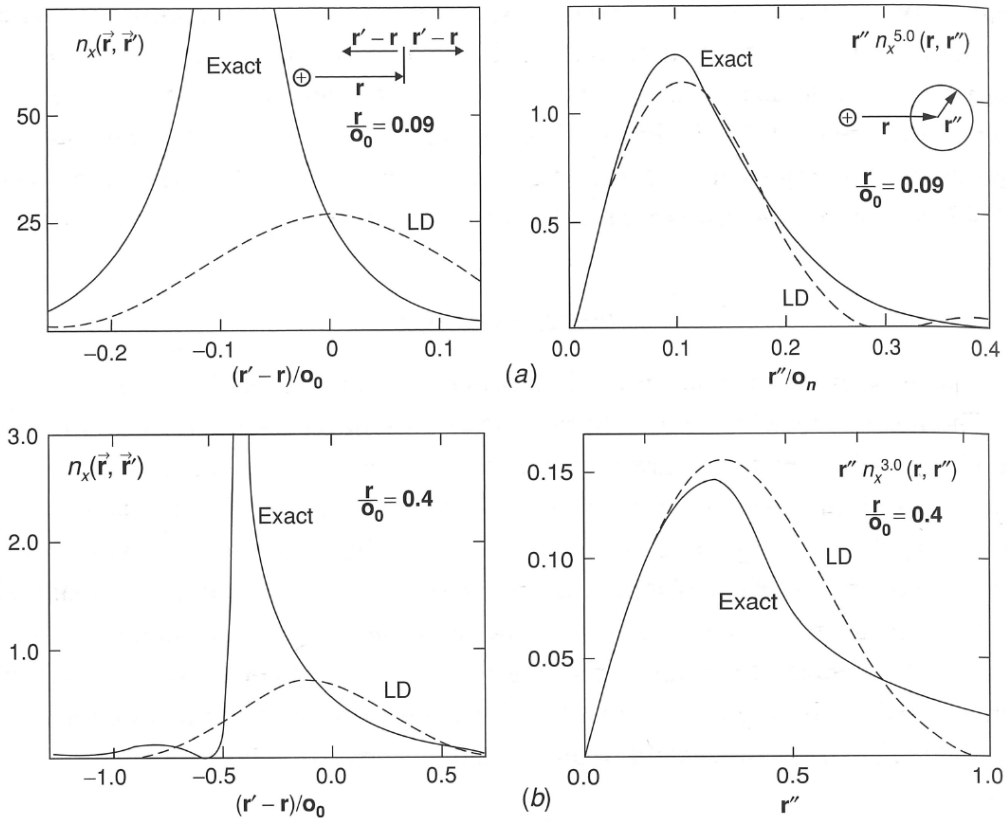

Figure 3.1: Reproduced from [7, 8]: Exchange hole in a Ne atom. Left: $n_x(\boldsymbol{r}, \boldsymbol{r}')$ plotted for two values of $|\boldsymbol{r}|$ as a function of $|\boldsymbol{u}| = |\boldsymbol{r}' - \boldsymbol{r}|$ along a line through the nucleus. Right: The spherically averaged exchange hole as a function of the relative distance $|\boldsymbol{u}|$. Exact results (solid lines) are compared to the local density approximation (dashed lines).

3.5.3 Local Density Approximation

While the expressions for $E_{xc}[n]$ derived in the previous section, 3.43 or 3.46, are important to gain fundamental insights, in practice approximations have to be made. The most simple and still widely used approximation is the local density approximation (LDA), or indeed the local spin density approximation (LSDA). It has already been proposed in the original work by Kohn and Sham [5]

$$E_{xc}^{\mathrm{LDA}}[n] = \int \mathrm{d}^3r\, n(\boldsymbol{r}) e_{xc}^{\mathrm{unif}}\left(n(\boldsymbol{r})\right) \tag{3.47}$$

$$E_{xc}^{\mathrm{LSDA}}[n_\uparrow, n_\downarrow] = \int \mathrm{d}^3r\, n(\boldsymbol{r}) e_{xc}^{\mathrm{unif}}\left(n_\uparrow(\boldsymbol{r}), n_\downarrow(\boldsymbol{r})\right). \tag{3.48}$$

Here $n(\boldsymbol{r})$ and $n_\uparrow(\boldsymbol{r}), n_\downarrow(\boldsymbol{r})$ are the density and spin densities of the inhomogeneous system, and e_{xc}^{unif} is the exchange-correlation energy per particle of a uniform electron gas of charge density n. Thus, the local (spin) density approximation means that the total exchange-correlation energy of some density distribution $n(\boldsymbol{r})$ is the sum of local contributions of an electron gas with density $n(\boldsymbol{r})$ at $\boldsymbol{r}$ assumed to have the same exchange-correlation energy as the uniform electron gas of the same density.

The exchange and correlation energy of the uniform electron gas, for the non spin-polarized case with $n_\uparrow = n_\downarrow = \frac{1}{2}n$ has already been discussed in Sec. 2.3. Combining Eqs. 2.59 for the exchange and 2.66 for the correlation contribution, we have[2]

$$e_{xc}^{\mathrm{unif}}(r_s) = -\frac{3}{4\pi}\frac{(9\pi/4)^{\frac{1}{3}}}{r_s} - 2c_0(1+\alpha_1 r_s)\ln\left[1 + \frac{1}{2c_0\left(\beta_1 r_s^{1/2} + \beta_2 r_s + \beta_3 r_s^{3/2} + \beta_4 r_s^2\right)}\right], \tag{3.49}$$

while for the spin-polarized case characterized by the spin polarization ζ

$$\zeta = \frac{n_\uparrow - n_\downarrow}{n_\uparrow + n_\downarrow}, \tag{3.50}$$

generalized expressions for $e_{xc}^{\mathrm{unif}}(r_s, \zeta)$ have been summarized by Perdew and Wang [25].

In order to perform self-consistent Kohn-Sham calculations, one has to compute the exchange-correlation potential by performing the functional derivative of 3.48 with respect to the density

$$v_{xc,\sigma}^{\mathrm{LSDA}}(\boldsymbol{r}) = \frac{\delta E_{xc}^{\mathrm{LSDA}}[n_\uparrow, n_\downarrow]}{\delta n_\sigma(\boldsymbol{r})} = \frac{\partial}{\partial n_\sigma}\left[(n_\uparrow + n_\downarrow) e_{xc}^{\mathrm{unif}}(n_\uparrow, n_\downarrow)\right]. \tag{3.51}$$

[2]For an alternative derivation of the exchange energy of the uniform electron gas based on $E_x[n]$ in terms of the exchange-hole, the interested reader is referred to Ref. [1].

For instance, with $E_x^{\mathrm{LDA}}[n] = -\int \mathrm{d}^3r\, n(\boldsymbol{r})\frac{3}{4\pi}(3\pi^2 n)^{1/3}$ the exchange potential is given by

$$v_x^{\mathrm{LDA}}(\boldsymbol{r}) = \frac{\delta E_x^{\mathrm{LDA}}[n]}{\delta n(\boldsymbol{r})} = \frac{\partial}{\partial n}\left[\frac{3}{4\pi}(3\pi^2)^{\frac{1}{3}} n^{\frac{4}{3}}\right] = \frac{[3\pi^2 n(\boldsymbol{r})]^{\frac{1}{3}}}{\pi} = \frac{k_F(\boldsymbol{r})}{\pi}. \tag{3.52}$$

In a similar manner, the correlation potential can be obtained

$$v_c^{\mathrm{LDA}}(\boldsymbol{r}) = \frac{\delta E_c^{\mathrm{LDA}}[n]}{\delta n(\boldsymbol{r})} = \frac{\partial}{\partial n}[n \cdot e_c(n)] = e_c(n(\boldsymbol{r})) + n\frac{\partial e_c(n)}{\partial n}. \tag{3.53}$$

As an example of how the local Fermi wave vector $k_F(\boldsymbol{r})$ or the local Wigner-Seitz radius $r_s(\boldsymbol{r})$ looks like, in Fig. 3.2 we show results of a self-consistent DFT calculation for the H_2 molecule and bulk Na in the bcc structure. In the case of the H_2 molecule, k_F and r_s is depicted in the xy-plane containing the H_2 bond. The two local maxima in $k_F(x, y, z = z_0)$ correspond to the positions of the two hydrogen atoms. For bcc-Na, we plot k_F and r_s for a plane which is parallel to the basal plane of the cube and goes through the Na atom in the body-centred position. Here, the shell-structure of the inner two shells (1s and 2s/2p) becomes visible. In the interstitial region between the atoms (corners of the plot region), fairly constant values for k_F and r_s, respectively, are found indicating the free-electron like behaviour of the 3s valence electron.

Regardless of the fact that the L(S)DA neglects any dependence on the gradient of the density, it has proved to be remarkably accurate, useful, and hard to improve upon. Ref [1] lists a number of reasons for this success of which we here mention the most important ones: By construction, the LDA is exact for a uniform density and nearly-exact for slowly varying densities, features that make LDA well suited to the description of simple metals (such as Na). It satisfies $E_x < 0$ and $E_c < 0$ and the so-called coordinate-scaling relations, and it has the correct low-density behavior for E_c [1]. Moreover, the LDA approximation to the exchange and correlation holes obey the correct sum rules although the shape of the hole may be in error (see also Fig. 3.1).

However, there is certainly room for improvement because there are also a number of deficiencies of the LDA. (i) Obviously, the LDA does not incorporate inhomogeneity or gradient corrections to the exchange-correlation hole near the electron. (ii) It does not obey the correct coordinate-scaling relation of $E_c[n]$ at high densities ($r_s \to 0$), because the uniform electron gas shows a $\ln r_s$ divergence. Among others, (iii) the LDA is also not exact in the one-electron limit, thus the correlation does not vanish and the exchange does not compensate for the self-interaction. The so-called generalized gradient approximation (GGA), to be derived in the next Section 3.5.4, will preserve all the good properties of the LDA and eliminate the bad features (i) and (ii) listed above.

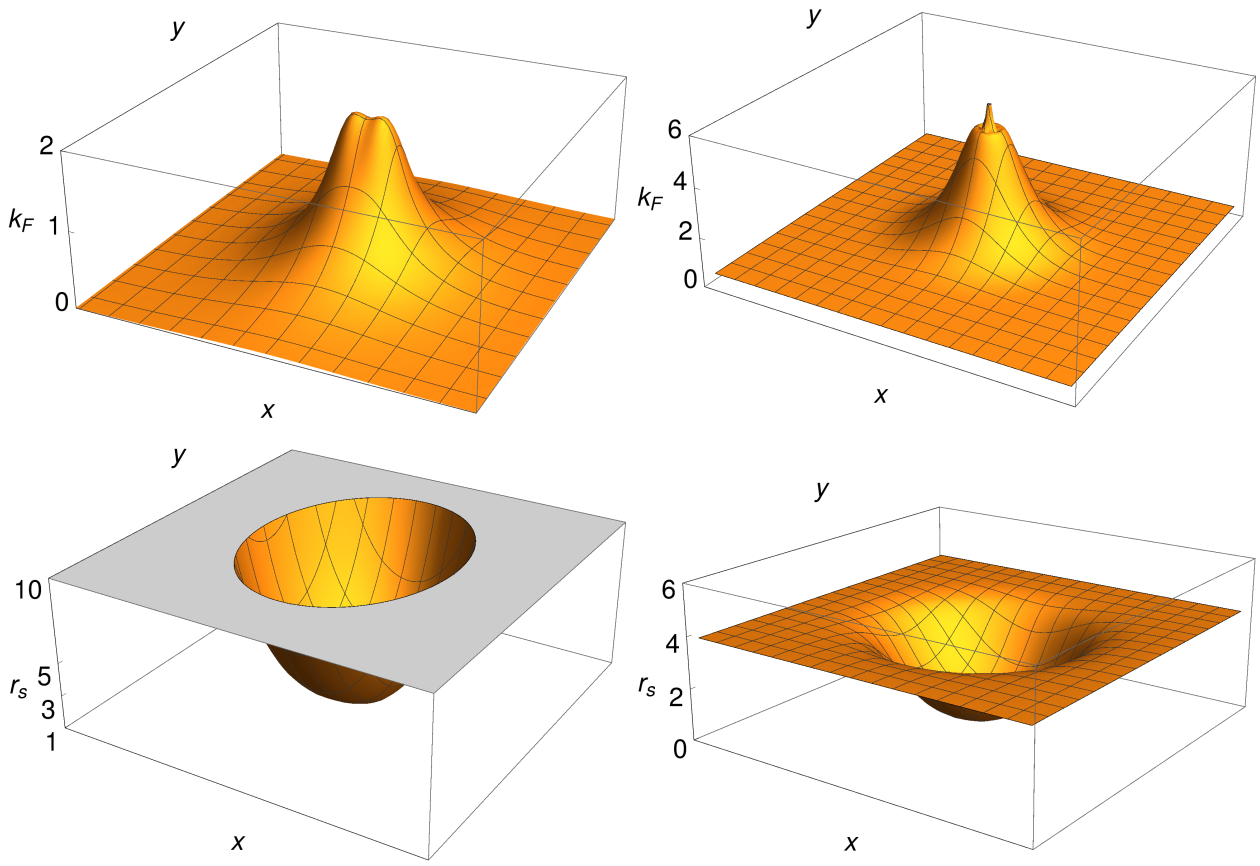

Figure 3.2: The Fermi wave vector $k_F(x, y, z = z_0)$ (top) and the Wigner-Seitz radius $r_s(x, y, z = z_0)$ (bottom) for the H_2 molecule (left) and bulk Na (right). A planar cut through the H–H bond and through the central Na atom of the bcc-unit cell is shown, respectively.

3.5.4 Generalized Gradient Approximation

The basic idea of gradient corrections to $E_{xc}[n]$ is to introduce a dependence on the gradient of the density $\nabla n(\boldsymbol{r})$. Instead of using the density gradient $\nabla n(\boldsymbol{r})$ directly as a measure for density inhomogeneity, one defines the dimensionless quantity s, the *reduced density gradient*, which is a measure for the relative change of the density on the scale of the Fermi wave length $\lambda_F = \frac{2\pi}{k_F}$

$$s = \left| \frac{1}{4\pi} \frac{\partial n}{\partial \left(\frac{\boldsymbol{r}}{\lambda_F}\right)} \Big/ n \right| = \frac{|\nabla n|}{2k_F n} = \cdots = \frac{3}{2}\left(\frac{4}{9\pi}\right)^{1/3} |\nabla r_s|. \tag{3.54}$$

In the last step of the above equation, we have expressed the reduced density gradient in terms of a gradient of the Wigner-Seitz parameter r_s. When calculated for real systems, that is atoms, molecules or solids, the most important range of s is $0 \leq s \leq 1$, the range $1 \leq s \leq 3$ is already less prominent,

while $s > 3$ only applies to the exponential tail of the density is therefore unimportant with respect to the total energy of the system. In order to illustrate how this reduced density gradient appears in a real system, in Fig. 3.3 we show the gradient $s(\boldsymbol{r})$ for the two same systems as above, namely the hydrogen molecule and bulk Na, respectively. As noted above, for a bulk system such as Na, s does not increase above 2 or so, and clearly approaches zero in the interstitial region with almost constant electron density. For a finite system, such as the H_2 molecule, the s attains large values in the density tail. But because for total energy considerations these regions are weighted by the electron density, such regions of large s (cut-off in the figure) do not contribute significantly.

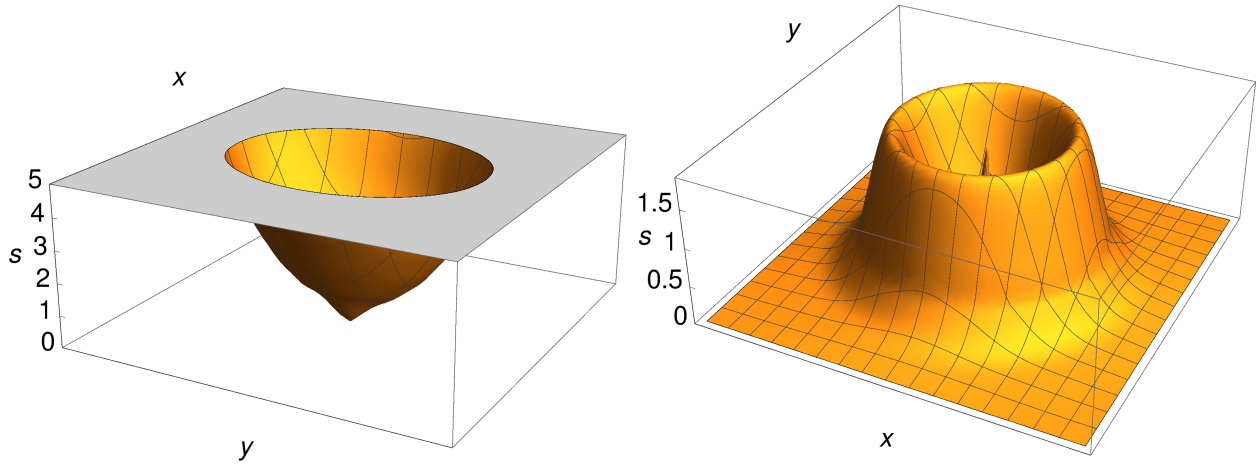

Figure 3.3: The reduced density gradient parameter $s(x, y, z = z_0)$ as defined in Eq. 3.54 for the H_2 molecule (left) and bulk Na (right). A planar cut through the H–H bond and through the central Na atom of the bcc-unit cell is shown, respectively.

Apart from the length scale k_F which introduces a length scale on which density variations are measured and which is relevant for the exchange-hole, Thomas-Fermi screening, characterized by the Thomas-Fermi wave vector k_s, introduces a second length scale which is in fact the important length scale for the correlation hole. For instance, the potential ϕ of a point charge inside an electron gas with a Fermi wave vector k_F can be shown to be screened as

$$\phi(r) = \frac{e^{-k_s r}}{r} \qquad \text{with} \qquad k_s = \left(\frac{4k_F}{\pi a_0}\right)^{\frac{1}{2}} = \cdots = \left(\frac{4}{\pi}\right)^{\frac{1}{2}} \left(\frac{9\pi}{4}\right)^{\frac{1}{6}} \frac{1}{r_s^{1/2}}. \tag{3.55}$$

In the first expression for k_s, we have re-introduced the Bohr radius a_0, which is actually 1 in atomic units, to better illustrate that k_s indeed is an inverse length. Using k_s in place of k_F, we can define a

second reduced gradient in an analogous way as above which is commonly denoted as t:

$$t = \left| \frac{1}{4\pi} \frac{\partial n}{\partial \left(\frac{\boldsymbol{r}}{\lambda_s}\right)} \Big/ n \right| = \frac{|\nabla n|}{2k_s n} = \cdots = \left(\frac{\pi}{4}\right)^{\frac{1}{2}} \left(\frac{9\pi}{4}\right)^{\frac{1}{6}} \frac{s}{r_s^{1/2}}. \tag{3.56}$$

Naively, one could use the reduced gradients s and t to construct a Taylor-like expansion of the exchange and correlation energies, respectively. However, such an approach, termed gradient expansion approximation (GEA), turns out to be not successful and in fact worsens numerical results compared to the LDA as is explained in more detail in Ref. [1]. The reason is that for actual systems, $s \ll 1$ and $t \ll 1$ is not fulfilled (compare Fig. 3.3), such high order terms of s and t would be required to reach a proper description, while taking into account only low-order terms in the expansion may lead to improperly positive correlation energies for atoms. As a remedy for this problem, the *generalized gradient approximation* (GGA) has been developed. While there is only one way to do a local density approximation (because there is only one uniform electron gas), there are numerous ways to devise a GGA. One strategy is to develop GGA's by fitting it to a test set of calculations. Another approach, the one that we briefly explain here, is to devise a GGA in a way as to fulfil as many as possible constraints of the exact exchange-correlation functional and at the same time maintain all the good properties of the LDA. In particular, we want to follow the work of Perdew, Burke, Ernzerhof entitled "Generalized Gradient Approximation Made Simple" [10] which has already been mentioned in Fig. 1.1 as the currently most cited paper in Physical Review Letters. Their exchange-correlation functional, commonly abbreviated as PBE-GGA or simply PBE, is probably the most-widely used one among physicists[3] and is defined as follows

$$E_x^{\mathrm{GGA}}[n] = \int \mathrm{d}^3r\, n\, e_x^{\mathrm{unif}}(n) F_x(s) \tag{3.57}$$

$$E_c^{\mathrm{GGA}}[n_\uparrow, n_\downarrow] = \int \mathrm{d}^3r\, n\, \left[e_c^{\mathrm{unif}}(n) + H(r_s, \zeta, t)\right] \tag{3.58}$$

$$E_{xc}^{\mathrm{GGA}}[n_\uparrow, n_\downarrow] = \int \mathrm{d}^3r\, n\, e_x^{\mathrm{unif}}(n) F_{xc}(r_s, \zeta, s). \tag{3.59}$$

Here, ζ is the spin polarization as defined in 3.50, and the quantities n, r_s, s, and t are assumed to be functions of $\boldsymbol{r}$. The functions $F_x(s)$, $H(r_s, \zeta, t)$ and $F_{xc}(r_s, \zeta, t)$ are drawn in Fig. 3.4 for the non-spinpolarized case of $\zeta = 0$. Without going into the details of the derivations that led Perdew, Burke and Ernzerhof to the form of these enhancement functions F_x, H, and F_{xc}, we briefly outline their reasoning which was driven by their credo of (1) a non-empirical derivation, (2) universality, (3) simplicity and (4) accuracy [10].

[3] DFT practitioners which are by training chemists tend to use functionals which have been developed by fitting to a test set of molecules.

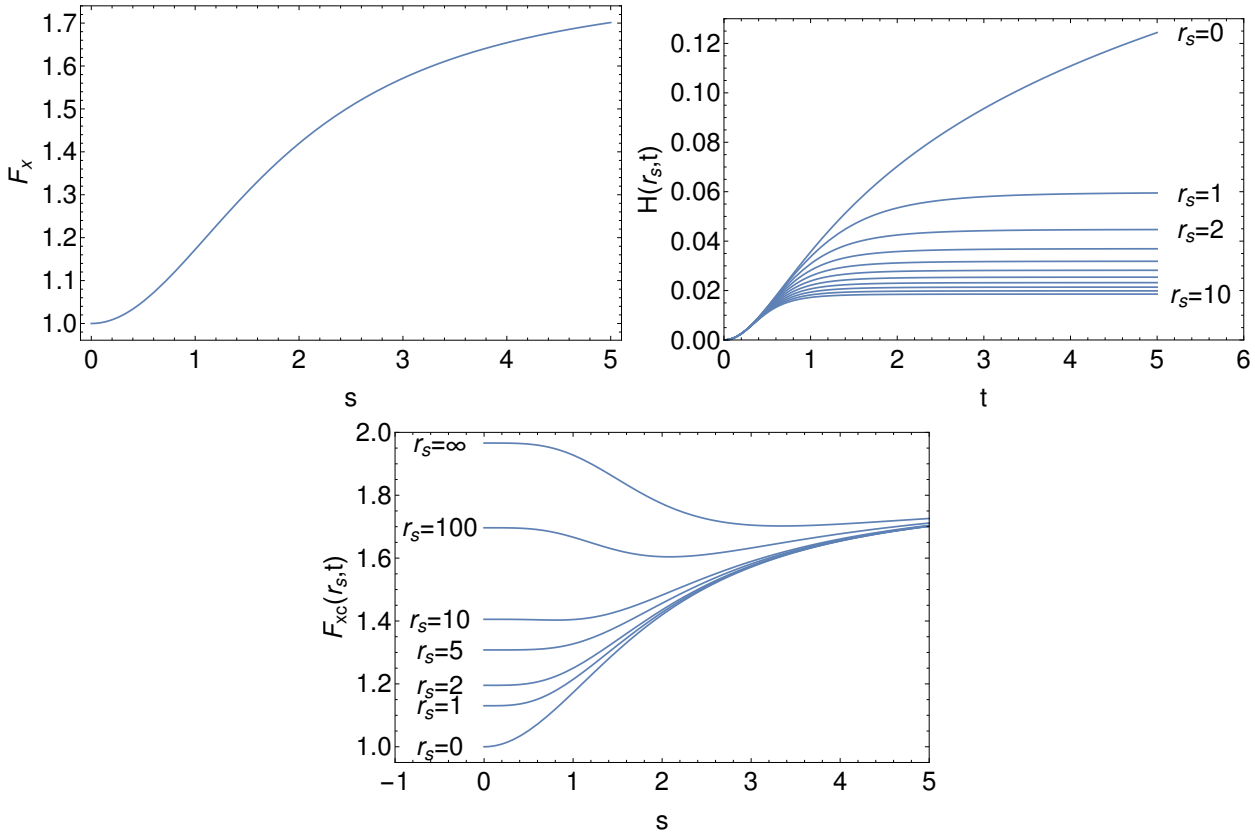

Figure 3.4: Enhancement factors $F_x(s)$, $H(r_s, \zeta, t)$ and $F_{xc}(r_s, \zeta, s)$ for $\zeta = 0$ for the GGA functionals defined in Eqs. 3.57–3.59 according to Perdew, Burke and Ernzerhof [10].

The enhancement function for the correlation energy, $H(r_s, t)$, should obey the following limits. In the slowly varying limit, $t \to 0$, it should behave as $H = \beta t^2$, where $\beta \approx 0.066725$ derived by Ma and Brückner [1]. In the rapidly varying limit, $t \to \infty$, correlations are expected to vanish since this is the only way the correct sum rule for the correlation hole can be satisfied, thus $H(r_s, t \to \infty) = -e_c^{\text{unif}}(r_s)$ to enable a cancellation of the terms in Eq. 3.58. Moreover, the uniform scaling relation for the exact correlation energy functional requires that $E_c[r_s \to 0]$ stays finite. Thus, the function $H(r_s \to 0, t)$ is constructed such that it cancels the logarithmic singularity of the correlation energy of the uniform electron gas mention in Sec. 2.3.4.

The enhancement factor for exchange, $F_x(s)$, is constructed from further exact requirements. The form of 3.57 as well as the correct uniform gas limit $s = 0$ is demanded by the exact scaling relations of the exchange energy and the requirement $F_x(0) = 1$. In the slowly varying limit, $s \to 0$, the function should behave as $F_x(s) = 1 + \mu s^2$. PBE makes the choice of $\mu = \frac{\pi^2}{3}\beta \approx 0.21951$ in order to cancel the corresponding t^2 expansion coefficient for the correlation part in order to retain the good linear response property of the LDA. Finally, the so-called Lieb-Oxford bound, and equality for the exact

exchange and correlation energy functionals, demands that $F_x(s) \leq 1.804$.

It should be noted that the Eq. 3.59 defining E_{xc} in terms of the exchange-correlation enhancement factor $F_{xc}(r_s, \zeta, s)$ is in fact redundant. E.g. for $\zeta = 0$, it is easy to verify that

$$F_{xc}(r_s, s) = F_x(s) + \frac{e_c^{\text{unif}}(r_s)}{e_x^{\text{unif}}(r_s)} + \frac{H(r_s, t)}{e_x^{\text{unif}}(r_s)}. \tag{3.60}$$

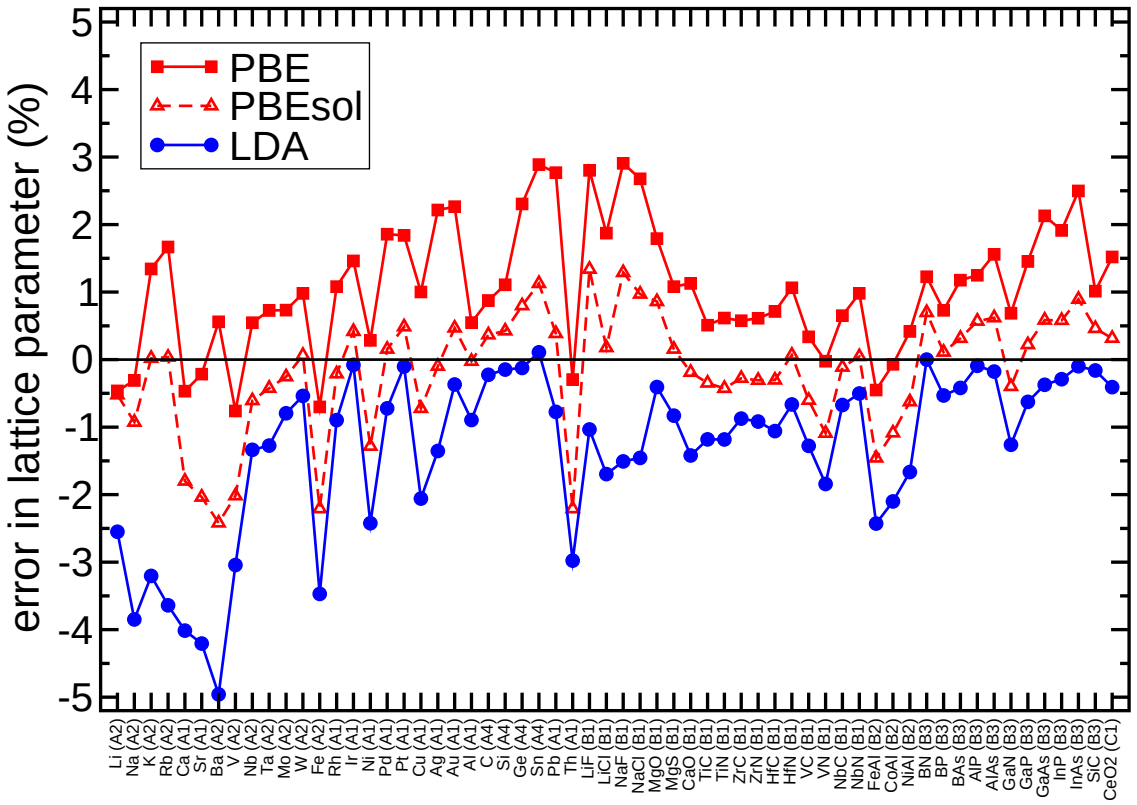

Figure 3.5: Relative error in the equilibrium lattice parameter as obtained within the LDA, the PBE-GGA [10] and the PBEsol-GGA [32] for 28 elemental and 32 binary bulk crystals. The data is reproduced from Ref. [33].

Before we conclude this section about the GGA, it may be interesting to see how it performs for typical solid state applications. In Figure 3.5 we have reproduced results from Ref. [33] and have plotted the relative error in the equilibrium lattice parameter for 28 elemental and 32 binary bulk crystals. For comparison, we also show the corresponding LDA results which consistently underestimate the lattice parameters of solids and typically also underestimate the bond lengths in molecules. In other words, LDA *overbinds*. Overall, the PBE-GGA presents an improvement over the LDA, however, in many

cases it overshoots and produces too large lattice parameters, respectively, bond lengths of molecules. Figure 3.5 also shows the results of another variant of the GGA, the so-called PBEsol [32], a slight modification of the original PBE presented above especially designed for solids.[4] In terms of the lattice parameters for the 60 bulk systems shown in Fig. 3.5, it clearly outperforms the PBE-GGA.

3.5.5 Jacob's Ladder

We have seen in the previous section how the GGA exchange-correlation functional can lead to an improvement of DFT results over conceptually simpler LDA results. As you may imagine, the GGA is not the end of the story, and even though the exact form of $E_{xc}[n]$ may remain unknown forever, there exists a hierarchy of more advanced approximations for the exchange-correlation functional.

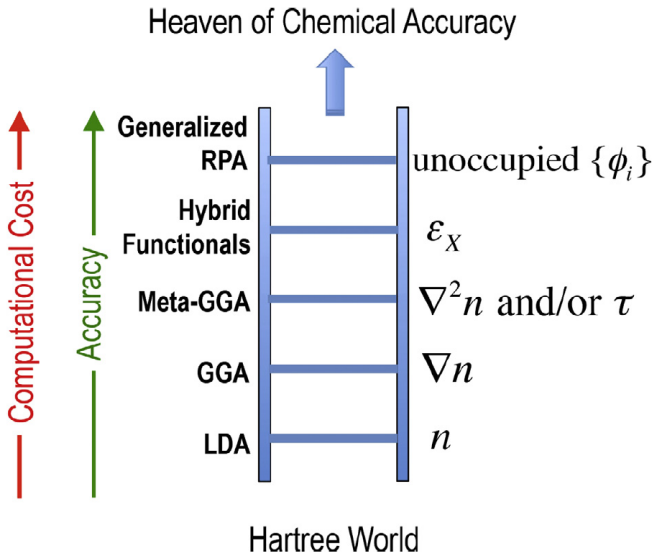

Figure 3.6: Reproduced from [34]: Jacob's ladder of density functional approximations to the exchange-correlation energy (as put forward by John P. Perdew [35]).

In her perspective article in Science entitled "In Pursuit of the "Divine" Functional" [36], Ann E. Mattsson describes a strategy for developing improved functionals commonly known as "Jacob's ladder" (see Fig. 3.6): *The first rung is the LDA, using only the electron density. The next rung holds the GGAs, where the gradient of the density adds refinement. The community is now [2002] working on the third rung, so-called meta-GGAs, where the kinetic energy density is introduced, thus the second derivative of the density. The fourth rung approaches the divine functional by treating exchange*

[4] In the PBEsol, the $s \to 0$ behaviour of $F_x(s)$ is determined by fixing $\mu = \frac{10}{81}$, thus using an exact value which has been derived for the slowly varying density. The value for $\beta \approx 0.046$ is guided by considerations for a jellium surface at the cost of violating the t^2 gradient expansion coefficient and, to a lesser extent, the exact cancellation of the exchange and correlation gradient corrections in the slowly varying limit [32].

exactly. For this to work, the exact exchange must be combined with a compatible correlation. The last rung retains the exact exchange and refines correlation by evaluating part of it exactly. The divine functional must have both exact exchange and exact correlation. The Jacob's ladder scheme, advanced by Perdew and co-workers, is the traditional strategy in the physics community and is an extension of the strategy that led to the GGAs. The philosophy is to keep everything that works in old functionals while adding capability. The strategy can be viewed as a ladder with five rungs, leading up to the divine functional, the ultimate goal in functional development. In the previous two Sections 3.5.3 and 3.5.4 we have already discussed the first two rungs, here we briefly describe the rungs three, four and five.

Third Rung: Meta-GGA

While the first and second rung of the ladder involve the density and its gradient, respectively, the third rung also includes the kinetic energy density which is related to the *second derivative* of the density. In its most general form, any so-called meta-GGA can be written in the following way [37]

$$E_{xc}[n_\uparrow, n_\downarrow] = \int \mathrm{d}^3r\, n\, e_{xc}(n_\uparrow, n_\downarrow, \nabla n_\uparrow, \nabla n_\downarrow, \tau_\uparrow, \tau_\downarrow), \tag{3.61}$$

where $n(\boldsymbol{r}) = n_\uparrow(\boldsymbol{r}) + n_\downarrow(\boldsymbol{r})$ is the total density, and

$$\tau_\sigma = \sum_i^{\text{occup}} \frac{1}{2}|\nabla\varphi_{i\sigma}(\boldsymbol{r})|^2 \tag{3.62}$$

is the kinetic energy density for the occupied Kohn-Sham orbitals $\varphi_{i\sigma}(\boldsymbol{r})$, which are nonlocal functionals of the density $n_\sigma(\boldsymbol{r})$. There are various strategies to define the form of the function e_{xc} inside the integral. Here, we only mention a recently developed functional of the meta-GGA type, the "strongly constrained and appropriately normed" (SCAN) meta-GGA which has been constructed based on all 17 known exact constraints appropriate for a semilocal functional, and a set of "appropriate norms" for which a semilocal function can be exact or nearly exact [38]. A benchmark test of this functional is summarized in Table 3.5.5. It suggests that SCAN is a major improvement over PBE (and much more so over LSDA), at nearly the same computational cost [38].

Fourth Rung: Hybrid Functionals

In Sec. 3.5.1, we have defined the exchange energy in Eq. 3.30 as

$$E_x[n] = \left\langle \Phi_n^{\min} \middle| \hat{V}_{ee} \middle| \Phi_n^{\min} \right\rangle - U[n], \tag{3.63}$$

Table 3.1: Reproduced from [38]: Mean error (ME) and mean absolute error (MAE) of SCAN and other semilocal functionals for the G3 set of molecules, the BH76 set of chemical barrier heights, the S22 set of weakly bonded complexes, and the LC20 set of solid lattice constants. (1 kcal/mol = 0.0434 eV). Further details can be found in Ref. [38].

	G 3^{HC} (kcal/mol)		G3 (kcal/mol)		BH76 (kcal/mol)		S22 (kcal/mol)		LC20(Å)	
	ME	MAE	ME	MAE	ME	MAE	ME	MAE	ME	MAE
LSDA	−5.6	13.0	−83.7	83.7	−15.2	15.4	2.3	2.3	−0.081	0.081
BLYP	1.8	6.2	3.8	9.5	−7.9	7.9	−8.7	8.8		
PBEsol	−4.1	6.5	−58.7	58.8	−11.5	11.5	−1.3	1.8	−0.012	0.036
PBE	−2.1	6.6	−21.7	22.2	−9.1	9.2	−2.8	2.8	0.051	0.059
TPSS	1.9	3.8	−5.2	5.8	−8.6	8.7	−3.7	3.7	0.035	0.043
M06 L	−0.2	4.6	−1.6	5.2	−3.9	4.1	−0.9	0.9	0.015	0.069
SCAN	−0.8	2.7	−4.6	5.7	−7.7	7.7	−0.7	0.9	0.007	0.016

where $\Phi_n^{\min}$ is the Slater determinant constructed from all occupied Kohn-Sham orbitals, $\hat{V}_{ee}$ is the electron-electron interaction operator, and $U[n]$ is the Hartree energy. The idea of *hybrid functionals* is to incorporate some fraction of this exact exchange, as given by the above expression, into the exchange-correlation functional. It turns out that such hybrid functionals provide improved accuracy in the description of the atomization energies, bond lengths, and vibrational frequencies of most molecules.

To understand why it is more reasonable to add only some *fraction* of exact exchange rather than using 3.63 entirely, we start with the coupling-constant expression given in Eq. 3.39 which we rewrite in the following way [39]

$$E_{xc} = \int_0^1 \mathrm{d}\lambda\, E_{xc,\lambda} \qquad \text{with} \qquad E_{xc,\lambda} = \left\langle \Psi_n^{\min,\lambda} \middle| \hat{V}_{ee} \middle| \Psi_n^{\min,\lambda} \right\rangle - U[n]. \tag{3.64}$$

A simple two-point approximation to this integral over the coupling-constant would give

$$E_{xc} \approx \frac{1}{2}(E_{xc,\lambda=0} + E_{xc,\lambda=1}) = \frac{1}{2}(E_x + E_{xc,\lambda=1}), \tag{3.65}$$

where we have used the fact that in the non-interacting case ($\lambda = 0$), there is no correlation and the $E_{xc,\lambda=0}$ reduces to the exchange given by 3.63. Becke, Perdew and co-worker have now reasoned [39] that local or semilocal density functionals are more accurate at the fully-interacting case ($\lambda = 1$), where the exchange-correlation hole is deeper and thus more localized around its electron than at the non-interacting case ($\lambda = 0$). Therefore, the unknown $E_{xc,\lambda=1}$ may be approximated by some semi-local approximation (sl) which could be, for instance, the LDA or a GGA. This reasoning leads

to Becke's half-half hybrid functional

$$E_{xc} = \frac{1}{2}(E_x + E^{\mathrm{sl}}_{xc,\lambda=1}) = E^{\mathrm{sl}}_{xc} + \frac{1}{2}(E_x - E^{\mathrm{sl}}_x). \tag{3.66}$$

In the last step we have assumed that density functional approximation also has a coupling-constant decomposition for which we approximate the integrand by a straight line as above

$$E^{\mathrm{sl}}_{xc} = \int_0^1 \mathrm{d}\lambda\, E^{\mathrm{sl}}_{xc,\lambda} \approx \frac{1}{2}(E^{\mathrm{sl}}_x + E^{\mathrm{sl}}_{xc,\lambda=1}). \tag{3.67}$$

Now it has been argued that in many cases the linear λ-dependence of $E^{\mathrm{sl}}_{xc,\lambda=1}$ and $E_{xc,\lambda}$ close to $\lambda = 1$ is not the best approximation, rather a more rapid decay is realistic as described by the following function describing the λ-dependence of the hybrid functional [39]

$$E^{\mathrm{hyb}}_{xc,\lambda} = E^{\mathrm{sl}}_{xc,\lambda} + (E_x - E^{\mathrm{sl}}_x)(1-\lambda)^{m-1}, \tag{3.68}$$

where $m \geq 1$ is a number controlling the how rapidly the correction to the sl-approximation vanishes as λ approaches 1. When performing the integral over λ, we obtain the expression

$$E^{\mathrm{hyb}}_{xc} = \int_0^1 \mathrm{d}\lambda\, E^{\mathrm{hyb}}_{xc,\lambda} = E^{\mathrm{sl}}_{xc} + \frac{1}{m}(E_x - E^{\mathrm{sl}}_x). \tag{3.69}$$

We see that with $m = 2$ we recover the half-half expression 3.66, and with $m = 4$, the value put forward by Perdew and co-workers, we obtain the so-called PBE0 hybrid functional defined as

$$E^{\mathrm{PBE0}}_{xc} = E^{\mathrm{PBE}}_{xc} + \frac{1}{4}(E_x - E^{\mathrm{PBE}}_x) = \frac{3}{4}E^{\mathrm{PBE}}_x + \frac{1}{4}E_x + E^{\mathrm{PBE}}_c. \tag{3.70}$$

where we have also specified the semi-local approximation to be the PBE-GGA discussed previously. PBE0 presents a significant improvement over the GGA description of molecular properties but it has also been used for solid state applications [40]. This can be attributed to the fact that the use of a fixed portion of the Fock exchange reduces the self-interaction error of the density functional (the unphysical self-interaction built into the Hartree energy is at least partially compensated for).

Apart from the *global* hybrid functionals discussed above, another possibility of incorporating a fraction of exact exchange is to use so-called *range-separated* hybrid functionals where the description of the exchange interaction is separated into a short- and a long-range part. In its most general form, the decomposition of the Coulomb kernel can be obtained using the construction

$$\frac{1}{r} = S_\gamma(r) + L_\gamma(r) = \underbrace{\frac{1 - [\alpha + \beta\,\mathrm{erf}(\gamma\, r)]}{r}}_{\text{short range}} + \underbrace{\frac{\alpha + \beta\,\mathrm{erf}(\gamma\, r)}{r}}_{\text{long range}}, \tag{3.71}$$

where $r = |\boldsymbol{r} - \boldsymbol{r}'|$ and γ is the parameter that defines the range separation related to a characteristic distance $\frac{2}{\gamma}$ at which the short-range interactions become negligible. The functions $S_\gamma(r)$ and $L_\gamma(r)$, which sum to $\frac{1}{r}$, are introduced to enable different expressions for the exchange in the short-range and long-range, respectively. The error function, $\mathrm{erf}(x)$ enables a smooth switching between short- and long-range Coulomb expressions. The exchange-correlation energy is then calculated as follows:

$$E_{xc} = \underbrace{(1-\alpha)E_{x,\mathrm{sl}}^{\mathrm{SR}} + \alpha\, E_{x,\mathrm{HF}}^{\mathrm{SR}}}_{\text{short range}} + \underbrace{(1-\alpha-\beta)E_{x,\mathrm{sl}}^{\mathrm{LR}} + (\alpha+\beta)E_{x,\mathrm{HF}}^{\mathrm{LR}}}_{\text{long range}} + E_{c,\mathrm{sl}}. \tag{3.72}$$

We see that in the short range, the fraction of Hartree-Fock exchange is given by the parameter $\alpha \in [0,1]$, while the semi-local expression (typically the LDA or GGA) is weighted by $1-\alpha$. In the long range, on the other hand, a different weight of Hartree-Fock and semi-local exchange is allowed for by introducing the parameter β. Thus, here the weight of Hartree-Fock exchange is $\alpha+\beta$, while the semi-local exchange expression gets the weight $1-\alpha-\beta$. For the correlation part, $E_{c,\mathrm{sl}}$, a semi-local expression is used, both, in short and long-range. Any range-separated hybrid functional on the "market of DFT-functionals" can be expressed by the Eqs. 3.71 and 3.72 and are defined by specifying the three parameters α, β and γ as well as the particular semi-local expression to be used.

There are different strategies to determine the parameter values for α, β and γ. One possibility is to fit the parameters α, β and γ such that a given test set of systems (mostly molecular test systems) are described as accurately as possible compared to reference value obtained from wave-function based quantum chemical methods.[5] Another possibility is to tune the parameters α, β and γ in such a way that the resulting functional fulfils as many exact properties as possible. This leads to the so-called optimally-tuned range-separated hybrids (OT-RSH) [41–43]. Here, α and γ are determined by enforcing the so-called "ionization potential theorem" and the "piece-wise linearity" to be discussed in Secs. 3.6.1 and 3.6.2, respectively. Because, the third parameter β governs the asymptotic behaviour for $r \to \infty$, it is chosen as

$$\frac{\alpha + \beta\,\mathrm{erf}(\gamma\, r)}{r} \longrightarrow_{r\to\infty} \frac{\alpha+\beta}{r} \equiv \frac{1}{\epsilon\, r} \quad \Rightarrow \quad \alpha + \beta = \frac{1}{\epsilon}. \tag{3.73}$$

To guarantee the correct asymptotic behaviour of the exchange interaction, β should be chosen according to the dielectric constant of the medium, thus $\epsilon = 1$ for isolated molecules, or $\epsilon = \epsilon_{\mathrm{bulk}}$ for bulk crystals [42, 43].

[5] Wave-function-based post-Hartree Fock methods will be discussed in the lecture "Modelling of Molecular Systems".

Fifth Rung: Random Phase Approximation

While the fourth rung of Jacob's ladder was dealing with systematic improvements of the *exchange* energy, the fifth rung aims at improvements of the *correlation* energy over the semi-local expressions, LDA, GGA or meta-GGA, discussed previously. In terms of computational complexity, we will see that while the calculation of the Hartree-Fock exchange energy requires *occupied* Kohn-Sham orbitals, the fifth rung expressions for the correlation energy will also involve *unoccupied* Kohn-Sham orbitals to account for effects such as polarization.

The starting point for the correlation energy is the adiabatic connection formula 3.43 discussed earlier, which is rewritten with the help of the *fluctuation-dissipation* theorem, which allows one to express the density fluctuation $\langle \delta n(\boldsymbol{r}) \delta n(\boldsymbol{r}') \rangle$ in terms of a density-density response χ at imaginary frequency [44, 45]

$$\rho_2(\boldsymbol{r}', \boldsymbol{r}) \equiv \langle \delta n(\boldsymbol{r}) \delta n(\boldsymbol{r}') \rangle = -\frac{1}{\pi} \int_0^\infty \chi(\boldsymbol{r}, \boldsymbol{r}', \omega = iu) \mathrm{d}u. \tag{3.74}$$

Here χ is the density-density response function (susceptibility) defined as the linear density response $\delta n(\boldsymbol{r}) \exp(ut)$ of the electrons to an externally applied electron potential energy perturbation $\delta V_{\text{ext}} \exp(ut)$,

$$\delta n(\boldsymbol{r}) = \int \mathrm{d}^3 r' \, \chi(\boldsymbol{r}, \boldsymbol{r}', iu) \delta V_{\text{ext}}(\boldsymbol{r}'), \tag{3.75}$$

where u is defined to be an imaginary frequency $u = i\omega$. Combining the 3.74 with 3.43 leads to the *adiabatic-connection fluctuation-dissipation* (ACFD) formula for the correlation energy [45]

$$\begin{aligned} E_c &= -\frac{1}{2\pi} \int_0^1 \mathrm{d}\lambda \int \mathrm{d}^3 r \int \mathrm{d}^3 r' \frac{1}{|\boldsymbol{r} - \boldsymbol{r}'|} \int_0^\infty \mathrm{d}u \left[\chi^\lambda(\boldsymbol{r}, \boldsymbol{r}', iu) - \chi^0(\boldsymbol{r}, \boldsymbol{r}', iu) \right] \\ &= -\frac{1}{2\pi} \int_0^1 \mathrm{d}\lambda \int_0^\infty \mathrm{d}u \, \mathrm{Tr} \left[v \cdot (\chi^\lambda(iu) - \chi^0(iu)) \right]. \end{aligned} \tag{3.76}$$

Here, χ^λ and χ^0 are the response functions for the interacting system with coupling strength λ and for the non-interacting case $\lambda = 0$, respectively. In the second line of the above equation we have used a short-hand notation for the "matrix-matrix" multiplication of the Coulomb-interaction, $v(\boldsymbol{r}, \boldsymbol{r}') = \frac{1}{|\boldsymbol{r} - \boldsymbol{r}'|}$ with the response function and the subsequent "trace" of the matrix.

Without any further approximation the still exact expression 3.76 cannot be evaluated. The most common and simple approximation, which is tractable for real systems, is the so-called *random phase approximation* (RPA). Here, the exchange-correlation kernel

$$f_{xc}^\lambda(\boldsymbol{r}, \boldsymbol{r}') = \frac{\delta E_{xc}^\lambda}{\delta n(\boldsymbol{r}) \delta n(\boldsymbol{r}')}, \tag{3.77}$$

which connects the interacting with the non-interacting response function via the following Dyson-like

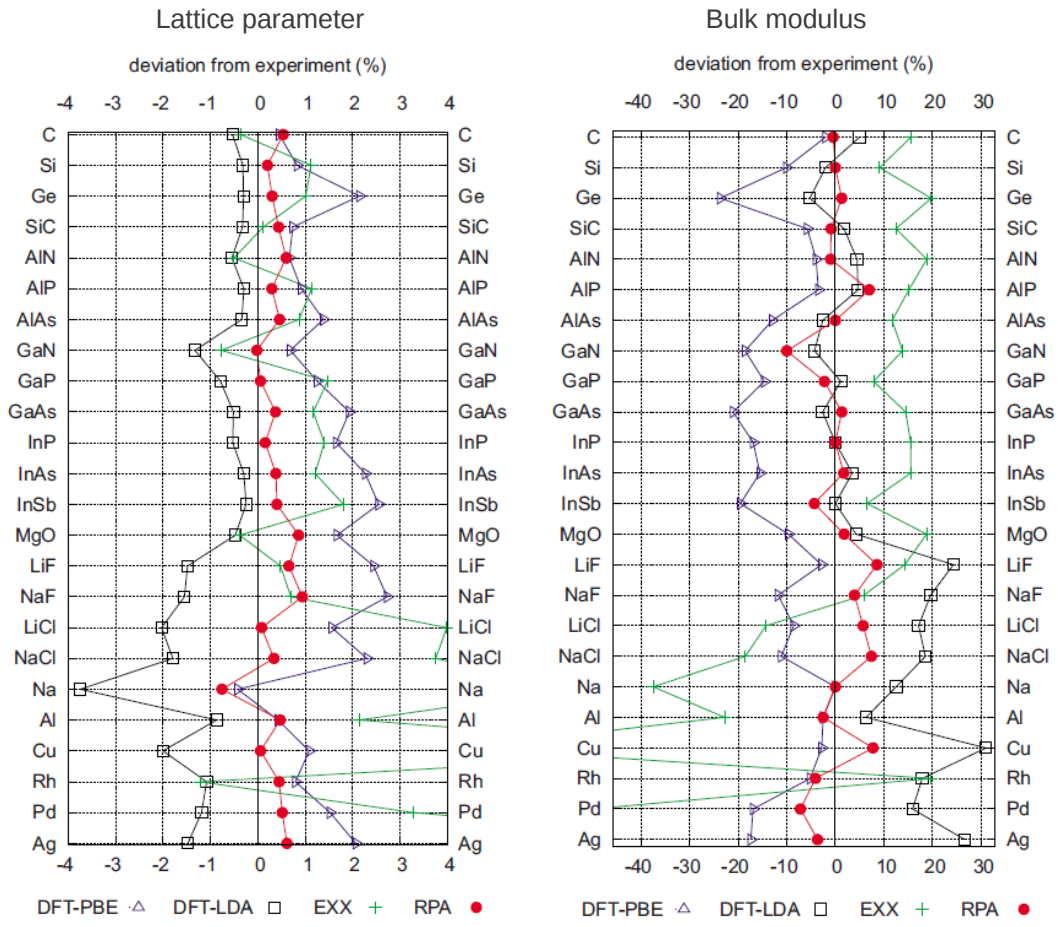

Figure 3.7: Reproduced from Ref. [46]: Relative error % of the theoretical lattice constants (left) and the theoretical bulk moduli (right) with respect to experiment.

equation

$$\left[\chi^{\lambda}\right]^{-1} = \left[\chi^{0}\right]^{-1} - \left[\lambda v + f_{xc}^{\lambda}\right] \approx \left[\chi^{0}\right]^{-1} - \lambda v. \tag{3.78}$$

is neglected. Note that here $\left[\chi^{\lambda}\right]^{-1}$ denotes the inverse of the matrix χ^{λ}. After some algebra, one obtains

$$E_c^{\mathrm{RPA}} = \frac{1}{2\pi}\int_0^{\infty} \mathrm{d}u\, \mathrm{Tr}\left[\ln(1-\chi^0 v) + v\chi^0\right], \tag{3.79}$$

where the non-interacting response function can be obtained from the Kohn-Sham orbitals [46].

To conclude this section and to show the performance of RPA calculations for real bulk systems, in Fig. 3.7 we show the relative error % of the theoretical lattice constants (left panel) and the theoretical bulk moduli (right panel) with respect to experiment. These results are reproduced from the work of Harl and Kresse [46].

3.5.6 Van der Waals Interactions

We begin this section with a quote from a recent review by Berland and co-workers [18]:

"Identified in 1873, there is a force that today attracts more interest than ever. It was first introduced in a doctoral thesis by Johannes Diderik van der Waals (vdW) ... It is present everywhere, but its variation from one environment to another and its complex manifestations still pose challenging questions nearly one hundred years after van der Waals was awarded the Nobel Prize in physics. These questions are relevant for such varied systems as soft matter, surfaces, and DNA, and in phenomena as different as supramolecular binding, surface reactions, and the dynamic properties of water. The term vdW includes the following forces between molecules: (i) two permanent dipoles (Keesom force), (ii) a permanent dipole and a corresponding induced dipole (Debye force), and (iii) two instantaneously induced dipoles (London dispersion force). In the condensed-matter community, typically just the latter, which has a nonclassical, true quantum mechanical, origin, is referred to as the vdW force. Like all non-relativistic electronic effects, the vdW interactions are present in the exact DFT functional. However, by construction, LDA and GGA neglect the long-range, nonlocal correlations that give rise to the vdW forces. Proper inclusion of vdW interactions in DFT calculations requires that the total energy functional depends on the electron density in a manner that reflects both the long-ranged and medium-ranged nature of vdW interactions."

The inclusion of vdW interactions within a first-principles DFT treatment can be achieved with the so-called Rutgers-Chalmers *van der Waals density functional* (vdW-DF) method which includes vdW forces by using a *nonlocal* exchange-correlation functional [18, 47]. We will restrict ourselves to briefly introduce this vdW-DF approach while alternative schemes, such as the Tkatchenko-Scheffler methods [19] or the popular semi-empirical methods due to Grimme [48] are outside the scope of these lecture notes.

The key to the vdW-DF method is the inclusion of a longrange piece of the correlation energy, $E_c^{nl}[n]$, a fully nonlocal functional of the density n. This piece is evaluated using a "plasmon" pole approximation for the inverse dielectric function, which satisfies known conservation laws, limits, sum rules, and invariances [49, 50]. Since the nonlocal dispersion forces are usually considered to arise from non-overlapping densities, the total correlation energy is divided into two contributions,

$$E_c[n] = E_c^0[n] + E_c^{nl}[n] \tag{3.80}$$

where $E_c^{nl}[n]$ accounts for the long-ranged dispersive interactions. The first term, $E_c^0[n]$, is, in principle, semi-local, but is treated by the LDA. This appears to be a reasonable approximation since it is exact in the limit of slowly varying densities. Hence, the *r*ecipe for treating correlation effects within the vdW-DF is

$$E_c^0[n] \approx E_c^{LDA}[n], \tag{3.81}$$

ensuring that no double-counting of non-local effects will occur. The non-local term can be considerably simplified by noting that the long-range interactions are less sensitive to the details of the system's dielectric response than the short-range terms, and it can be cat into the form [18]

$$E_c^{nl} = \frac{1}{2}\int \mathrm{d}^3r\mathrm{d}^3r' n(\boldsymbol{r})\phi(\boldsymbol{r},\boldsymbol{r}')n(\boldsymbol{r}'). \tag{3.82}$$

The details of the interaction between the electron density at point $\boldsymbol{r}$ and $\boldsymbol{r}'$ are hidden in the *non-local kernel* ϕ, which is, by construction, a generalized function of space coordinates, the electron densities n and their gradients, i.e., $\phi = \phi(|\boldsymbol{r}-\boldsymbol{r}'|, n(\boldsymbol{r}), n(\boldsymbol{r}'), \nabla n(\boldsymbol{r}), \nabla n(\boldsymbol{r}'))$. Introducing the quantities

$$d = |\boldsymbol{r}-\boldsymbol{r}'|\; q_0(\boldsymbol{r}) \tag{3.83}$$

$$d' = |\boldsymbol{r}-\boldsymbol{r}'|\; q_0(\boldsymbol{r}'), \tag{3.84}$$

where q_0 also depends on the density and its gradients, the kernel ϕ thus depends on $\boldsymbol{r}$ and $\boldsymbol{r}'$ only through d and d', so that it can be tabulated in advance in terms of these two variables, or better, in terms of the sum and difference of these two, i.e., D and δ defined by

$$D = \frac{1}{2}(d+d') \qquad 0 \le D \le \infty, \tag{3.85}$$

$$\delta = \frac{d-d'}{d+d'} \qquad 0 \le |\delta| \le 1. \tag{3.86}$$

When both, d and d' are large, the asymptotic form of $\phi(d,d')$ is

$$\phi \to -\frac{C}{d^2\; d'^2\; (d^2+d'^2)}, \tag{3.87}$$

with $C = 12(4\pi/9)^3 me^4$. Thus, the interaction energy has the correct r^{-6} dependence for large distances. Another important feature of the kernel function is that E_c^{nl} is strictly zero for systems with a uniform electron density, as was initially imposed by Eq. 3.80. Moreover, the form of Eq. 3.82 keeps the spirit of DFT in the sense that the total energy requires only the knowledge of the electron density and does not depend on any adjustable input parameter.

The theory of the van der Waals density functional discussed above is an approximation for the correlation energy only. In practice, one needs to approximate the exchange energy as well. The standard scheme is to use a GGA for exchange, where it is important to choose a flavor, the exchange part of which does not produce a binding that is not present when the exchange is treated exactly. In fact, such a spurious binding from exchange has been found for rare gas dimers, a feature absent for the exact Hartree-Fock exchange. Since revPBE [51] does not exhibit this property, it was suggested to use this functional in numerical calculations.

Summarizing, the total xc energy in vdW-DF theory is defined as

$$E_{xc} = E_x^{revPBE} + E_c^{LDA} + E_c^{nl}. \tag{3.88}$$

Sometimes, the vdW-DF is carried out in a post-scf manner. First, the electron density is obtained self-consistently by using some GGA, and, in the second step, the nonlocal correlation energy E_c^{nl} is evaluated using this density as an input. We note, however, that self-consistency has little effect on the atomic interaction energy as shown by Thonhauser et al. [52] for the systems investigated so far. This should be particularly true for weakly interacting systems where one does not expect significant charge redistributions arising through the nonlocal interactions.

3.6 Interpretation of Kohn-Sham Energies

When deriving the Kohn-Sham equations 3.26 in Sec. 3.4, we have introduced the auxiliary system of non-interacting electrons with the purpose of enabling the calculation of the charge density $n(\boldsymbol{r})$ using 3.27, and in turn, of the total ground state energy, $E[n(\boldsymbol{r})]$, which is a functional of the density. The Kohn-Sham energies ε_i as well as the Kohn-Sham orbitals $\varphi_i(\boldsymbol{r})$, on the other hand, have not (yet) received any physical interpretation. It is of course tempting to interpret – similarly as Koopmans' theorem dictates for the Hartree-Fock method – as excitation energies. Thus, for a periodic system with $i \to (n\boldsymbol{k})$, the Kohn-Sham energies could be interpreted as the band structure $\varepsilon_{n\boldsymbol{k}}$ of the crystal. This is indeed regularly done in many practical applications of DFT, however, it may also lead to severe problems. The most prominent example is the underestimation of the band gap of semiconductors or insulators by as much as 50% whose origin will be discussed in Sec. 3.6.3. Before, we review in the next section, the so-called Janak's Theorem which can be viewed as the analogue of Koopmans' theorem for density functional theory.

3.6.1 Janak's Theorem

In his seminal paper from 1978 [53], Janak has derived a relation between the highest occupied Kohn-Sham orbital and the change in total energy with respect to orbital occupation which we will review here.

The formal extension of density functional theory to the case of *fractional occupations* has been demonstrated by Perdew an co-workers [54]. Denoting the fractional occupation of orbital φ_i as $f_i \in [0, 1]$, the charge density can be obtained from the following generalized expression

$$n(\boldsymbol{r}) = \sum_j f_j |\varphi_j(\boldsymbol{r})|^2. \tag{3.89}$$

The generalization of the total energy functional 3.28 for the case of fractional occupations is then given by

$$\tilde{E}[n] = \tilde{T}_s[n] + U[n] + E_{xc}[n] + \int \mathrm{d}^3 r \, v(\boldsymbol{r}) n(\boldsymbol{r}) \tag{3.90}$$

Here the "tilde" above E and T_s indicates that the definitions for these quantities need to be adjusted when allowing for fractional occupations. Similarly as for the charge density, we define the kinetic energy functional $\tilde{T}_s[n]$ as

$$\tilde{T}_s[n] = \sum_j f_j t_j \qquad \text{with} \qquad t_j = \int \mathrm{d}^3 r \varphi_j^*(\boldsymbol{r}) \left(-\frac{1}{2}\Delta \right) \varphi_j(\boldsymbol{r}). \tag{3.91}$$

We now want to prove Janak's theorem which states that the partial derivative of the total energy with respect to the occupation f_i of the i-th orbital equals the Kohn-Sham energy ε_i of the respective orbital, thus

$$\frac{\partial \tilde{E}}{\partial f_i} = \varepsilon_i. \tag{3.92}$$

We begin with the derivative with respect to the kinetic energy which gives

$$\frac{\partial \tilde{T}_s}{\partial f_i} = t_i + \sum_j f_j \frac{\partial t_j}{\partial f_i}. \tag{3.93}$$

The second term in the above equation arises because a change of occupation in orbital i will obviously change the electron density and thus also alter all other orbitals j and thereby modify the kinetic energy t_j of orbital j. This term, $\frac{\partial t_j}{\partial f_i}$, will be evaluated further below. Before doing so, we consider how the Hartree energy U and the exchange-correlation energy E_{xc} change with f_i by applying the chain rule of differentiation

$$\frac{\partial U}{\partial f_i} = \int \mathrm{d}^3 r \underbrace{\frac{\delta U}{\delta n(\boldsymbol{r})}}_{=v_H(\boldsymbol{r})} \cdot \frac{\partial n(\boldsymbol{r})}{\partial f_i} = \int \mathrm{d}^3 r \, v_H(\boldsymbol{r}) \left[|\varphi_i(\boldsymbol{r})|^2 + \sum_j f_j \frac{\partial |\varphi_j(\boldsymbol{r})|^2}{\partial f_i} \right]. \tag{3.94}$$

Here, we have made use of the definition of the Hartree potential $v_H(\boldsymbol{r})$ as the functional derivative of the Hartree energy with respect to the density, and applied the product rule to the derivative of the density as defined in 3.89. Again, because the occupation of orbital i changes the density, also the orbital j will be affected. Using the same arguments, also the derivative of the exchange-correlation energy and the external energy $V_{\text{ext}}[n] = \int \mathrm{d}^3 r \, v(\boldsymbol{r}) n(\boldsymbol{r})$ with respect to the occupation number f_i can

be obtained:

$$\frac{\partial E_{xc}}{\partial f_i} = \int \mathrm{d}^3 r \underbrace{\frac{\delta E_{xc}}{\delta n(\boldsymbol{r})}}_{=v_{xc}(\boldsymbol{r})} \cdot \frac{\partial n(\boldsymbol{r})}{\partial f_i} = \int \mathrm{d}^3 r \, v_{xc}(\boldsymbol{r}) \left[|\varphi_i(\boldsymbol{r})|^2 + \sum_j f_j \frac{\partial |\varphi_j(\boldsymbol{r})|^2}{\partial f_i} \right], \tag{3.95}$$

$$\frac{\partial V_{\mathrm{ext}}}{\partial f_i} = \int \mathrm{d}^3 r \underbrace{\frac{\delta V_{\mathrm{ext}}}{\delta n(\boldsymbol{r})}}_{=v(\boldsymbol{r})} \cdot \frac{\partial n(\boldsymbol{r})}{\partial f_i} = \int \mathrm{d}^3 r \, v(\boldsymbol{r}) \left[|\varphi_i(\boldsymbol{r})|^2 + \sum_j f_j \frac{\partial |\varphi_j(\boldsymbol{r})|^2}{\partial f_i} \right]. \tag{3.96}$$

In order to evaluate Eq. 3.93 further, we first rewrite t_i with the help of the Kohn-Sham equations as

$$t_i = \int \mathrm{d}^3 r \varphi_i^*(\boldsymbol{r}) \left(-\frac{1}{2}\Delta \right) \varphi_i(\boldsymbol{r}) = \varepsilon_i - \int \mathrm{d}^3 r \underbrace{\left[v_H(\boldsymbol{r}) + v_{xc}(\boldsymbol{r}) + v(\boldsymbol{r}) \right]}_{=v_s(\boldsymbol{r})} |\varphi_i(\boldsymbol{r})|^2, \tag{3.97}$$

and then find for the derivative

$$\frac{\partial t_j}{\partial f_i} = \int \mathrm{d}^3 r \frac{\partial \varphi_j^*}{\partial f_i} \left(-\frac{1}{2}\Delta \right) \varphi_j + c.c., \tag{3.98}$$

where *c.c.* indicates the complex conjugate of the preceding terms. By adding the contributions together, we obtain

$$\begin{aligned}
\frac{\partial \tilde{E}}{\partial f_i} &= \frac{\partial \tilde{T}_s}{\partial f_i} + \frac{\partial U}{\partial f_i} + \frac{\partial E_{xc}}{\partial f_i} + \frac{\partial V_{\mathrm{ext}}}{\partial f_i} \\
&= \varepsilon_i - \int \mathrm{d}^3 r \, v_s(\boldsymbol{r}) |\varphi_i(\boldsymbol{r})|^2 + \sum_j f_j \frac{\partial t_j}{\partial f_i} + \int \mathrm{d}^3 r \, v_s(\boldsymbol{r}) \left[|\varphi_i(\boldsymbol{r})|^2 + \sum_j f_j \frac{\partial |\varphi_j(\boldsymbol{r})|^2}{\partial f_i} \right] \\
&= \varepsilon_i + \sum_j f_j \left[\frac{\partial t_j}{\partial f_i} + \int \mathrm{d}^3 r \, v_s(\boldsymbol{r}) \frac{\partial |\varphi_j(\boldsymbol{r})|^2}{\partial f_i} \right].
\end{aligned} \tag{3.99}$$

When inserting 3.98 into 3.99 and using the product rule for $\frac{\partial |\varphi_j|^2}{\partial f_i} = \frac{\partial \varphi_j^*}{\partial f_i}\varphi_j + c.c.$, we find

$$\begin{aligned}
\frac{\partial \tilde{E}}{\partial f_i} &= \varepsilon_i + \sum_j f_j \left[\int \mathrm{d}^3 r \frac{\partial \varphi_j^*}{\partial f_i} \underbrace{\left(-\frac{1}{2}\Delta + v_s \right) \varphi_j}_{=\varepsilon_j \varphi_j} + c.c. \right] \\
&= \varepsilon_i + \sum_j f_j \varepsilon_j \frac{\partial}{\partial f_i} \underbrace{\int \mathrm{d}^3 r |\varphi_j(\boldsymbol{r})|^2}_{=1} \\
&= \varepsilon_i.
\end{aligned} \tag{3.100}$$

Thus, by using the Kohn-Sham equations once more and noting that the orbitals are normalized, we have proven Janak's theorem.

In the mathematical derivations outlined above we did not make assumptions on which orbital's occupation we were changing. It appears that 3.100 is correct for any orbital i. However, to remain in the electronic ground state, there are only two possibilities when starting from an M-electron ground state where M is an integer number: (i) removal of an electron from the highest occupied orbital φ_M with the orbital energy ε_M, thus altering f_M, or (ii) addition of an electron to the lowest unoccupied orbital φ_{M+1} with the orbital energy ε_{M+1}, thus altering f_{M+1}. All other possibilities, would lead to a system which is no longer in its electronic ground state but rather represent an excited state. In the latter situation density functional theory can no longer be applied.

3.6.2 Picewise Linearity of $E(N)$

We can now use Janak's theorem to connect the M-electron system with the $M+1$ electron system, and respectively, the M-electron system with the $M-1$ electron system. Let us start with the former and denote the fractional charge that we put into the orbital $M+1$ as $f_{M+1} = \omega$. Denoting the total energy of the M-electron system as $E(M)$ and the total energy of the $M+1$-electron system as $E(M+1)$, we have

$$-A(M) \equiv E(M+1) - E(M) = \int_0^1 \mathrm{d}f_{M+1} \frac{\partial \tilde{E}}{\partial f_{M+1}} = \int_0^1 \mathrm{d}\omega\, \varepsilon_{M+1}(M+\omega) = \varepsilon_{M+1}(M+\delta). \quad (3.101)$$

Here, we have introduced the *electron affinity* which is defined to be the negative of the total energy difference of the $M+1$ and the M-electron systems, and we have made use of Janak's theorem. In the last step of the above equation, we have used the fact that – from very general arguments to be outlined below – the total energy $E(N)$ as a function of electron number, where N is allowed to be non-integer, is a *piece-wise linear function* as illustrated in Fig. 3.8. As a consequence, it does not matter where in the interval $(M, M+1)$ we take the derivative, and the orbital energy $\varepsilon_{M+1}(N)$ remains constant over the open interval $N \in (M, M+1)$. In analogy to Eq. 3.101, we can also gradually remove an electron from the highest occupied orbital which leads us to the definition of the *ionization potential* of the M-electron system denoted as $I(M)$:

$$-I(M) \equiv E(M) - E(M-1) = \int_0^1 \mathrm{d}f_M \frac{\partial \tilde{E}}{\partial f_M} = \int_0^1 \mathrm{d}\omega\, \varepsilon_M(M-1+\omega) = \varepsilon_M(M-\delta). \quad (3.102)$$

In the last step of the above equation we have again used the fact that $E(N)$ is a piecewise linear

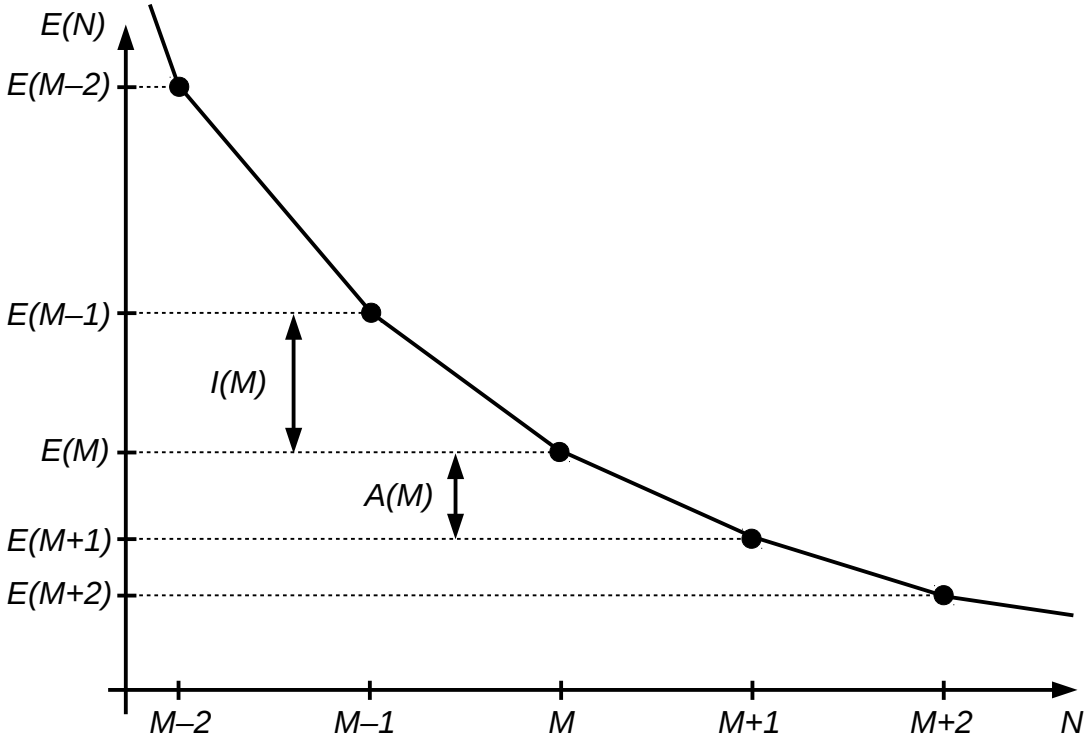

Figure 3.8: Principal behaviour of the total energy E as a function of the non-integer electron number N. The energies at the integer particle numbers $M-2$, $M-1$, M, $M+1$ and $M+2$ are indicated and the definitions of the electron affinity, $A(M)$ and ionization potential $I(M)$ of the M-electron system are given.

function. This fact is a consequence of the *convex condition* of $E(N)$ which can be expressed as follows:

$$E(M) < \frac{1}{2}\left[E(M+1) + E(M-1)\right]. \tag{3.103}$$

In other words, this means that for a given system of M interacting electrons, the ionization potential $I(M)$ is always larger than the electron affinity. The cost of removing an electron from the M-electron system is larger than the energy gain of adding an additional electron to the system, because the added electron experiences an enhanced Coulomb repulsion.

In order to understand the piecewise linear behaviour of $E(N)$ depicted in Fig. 3.8, we have to recall how a system of a non-integer number of electrons can be treated. For an integer number of electrons, M, the ground state wave function is a pure state denoted as Ψ_M, while for a non-integer number the system has to be described by a *statistical mixture* of several pure states with some probabilities. For instance, take the two pure states Ψ_M and Ψ_{M+1} corresponding to the ground state of the M and $M+1$ electron systems with the weights $(1-\omega)$ and ω, respectively. Then the corresponding electron densities, denoted as $n_M(\boldsymbol{r})$ and $n_{M+1}(\boldsymbol{r})$ and computed in the usual manner 3.2, integrate

to $N = M + \omega$ electrons

$$N = (1-\omega)\int \mathrm{d}^3 r\, n_M(\boldsymbol{r}) + \omega \int \mathrm{d}^3 r\, n_{+1}(\boldsymbol{r}) = (1-\omega)M + \omega(M+1) = M + \omega. \tag{3.104}$$

Thus, we see that such a statistical mixture with the weights given above and $\omega \in [0,1]$ indeed describes a system containing $M + \omega$ electrons. In a similar manner, the total energy of the $M + \omega$ system is given by

$$E(N) = (1-\omega)E[n_M] + \omega E[n_{M+1}] = (1-\omega)E(M) + \omega E(M+1). \tag{3.105}$$

This equation describes a linear interpolation between the total energy values at the integer numbers M and $M+1$, respectively. If one were to include more pure states, such as Ψ_{M+2} or Ψ_{M-1}, in order to describe the $M+\omega$ system, one would always end up with larger energies, thus not find the ground state. Expressed in mathematical terms, a linear interpolation always overestimates a convex function. Thus, the ground state of the $M+\omega$ system is indeed described only by the pure states Ψ_M and Ψ_{M+1} with weights $(1-\omega)$ and ω, respectively, leading to the piecewise linear dependence of $E(N)$ with *derivative discontinuities* at integer values.

It should be noted that most approximate exchange-correlation functionals used in practice have a non-linear behaviour between integers and lack the derivative discontinuities in the energy. This is illustrated in Fig. 3.9 for the C atom and the H_2O molecule. For instance, the PBE-GGA functional leads to a smooth convex function $E(N)$ for the C atom with a positive curvature $C = \frac{\mathrm{d}^2 E}{\mathrm{d}N^2}$, while the Hartree-Fock calculation (HF) yields a concave function with a negative curvature. There is a class of functionals, so-called range-separated hybrid functionals, where the range-separation parameter γ can be tuned such to yield an almost vanishing curvature, thereby restoring the piecewise linear behaviour expected for the exact functional. This is illustrated in the right panel of Fig. 3.9 for the H_2O molecule.

We conclude this section by noting that deviations from the perfect linear $E(N)$ behaviour, which most approximate functionals show, have profound consequences, for instance, it leads to too small chemical barriers, problems in the description of long-range charge transfer excitations or dissociating molecules, and to an underestimation of band gaps which will be explained in the next section.

3.6.3 The Band Gap Problem

The fundamental energy gap, E_{gap}, of a system of M electrons and the center of the gap, E_{center}, can be defined in terms of the ionization potential $I(M)$ and the electron affinity $A(M)$ (see e.g. Perdew

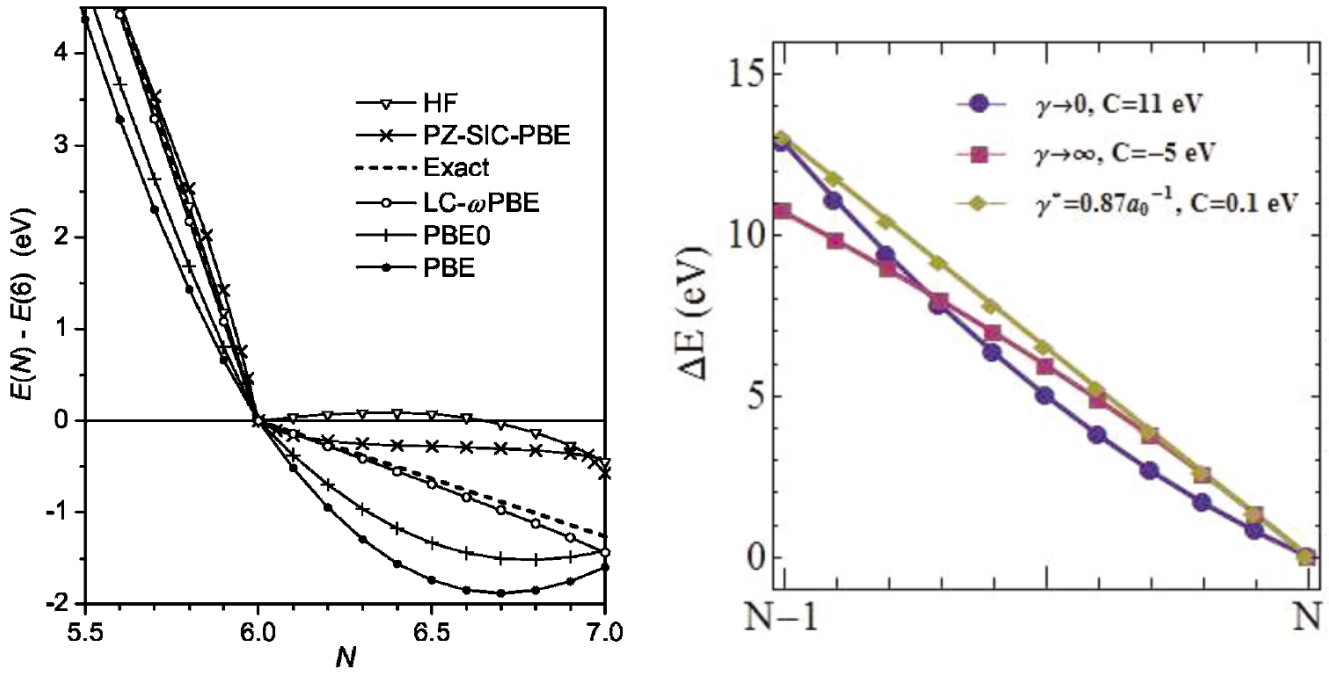

Figure 3.9: Left from Ref. [55]: Total energy of the C atom as a function of the electron number N computed for various functionals. Right from Ref. [41]: Total energy difference with respect to the neutral, $N = 10$ electron system as a function of the particle number N for the H_2O molecule, calculated with the Baer-Neuhauser (BN) functional with $\gamma = 0$, $\gamma \to \infty$, and the optimally tuned $\gamma = 0.87$. The average curvature, $C = \frac{\mathrm{d}^2E}{\mathrm{d}N^2}$, is indicated for each functional.

and Levy [56])

$$E_{\mathrm{gap}} = I(M) - A(M) \tag{3.106}$$

$$E_{\mathrm{center}} = -\frac{1}{2}\left[I(M) + A(M)\right]. \tag{3.107}$$

Using the Eqs. 3.101 and 3.102 to express E_{gap} and E_{center} in terms of Kohn-Sham energies instead of total-energy-derived quantities, we thus find

$$E_{\mathrm{gap}} = \varepsilon_{M+1}(M+\delta) - \varepsilon_M(M-\delta) \tag{3.108}$$

$$E_{\mathrm{center}} = \frac{1}{2}\left[\varepsilon_{M+1}(M+\delta) + \varepsilon_M(M-\delta)\right]. \tag{3.109}$$

The appearance of the infinitesimal charge δ in the above equations is crucial because of a derivative discontinuity of the potential as illustrated below

$$\delta \quad \longleftrightarrow \quad \delta n(\boldsymbol{r}) \quad \longleftrightarrow \quad \delta v_s(\boldsymbol{r}) + \Delta_{xc} \tag{3.110}$$

The infinitesimal charge δ results in an infinitesimal change in the electron density $\delta n(\boldsymbol{r})$ which in turn is connected with an infinitesimal change in the Kohn-Sham potential $\delta v_s(\boldsymbol{r})$. Because, according to the Hohenberg-Kohn theorem, the density determines the potential uniquely only up to an additive constant, we also must allow for the constant Δ_{xc}. This is the so-called derivative discontinuity of the exchange-correlation potential which can be defined in the following way

$$\Delta_{xc} = \left.\frac{\delta E_{xc}}{\delta n(\boldsymbol{r})}\right|_{M+\delta} - \left.\frac{\delta E_{xc}}{\delta n(\boldsymbol{r})}\right|_{M-\delta} \tag{3.111}$$

Thus, the band gap can be written as the sum of the Kohn-Sham band gap, ε_{gap}, and the derivative discontinuity

$$E_{\text{gap}} = \underbrace{\varepsilon_{M+1}(M) - \varepsilon_M(M)}_{\varepsilon_{\text{gap}}} + \Delta_{xc}. \tag{3.112}$$

Experience shows that Δ_{xc} is a substantial part of the band gap. As a result the Kohn-Sham band gap ε_{gap} calculated with approximate functionals such as the LDA or the GGA amounts to only about 50% of the true band gap. This is illustrated in Fig. 3.10 for a number of bulk semiconductors and insulators. Note that in this figure, MBJLDA refers to a meta-GGA functional (third rung of Jacob's ladder), the so-called modified Becke-Johnson LDA functional as proposed by Tran and Blaha [57] and HSE is the range-separated hybrid functional (fourth rung of the ladder) according Heyd, Scuseria and Ernzerhof [58]. The data points labelled as G_0W_0 and GW are results from many-body perturbation theory whose description is beyond the scope of this lecture [59, 60].

The center of the gap, on the other hand, can be obtained exactly from the Kohn-Sham band structure

$$E_{\text{center}} = \frac{1}{2}\left[\varepsilon_{M+1}(M) + \varepsilon_M(M)\right] \equiv \mu. \tag{3.113}$$

This is because the definition of the gap center coincides with the chemical potential μ which, by construction, is equal for the auxiliary Kohn-Sham system and the physical system of interacting electrons. Therefore, the exchange-correlation potential at the integer electron number M is the average of the right and left functional derivatives of E_{xc}

$$\left.\frac{\delta E_{xc}}{\delta n(\boldsymbol{r})}\right|_{M} = \frac{1}{2}\left[\left.\frac{\delta E_{xc}}{\delta n(\boldsymbol{r})}\right|_{M+\delta} + \left.\frac{\delta E_{xc}}{\delta n(\boldsymbol{r})}\right|_{M-\delta}\right] \tag{3.114}$$

Note that for a metal (no gap), by definition $I(M) = A(M)$ and there is also no derivative discontinuity. Hence, the highest occupied Kohn-Sham orbital, $\mu = \varepsilon_M(M)$, equals the negative of the work function Φ [53]

$$\mu = -\Phi. \tag{3.115}$$

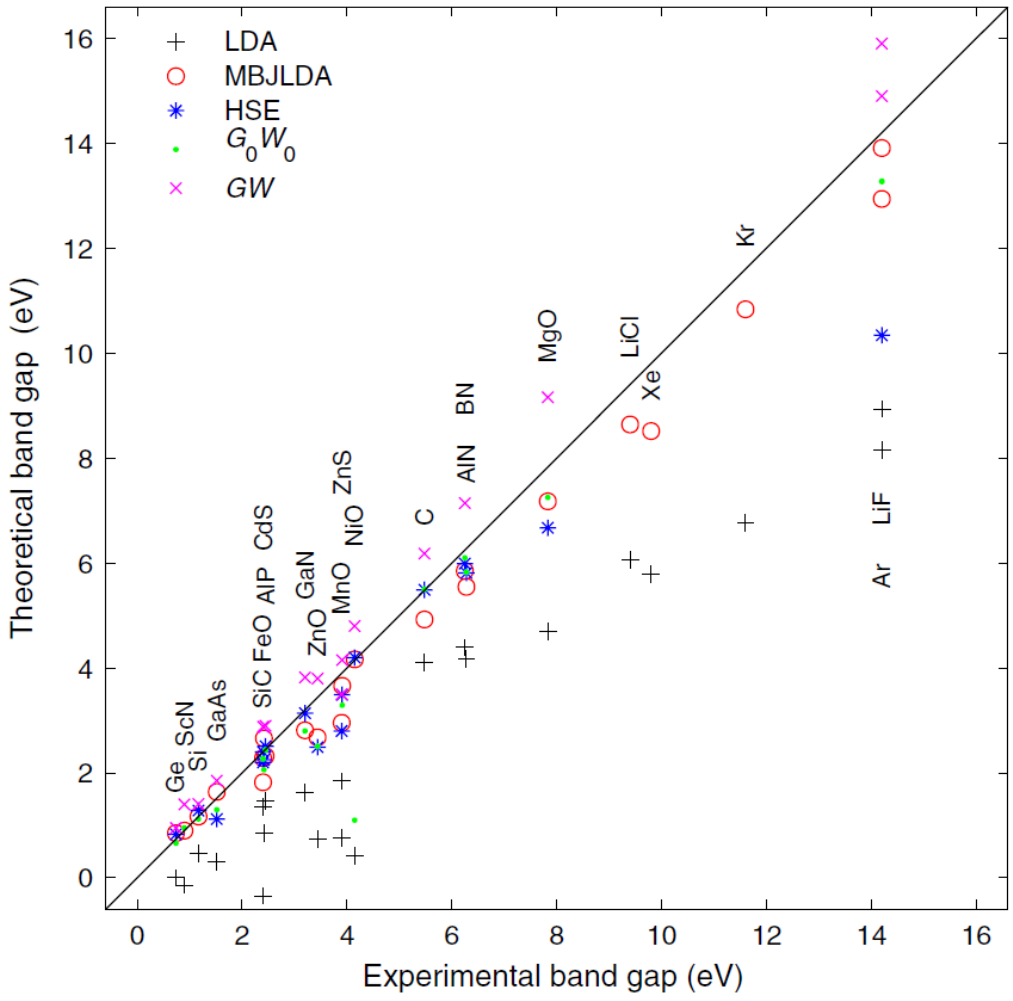

Figure 3.10: Left from Ref. [57]: Theoretical versus experimental band gaps for various bulk semiconductors and insulators obtained with various DFT functionals (LDA, MBJLDA, HSE) and many-body perturbation theory (G_0W_0, GW).

Chapter 4

Density Functional Theory in Practice

4.1 Introduction

As already highlighted in the introductory Section 1.3, the popularity of density functional methods in theoretical solid state physics and quantum chemistry (but indeed also for related fields such as materials science, biochemistry, ...) is ever growing (compare Fig. 1.1). Not least this is due to the availability of numerically efficient software packages for DFT applications. The mere number of available DFT software packages is truly overwhelming. This can be appreciated from this impressive list: DFT-packages. A characteristic feature of a given DFT software package is the type of *basis functions* it uses for solving the Kohn-Sham equations 1.9. Principally, the solution of the Kohn-Sham equations is accomplished by expanding the Kohn-Sham orbitals $\psi_j(\boldsymbol{r})$ into known basis functions $\phi_i(\boldsymbol{r})$:

$$\psi_j(\boldsymbol{r}) = \sum_i c_i^{(j)} \phi_i(\boldsymbol{r}). \tag{4.1}$$

A major distinction arises from the type of boundary conditions which the basis functions are designed to fulfill, specifically, whether periodic boundary conditions, which are suitable for crystalline solids, are imposed or not. In these lecture notes, we only cover such basis sets, and in particular we briefly describe the main ideas behind a *plane wave basis set* (Sec. 4.2) and an *augmented plane wave basis set* (Sec. 4.3).

As a side note, we refer to a recent publication [61], which compares the calculated values for the equation of states for 71 elemental crystals from 15 different widely used DFT codes employing 40 different potentials. Although there were variations in the calculated values, most recent codes and methods converged toward a single value, with errors comparable to those of experiment.

4.2 Plane Wave Basis

As outlined in Sec. 2.1.1, in the case of translational symmetry, the Kohn-Sham potential is translationally invariant$v_s(\boldsymbol{r}+\boldsymbol{R}) = v_s(\boldsymbol{r})$, and the Kohn-Sham orbitals $\psi_{\boldsymbol{k}}(\boldsymbol{r})$ are Bloch-waves. Thus, they can be written as a product of a plane wave and a lattice periodic function $u_{\boldsymbol{k}}(\boldsymbol{r})$ with $\boldsymbol{k}$ denoting a wave vector within the first Brillouin zone

$$\psi_{\boldsymbol{k}}(\boldsymbol{r}) = e^{i\boldsymbol{k}\cdot\boldsymbol{r}} u_{\boldsymbol{k}}(\boldsymbol{r}) \qquad \text{with} \qquad u_{\boldsymbol{k}}(\boldsymbol{r}+\boldsymbol{R}) = u_{\boldsymbol{k}}(\boldsymbol{r}). \tag{4.2}$$

A natural choice of basis functions $\phi(\boldsymbol{r})$ is to use the plane waves $e^{i\boldsymbol{G}\boldsymbol{r}}$, thus

$$\phi_{\boldsymbol{G}}(\boldsymbol{r}) = \frac{1}{\sqrt{\Omega}} e^{i\boldsymbol{G}\boldsymbol{r}}, \tag{4.3}$$

where $\boldsymbol{G}$ is a reciprocal lattice vector. Then, according to Eq. 2.21, the Kohn-Sham orbitals are expanded in the following way

$$\psi_{\boldsymbol{k}}(\boldsymbol{r}) = e^{i\boldsymbol{k}\boldsymbol{r}} \sum_{\boldsymbol{G}} c_{\boldsymbol{G}}(\boldsymbol{k}) \phi_{\boldsymbol{G}}(\boldsymbol{r}) = \sum_{\boldsymbol{G}} c_{\boldsymbol{G}}(\boldsymbol{k}) \phi_{\boldsymbol{k}+\boldsymbol{G}}(\boldsymbol{r}) = \frac{1}{\sqrt{\Omega}} \sum_{\boldsymbol{G}} c_{\boldsymbol{G}}(\boldsymbol{k}) e^{i(\boldsymbol{k}+\boldsymbol{G})\boldsymbol{r}}, \tag{4.4}$$

where the expansion coefficients $c_{\boldsymbol{G}}(\boldsymbol{k})$ are the Fourier coefficients for a particular Bloch wave at a given wave vector $\boldsymbol{k}$. Similarly, also the electron density $n(\boldsymbol{r})$ and the Kohn-Sham potential $v_s(\boldsymbol{r})$ may be expanded in a Fourier series owing to the lattice periodicity, $n(\boldsymbol{r}+\boldsymbol{R}) = n(\boldsymbol{r})$ and $v_s(\boldsymbol{r}+\boldsymbol{R}) = v_s(\boldsymbol{r})$, respectively. Thus we have (compare Eq. 2.21):

$$n(\boldsymbol{r}) = \frac{1}{\Omega} \sum_{\boldsymbol{G}} \tilde{n}(\boldsymbol{G}) e^{i\boldsymbol{G}\boldsymbol{r}} \tag{4.5}$$

$$v_s(\boldsymbol{r}) = \frac{1}{\Omega} \sum_{\boldsymbol{G}} \tilde{v}_s(\boldsymbol{G}) e^{i\boldsymbol{G}\boldsymbol{r}}. \tag{4.6}$$

4.2.1 Secular equation

When inserting the plane wave expansion 4.4 into the Kohn-Sham equations

$$\hat{H}\psi_{\boldsymbol{k}}(\boldsymbol{r}) = \varepsilon_{\boldsymbol{k}} \psi_{\boldsymbol{k}}(\boldsymbol{r}), \tag{4.7}$$

we transform the differential eigenvalue problem into a matrix eigenvalue equation which is also termed the *secular equation*:

$$\sum_{\boldsymbol{G}'} H_{\boldsymbol{G}\boldsymbol{G}'}(\boldsymbol{k}) c_{\boldsymbol{G}'}(\boldsymbol{k}) = \varepsilon_{\boldsymbol{k}}\, c_{\boldsymbol{G}}(\boldsymbol{k}). \tag{4.8}$$

Here we have introduced the Hamiltonian matrix $H_{\boldsymbol{G}\boldsymbol{G}'}(\boldsymbol{k})$ with the matrix indices $\boldsymbol{G}$ and $\boldsymbol{G}'$

$$H_{\boldsymbol{G}\boldsymbol{G}'}(\boldsymbol{k}) = \frac{1}{\Omega}\int \mathrm{d}^3r\, e^{-i(\boldsymbol{k}+\boldsymbol{G})\boldsymbol{r}}\hat{H}e^{i(\boldsymbol{k}+\boldsymbol{G}')\boldsymbol{r}}, \tag{4.9}$$

and used the fact that the plane waves are orthonormal, thus the overlap matrix is given by the identity matrix

$$S_{\boldsymbol{G}\boldsymbol{G}'}(\boldsymbol{k}) = \frac{1}{\Omega}\int \mathrm{d}^3r\, e^{-i(\boldsymbol{k}+\boldsymbol{G})\boldsymbol{r}}e^{i(\boldsymbol{k}+\boldsymbol{G}')\boldsymbol{r}} = \frac{1}{\Omega}\int \mathrm{d}^3r\, e^{-i(\boldsymbol{G}-\boldsymbol{G}')\boldsymbol{r}} = \delta_{\boldsymbol{G}\boldsymbol{G}'}. \tag{4.10}$$

We can further split the Hamilton matrix 4.9 into a kinetic energy matrix and a potential energy matrix $H_{\boldsymbol{G}\boldsymbol{G}'}(\boldsymbol{k}) = T_{\boldsymbol{G}\boldsymbol{G}'}(\boldsymbol{k}) + V_{\boldsymbol{G}\boldsymbol{G}'}$, where

$$\begin{aligned} T_{\boldsymbol{G}\boldsymbol{G}'}(\boldsymbol{k}) &= \frac{1}{\Omega}\int \mathrm{d}^3r\, e^{-i(\boldsymbol{k}+\boldsymbol{G})\boldsymbol{r}}\left(-\frac{1}{2}\Delta\right)e^{i(\boldsymbol{k}+\boldsymbol{G}')\boldsymbol{r}} \\ &= \frac{|\boldsymbol{k}+\boldsymbol{G}'|^2}{2\Omega}\int \mathrm{d}^3r\, e^{-i(\boldsymbol{k}+\boldsymbol{G})\boldsymbol{r}}e^{i(\boldsymbol{k}+\boldsymbol{G}')\boldsymbol{r}} \\ &= \frac{|\boldsymbol{k}+\boldsymbol{G}'|^2}{2}\delta_{\boldsymbol{G}\boldsymbol{G}'}, \end{aligned} \tag{4.11}$$

and

$$\begin{aligned} V_{\boldsymbol{G}\boldsymbol{G}'} &= \frac{1}{\Omega}\int \mathrm{d}^3r\, e^{-i(\boldsymbol{k}+\boldsymbol{G})\boldsymbol{r}}v_s(\boldsymbol{r})e^{i(\boldsymbol{k}+\boldsymbol{G}')\boldsymbol{r}} = \frac{1}{\Omega}\int \mathrm{d}^3r\, e^{-i(\boldsymbol{G}-\boldsymbol{G}')\boldsymbol{r}}v_s(\boldsymbol{r}) \\ &= \frac{1}{\Omega^2}\int \mathrm{d}^3r\, e^{-i(\boldsymbol{G}-\boldsymbol{G}')\boldsymbol{r}}\sum_{\boldsymbol{G}''}\tilde{v}_s(\boldsymbol{G}'')e^{i\boldsymbol{G}''\boldsymbol{r}} \\ &= \frac{1}{\Omega^2}\sum_{\boldsymbol{G}''}\tilde{v}_s(\boldsymbol{G}'')\int \mathrm{d}^3r\, e^{-i(\boldsymbol{G}-\boldsymbol{G}'-\boldsymbol{G}'')\boldsymbol{r}} = \frac{1}{\Omega}\sum_{\boldsymbol{G}''}\tilde{v}_s(\boldsymbol{G}'')\delta_{\boldsymbol{G}-\boldsymbol{G}',\boldsymbol{G}''} \\ &= \frac{1}{\Omega}\tilde{v}_s(\boldsymbol{G}-\boldsymbol{G}'). \end{aligned} \tag{4.12}$$

Thus, we notice that the kinetic energy matrix $T_{\boldsymbol{G}\boldsymbol{G}'}(\boldsymbol{k})$ is already diagonal and the diagonal elements are given by the kinetic energy associated with the plane wave $e^{i(\boldsymbol{k}+\boldsymbol{G}')\boldsymbol{r}}$. This is of course to be expected since plane waves are the eigenfunctions of the kinetic energy operator. Also the potential energy matrix $V_{\boldsymbol{G}\boldsymbol{G}'}$ acquires a simple form in the plane wave representation. Its matrix elements turn out to be independent of the Bloch vector $\boldsymbol{k}$ and are given by the Fourier coefficients $\tilde{v}_s$ of the Kohn-Sham potential, which can be computed numerically in an efficient manner by employing fast Fourier transform (FFT) algorithms.

4.2.2 Plane wave cut-off and convergence

The real space representation of the Kohn-Sham equations 4.7 are entirely equivalent to the momentum space representation 4.8 provided that the summation over $\boldsymbol{G}'$ includes all (infinite) reciprocal space vectors. In practice, however, one has to truncate the sum at a cut-off wave number G_{cut}

$$\sum_{\boldsymbol{G}'}^{|\boldsymbol{G}'|\leq G_{\text{cut}}} H_{\boldsymbol{G}\boldsymbol{G}'}(\boldsymbol{k}) c_{\boldsymbol{G}'}(\boldsymbol{k}) = \varepsilon_{\boldsymbol{k}}\, c_{\boldsymbol{G}}(\boldsymbol{k}). \tag{4.13}$$

Thus, the summation runs over all reciprocal space vectors $\boldsymbol{G}'$ which lie within a sphere of radius G_{cut} in momentum space, and the Hamiltonian matrix only needs to be calculated for those $\boldsymbol{G}$ vectors. It is common practice to characterize this plane wave cut-off with the cut-off energy $E_{\text{cut}} = \frac{G_{\text{cut}}^2}{2}$ which is the kinetic energy associated with the cut-off wave vector. For a given unit cell volume Ω_0 and a given cut-off vector G_{cut} we can estimate the number of reciprocal space vectors inside the cut-off sphere $N_{\boldsymbol{G}}$ and thus the size of the Hamiltonian matrix according to

$$N_{\boldsymbol{G}} \approx \frac{\frac{4}{3}\pi G_{\text{cut}}^3}{\frac{(2\pi)^3}{\Omega_0}} = \frac{1}{6\pi^2}\Omega_0\, G_{\text{cut}}^3 = \frac{1}{6\pi^2}\Omega_0 (2E_{\text{cut}})^{\frac{3}{2}}. \tag{4.14}$$

Since the computational time (CPU) for determining the eigenvalues of a dense (=not sparse) $N_{\boldsymbol{G}} \times N_{\boldsymbol{G}}$ matrix scales with the third power of the matrix size, we can estimate the computational time as

$$CPU \sim \Omega_0^3\, G_{\text{cut}}^9 \sim \Omega_0^3 E_{\text{cut}}^{\frac{9}{2}}. \tag{4.15}$$

Thus, for a fixed unit cell volume which is determined by the system under study, the convergence of the results with respect to the plane wave cut-off is crucial. If the convergence with the plain wave cut-off would be easy and straight forward, then the lecture notes could end here, and in fact, there would be no need for the various electronic structure methods and the numerous software packages mentioned earlier: DFT-packages. However, life is not that simple. There are two reasons why the convergence with respect to the plane wave cut-off is slow, in fact so slow, that no meaningful calculation is possible even for the most simple crystalline solids such as the simple free-electron-like metal Na. First, *core electrons*, *i.e.* those electrons which are spatially localized close to the atomic nucleus, for instance the 1s electrons of Na, are difficult to describe with plane waves which are more suitable for delocalized (=extended) states. Second, also the convergence for *valence electrons*, such as the 3s electron forming the conduction band in Na, turns out to be problematic. This is because of the nodal structure of the radial part of the 3s-like wave functions close to the atomic nucleus. Only in the regions approximately half-way between the atomic nuclei (the so called *interstitial region*) the potential landscape is comparably flat and hence plane wave are a good description for the wave

functions. Close to the atomic nuclei, on the other hand, the potential felt by the electron remains $\sim \frac{1}{r}$-like and the resulting nodal structure, which is necessary to remain the orthogonality to the core sates, would require an impractically large plane wave cut-off. One solution to this problem is the so-called pseudo-potential concept to be presented in the next section.

4.2.3 The pseudo-potential concept

A *pseudopotential* is an effective potential constructed to replace the all-electron potential (full-potential) such that core states are eliminated and the valence electrons are described by pseudo-wavefunctions with significantly fewer nodes close to the atomic nuclei (compare Fig. 4.1). This allows these pseudo-wavefunctions to be described with far fewer plane waves, thus making a plane-wave basis set practical to use. In this approach usually only the chemically active valence electrons are dealt with explicitly, while the core electrons are "frozen", being considered together with the nuclei as rigid non-polarizable ion cores.

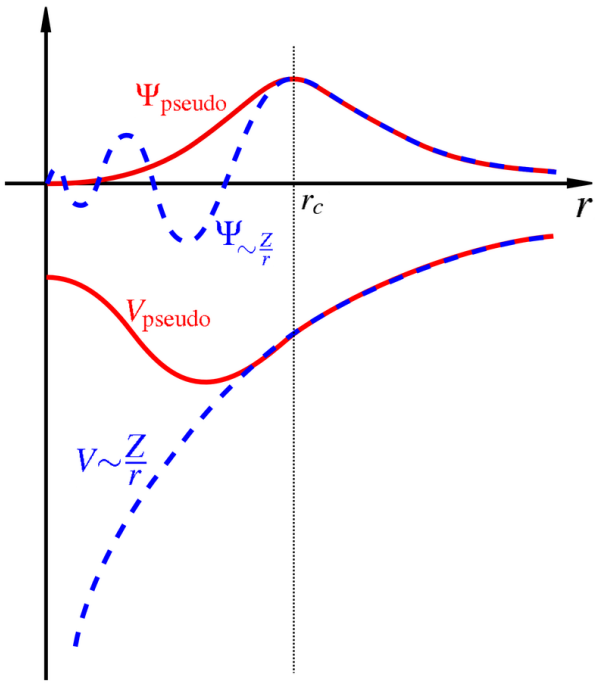

Figure 4.1: Comparison of a wavefunction in the Coulomb potential of the nucleus (blue) to the one in the pseudopotential (red). The real and the pseudo wavefunction and potentials match above a certain cutoff radius r_c.

Popular DFT software packages which are using a plane wave basis and employing the pseudo-potential concept and/or the more modern and accurate projector augmented wave (PAW) scheme are `ABINIT`, `Quantum-Espresso` or `VASP`.

There are various schemes to construct such pseudo-potentials from first-principles including so-called norm-conserving pseudo-potentials [62], ultra-soft pseudo-potentials [63] or the now widely used potentials based on the projector augmented wave (PAW) method [64]. In these lecture notes, however, we restrict ourselves to demonstrate only the main principle of the pseudo-potential concept.

To this end, let us consider the Kohn-Sham equations for a free atom

$$\hat{H}\,|\psi_i\rangle = E_i\,|\psi_i\rangle\,. \tag{4.16}$$

Here i comprises the set of quantum numbers $i = (nlm)$, thus the principal quantum number n, the angular quantum number l and the magnetic quantum number m. Because of the Hermiticity of the Hamiltonian, the orbitals are orthonormal

$$\langle\psi_i\,|\,\psi_j\rangle = \delta_{ij}. \tag{4.17}$$

In a next step, we must decide which if the states $|\psi_i\rangle$ we want to treat as valence (v) electrons and which we considers as core (c) electrons which are assumed not to participate in the bonding to neighboring atoms. For instance, in the case of an Aluminum atom with a total number of $Z = 13$ electrons and the electron configuration $1s^2 2s^2 2p^6 3s^2 3p^1$, it is reasonable to choose $N_c = 10$ core electrons ($1s^2 2s^2 2p^6$) and $N_v = 3$ valence electrons ($3s^2 3p^1$). We then attempt to decompose the true, physical wave function of a valence state $|\psi_v\rangle$ with its full nodal structure into a smooth *pseudo wave function* $|\phi_v\rangle$ and terms which should recover the nodal structure close to the atomic nucleus,

$$|\psi_v\rangle = |\phi_v\rangle + \sum_{c'} \alpha_{c'v}\,|\psi_{c'}\rangle \tag{4.18}$$

where the summation runs over all core states c'. We can determine the yet unknown coefficients $\alpha_{c'v}$ by acting on this equation with $\langle\psi_c|$ and using the orthonormality of $\langle\psi_c|$ with $|\psi_v\rangle$ and $|\psi_{c'}\rangle$, we find

$$\alpha_{cv} = -\,\langle\psi_c\,|\,\phi_v\rangle\,. \tag{4.19}$$

We can thus rewrite the connection between the physical wave valence state $|\psi_v\rangle$ and the pseudo valence state $|\phi_v\rangle$ in the following way

$$|\psi_v\rangle = \left(1 - \sum_c |\phi_c\rangle\,\langle\phi_c|\right)|\phi_v\rangle \tag{4.20}$$

By inserting this expression into the Kohn-Sham eigenvalue equation 4.16, we can derive an eigenvalue

equation for the pseudo-wave function $|\phi_v\rangle$

$$\left[\hat{H} - \sum_c (E_c - E_v) \, |\phi_c\rangle \, \langle\phi_c|\right] |\phi_v\rangle = E_v \, |\phi_v\rangle \tag{4.21}$$

$$\left[-\frac{1}{2}\Delta + v_s^{\mathrm{PP}}\right] |\phi_v\rangle = E_v \, |\phi_v\rangle \, . \tag{4.22}$$

In the latter equation, we have introduced the *pseudo potential* v_s^{PP} which we have defined as the sum of the all-electron (AE) Kohn-Sham potential v_s^{AE} and a term, which is spatially confined to the region of the core-electrons. It smoothens the potential in the vicinity of the atomic nucleus such that the rapid oscillations of the wave function close to the nucleus are removed

$$v_s^{\mathrm{PP}} = v_s^{\mathrm{AE}} - \sum_c (E_c - E_v) \, |\phi_c\rangle \, \langle\phi_c| \, . \tag{4.23}$$

While this form of the pseudo potential illustrates main idea behind the pseudo potential concept, for practical use it is still not convenient enough since Eq. 4.23 defines a *non-local* and *energy-dependent* form of a pseudo-potential. For details on how to construct more efficient versions of pseudo-potentials, which is outside the scope of this lecture, we refer to the literature [62].

4.3 Augmented Basis Functions

We have seen in the previous section, that plane waves are not a suitable choice of basis functions to account for the rapid oscillations of the wave functions close to the atomic nuclei. It was the idea of Slater [65] to *augment* the plane waves by atomic-like functions in the vicinity of the atomic nuclei. Since Slater first proposed the method in 1937, the augmented plane wave (APW) method and its descendents has been among the most popular schemes for solving the electronic structure problem for crystalline systems within the framework of density-functional theory. In part, this popularity arose from the fact that the APW method in its modern general potential, and linearized forms combines a conceptual simplicity with high accuracy for a general system.

In particular, the full-potential Linearized Augmented Plane Wave (FP-LAPW) method is one of the most accurate methods used for the solution of the Kohn-Sham equations for crystalline systems. This section gives a short introduction into the LAPW formalism. A more detailed description of the LAPW method can be found elsewhere [66]. Popular DFT software packages which are utilizing the LAPW method are `WIEN2k` or `exciting`.

The idea of the LAPW method is to divide the unit cell into two different regions: non-overlapping *spheres* around the positions of the nuclei, and the remaining *interstitial* region, schematically depicted

in Fig. (4.2). In the two regions, different sets of basis functions are used for the wave functions as well as for the electron density and the crystal potential. The choice of these basis functions is guided by the observation that near the nuclei the wave functions remain atomic-like even in a crystalline environment, whereas they are more plane-wave like between the atoms. The same argument also applies for the density as well as for the potential.

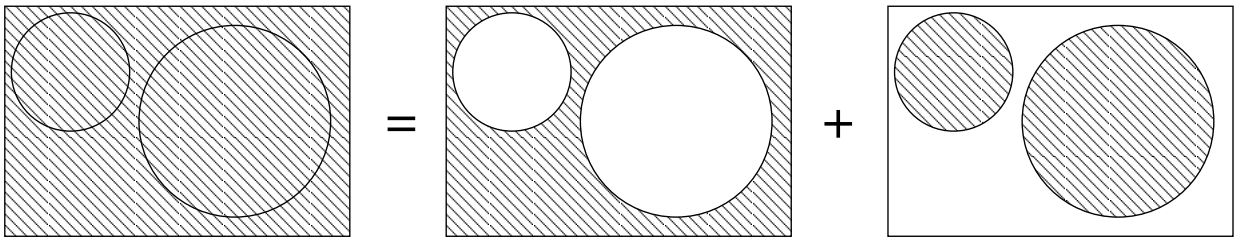

Figure 4.2: Splitting of the unit cell volume into the interstitial and the spheres region, which is also often referred to as the muffin–tin region.

4.3.1 The LAPW Basis

In the LAPW method, normalized plane waves are used as basis functions within the interstitial region (I),

$$\phi_{\boldsymbol{k}+\boldsymbol{G}}(\boldsymbol{r}) = \frac{1}{\sqrt{\Omega}} e^{i(\boldsymbol{k}+\boldsymbol{G})\boldsymbol{r}} \qquad \boldsymbol{r} \in I, \tag{4.24}$$

On the other hand, atomic radial functions and spherical harmonics are used to represent the wave function inside the atomic sphere α

$$\phi_{\boldsymbol{k}+\boldsymbol{G}}(\boldsymbol{r}) = \sum_{l=0}^{l_{max}} \sum_{m=-l}^{+l} [A_{lm}^{\alpha}(\boldsymbol{k}+\boldsymbol{G}) u_l(r_\alpha, E_l) + B_{lm}^{\alpha}(\boldsymbol{k}+\boldsymbol{G}) \dot{u}_l(r_\alpha, E_l)] Y_{lm}(\hat{r}_\alpha). \tag{4.25}$$

Here, $\boldsymbol{r}_\alpha$ denotes the position vector shifted by the position $\boldsymbol{R}_\alpha$ of atom α with the sphere radius R_α

$$\boldsymbol{r}_\alpha = \boldsymbol{r} - \boldsymbol{R}_\alpha, \qquad |\boldsymbol{r}_\alpha| \leq R_\alpha. \tag{4.26}$$

The radial wave functions $u_l(r_\alpha, E_l)$ and their *energy* derivatives $\dot{u}_l(r_\alpha, E_l)$ are determined from a numerical integration of the radial part of the Schrödinger equation (4.27) and its energy derivative (4.28)

$$[\hat{T} + v_{\text{eff}}(r_\alpha)] u_l(r_\alpha, E_l) Y_{lm}(\hat{r}_\alpha) = E_l u_l(r_\alpha, E_l) Y_{lm}(\hat{r}_\alpha), \tag{4.27}$$

$$[\hat{T} + v_{\text{eff}}(r_\alpha)] \dot{u}_l(r_\alpha, E_l) Y_{lm}(\hat{r}_\alpha) = [E_l \dot{u}_l(r_\alpha, E_l) + u_l(r_\alpha, E_l)] Y_{lm}(\hat{r}_\alpha). \tag{4.28}$$

In this context, the energies E_l are not eigenvalues, but chosen, fixed expansion energies, the *linearization* energies. The radial functions fulfill the following normalization conditions

$$\int_0^{R_\alpha} r^2 u_l^2(r)\mathrm{d}r = 1, \tag{4.29}$$

$$\int_0^{R_\alpha} r^2 u_l(r)\dot{u}_l(r)\mathrm{d}r = 0. \tag{4.30}$$

In addition we define the following integral

$$N_l \equiv \int_0^{R_\alpha} r^2 \dot{u}_l(r)\mathrm{d}r. \tag{4.31}$$

The coefficients $A_{lm}^\alpha(\boldsymbol{k}+\boldsymbol{G})$ and $B_{lm}^\alpha(\boldsymbol{k}+\boldsymbol{G})$ entering the expression (4.25) are chosen such, that the basis functions are continuous up to the first derivative at the sphere boundaries. These two conditions determine the coefficients A_{lm} and B_{lm}

$$A_{lm}^\alpha(\boldsymbol{k}+\boldsymbol{G}) = \frac{4\pi}{\sqrt{\Omega}} i^l Y_{lm}^*(\widehat{\boldsymbol{k}+\boldsymbol{G}}) c_l^\alpha(\boldsymbol{k}+\boldsymbol{G}) R_\alpha^2 e^{i(\boldsymbol{k}+\boldsymbol{G})\boldsymbol{R}_\alpha}, \tag{4.32}$$

$$B_{lm}^\alpha(\boldsymbol{k}+\boldsymbol{G}) = \frac{4\pi}{\sqrt{\Omega}} i^l Y_{lm}^*(\widehat{\boldsymbol{k}+\boldsymbol{G}}) d_l^\alpha(\boldsymbol{k}+\boldsymbol{G}) R_\alpha^2 e^{i(\boldsymbol{k}+\boldsymbol{G})\boldsymbol{R}_\alpha}, \tag{4.33}$$

with the abbreviations

$$c_l^\alpha(\boldsymbol{k}+\boldsymbol{G}) = j_l'(|\boldsymbol{k}+\boldsymbol{G}|R_\alpha)\dot{u}_l(R_\alpha) - j_l(|\boldsymbol{k}+\boldsymbol{G}|R_\alpha)\dot{u}_l'(R_\alpha), \tag{4.34}$$

$$d_l^\alpha(\boldsymbol{k}+\boldsymbol{G}) = j_l(|\boldsymbol{k}+\boldsymbol{G}|R_\alpha)u_l'(R_\alpha) - j_l'(|\boldsymbol{k}+\boldsymbol{G}|R_\alpha)u_l(R_\alpha). \tag{4.35}$$

Here, j_l is the spherical Bessel function, and the primes (dots) denote partial derivatives with respect to the radius r (expansion energy E_l). Thus, the basis functions and their first derivatives are continuous in the whole unit cell. The second derivative, however, is discontinuous at the sphere boundary.

4.3.2 The secular equation

By expanding the Kohn-Sham orbitals in terms of LAPW basis functions $\phi_{\boldsymbol{k}+\boldsymbol{G}}(\boldsymbol{r})$ with their dual representation introduced in the previous subsection, the Kohn-Sham equations are transformed into a *generalized* matrix eigenvalue problem (Ritz's variational principle).

$$H_{\boldsymbol{G}\boldsymbol{G}'}(\boldsymbol{k}) C_{veG'}(\boldsymbol{k}) = \varepsilon S_{\boldsymbol{G}\boldsymbol{G}'}(\boldsymbol{k}) C_{veG'}(\boldsymbol{k}). \tag{4.36}$$

Here, $H_{\boldsymbol{GG'}}(\boldsymbol{k})$ are the matrix elements of the Kohn-Sham Hamiltonian with the basis functions $\phi_{\boldsymbol{k+G}}(\boldsymbol{r})$

$$H_{\boldsymbol{GG'}}(\boldsymbol{k}) = \int \mathrm{d}^3 r \phi^*_{\boldsymbol{k+G}}(\boldsymbol{r}) h(\boldsymbol{r}) \phi_{\boldsymbol{k+G'}}(\boldsymbol{r}), \tag{4.37}$$

and $S_{\boldsymbol{GG'}}(\boldsymbol{k})$ denotes the overlap matrix which is no longer diagonal

$$S_{\boldsymbol{GG'}}(\boldsymbol{k}) = \int \mathrm{d}^3 r \phi^*_{\boldsymbol{k+G}}(\boldsymbol{r}) \phi_{\boldsymbol{k+G'}}(\boldsymbol{r}). \tag{4.38}$$

Similar to the treatment of wave functions in the full-potential LAPW method, also the valence electron density as well as the Kohn-Sham potential is expanded in a dual representation in the full-potential LAPW method: spherical harmonics are used inside the muffin-tin spheres and plane waves are taken in the interstitial.

It is important to note that also in the FP-LAPW method there is a difference in the mathematical description of *valence* and *core* electrons. Valence electrons are characterized by the fact that their wave function is de-localized over the whole unit cell, in particular there is a non-vanishing probability for them to be located in the interstitial region. Energetically, valence electron states lie close to the Fermi level. On the other hand, *core* electrons are energetically much deeper an can therefore be assumed to be confined within one atomic sphere. Thus in the LAPW method, which is an *all*-electron method, core electrons are treated only inside the muffin-tin spheres, by solving the Schrödinger equation, or indeed the relativistic Dirac equation. More detailed information can be found in the book by David Singh [66].

Bibliography

[1] C. Fiolhais, F. Nogueira, and M. A. L. Marques, editors. *A Primer in Density Functional Theory*. Springer, Berlin, 2003.

[2] M. Born and R. Oppenheimer. Zur Quantentheorie der Molekeln. *Ann. Physik*, 84:457, 1927.

[3] W. Kohn. Nobel lecture: Electronic structure of matter-wave functions and density functionals. *Rev. Mod. Phys.*, 71:1253, 1999.

[4] P. Hohenberg and W. Kohn. Inhomogeneous electron gas. *Phys. Rev.*, 136:B864, 1964.

[5] W. Kohn and L. J. Sham. Self-consistent equations including exchange and correlation effects. *Phys. Rev.*, 140(4A):A1133–A1138, Nov 1965.

[6] W. Kohn. An essay on condensed matter physics in the twentieth century. *Rev. Mod. Phys.*, 71, 1999.

[7] R. O. Jones and O. Gunnarsson. The density functional formalism, its application and prospects. *Rev. Mod. Phys.*, 61:689, 1989.

[8] Richard M. Martin. *Electronic Structure: Basic Theory and Practical Methods*. Cambridge University Press, 2010.

[9] D. S. Sholl and J. A. Steckel. *Density Functional Theory: A Practical Introduction*. Wiley, 2009.

[10] J. P. Perdew, K. Burke, and M. Ernzerhof. Generalized Gradient Approximation Made Simple. *Phys. Rev. Lett.*, 77:3865–3868, 1996.

[11] F. D. Murnaghan. The compressibility of media under extreme pressures. *Proc. Nat. Acad. Sci. U.S.A.*, 3:244, 1944.

[12] R. Golesorkhtabar, P. Pavone, J. Spitaler, P. Puschnig, and C. Draxl. Elastic: A universal tool for calculating elastic constants from first principles. *Comp. Phys. Comm.*, 184:1861–1873, 2013.

[13] Dario Knebl. Shockley surface states from first principles. Master's thesis, University of Graz, 2013.

[14] Anton S. Bochkarev, Maxim N. Popov, Vsevolod I. Razumovskiy, Jürgen Spitaler, and Peter Puschnig. Ab initio study of cu impurity diffusion in bulk tin. *Phys. Rev. B*, 94:104303, 2016.

[15] L. Romaner, C. Ambrosch-Draxl, and R. Pippan. Effect of rhenium on the dislocation core structure in tungsten. *Phys. Rev. Lett.*, 104:195503, 2010.

[16] Daniel Scheiber, Reinhard Pippan, Peter Puschnig, and Lorenz Romaner. Ab initio calculations of grain boundaries in bcc metals. *Modelling Simul. Mater. Sci. Eng.*, 24:035013, 2016.

[17] P. Sony, P. Puschnig, D. Nabok, and C. Ambrosch-Draxl. Importance of Van Der Waals Interaction for Organic Molecule-Metal Junctions: Adsorption of Thiophene on Cu(110) as a Prototype. *Phys. Rev. Lett.*, 99:176401, 2007.

[18] Kristian Berland, Valentino R Cooper, Kyuho Lee, Elsebeth Schröder, T Thonhauser, Per Hyldgaard, and Bengt I Lundqvist. van der waals forces in density functional theory: a review of the vdw-df method. *Reports on Progress in Physics*, 78(6):066501, 2015.

[19] Jan Hermann, Robert A. DiStasio, and Alexandre Tkatchenko. First-principles models for van der waals interactions in molecules and materials: Concepts, theory, and applications. *Chemical Reviews*, 117:4714–4758, 2017.

[20] N.W. Ashcroft and N.D. Mermin. *Solid State Physics*. Saunders, Fort Worth, 1976.

[21] H. Sormann and E. Schachinger. Lecture Notes: Theoretische Festkörperphysik. TU Graz, Austria, 2012.

[22] James D. Patterson and Bernard C. Bailey. *Solid-State Physics - Introduction to the Theory*. Springer, 2007.

[23] Murray Gell-Mann and Keith A. Brueckner. Correlation energy of an electron gas at high density. *Phys. Rev.*, 106:364–368, Apr 1957.

[24] L. Onsager, L. Mittag, and M. J. Stephen. Integrals in the theory of electron correlations. *Annalen der Physik*, 473(1-2):71–77, 1966.

[25] J. P. Perdew and Y. Wang. Accurate and simple analytic representation of the electron-gas correlation energy. *Phys. Rev. B*, 45:13244, 1992.

[26] P. Nozieres and D. Pines. Correlation energy of a free electron gas. *Phys. Rev.*, 111(2):442–454, Jul 1958.

[27] D. M. Ceperly and B. J. Alder. Ground state of the electron gas by a stochastic method. *Phys. Rev. Lett.*, 45:566, 1980.

[28] D. M. Ceperly. Ground state of the fermion one-component plasma: A monte carlo study in two and three dimensions. *Phys. Rev. B*, 18:3126, 1978.

[29] W. Kohn. Density Functional Theory: Fundamentals and Applications. *Reprint from Highlights of Condensed- Matter Theory, Soc. Italiana di Fisica*, Course LXXXIX:4, 1985.

[30] M. Levy. Electron densities in search of hamiltonians. *Phys. Rev. A*, 26:1200, 1982.

[31] E. J. Baerends and O. V. Gritsenko. A quantum chemical view of density functional theory. *The Journal of Physical Chemistry A*, 101(30):5383–5403, 1997.

[32] John P. Perdew, Adrienn Ruzsinszky, Gabor I. Csonka, Oleg A. Vydrov, Gustavo E. Scuseria, Lucian A. Constantin, Xiaolan Zhou, and Kieron Burke. Restoring the density-gradient expansion for exchange in solids and surfaces. *Phys. Rev. Lett.*, 100(13):136406, 2008.

[33] Philipp Haas, Fabien Tran, and Peter Blaha. Calculation of the lattice constant of solids with semilocal functionals. *Phys. Rev. B*, 79(8):085104, 2009.

[34] G. Pilania, J.E. Gubernatis, and T. Lookman. Multi-fidelity machine learning models for accurate bandgap predictions of solids. *Computational Materials Science*, 129:156 – 163, 2017.

[35] John P. Perdew, Adrienn Ruzsinszky, Lucian A. Constantin, Jianwei Sun, and Gabor I. Csonka. Some fundamental issues in ground-state density functional theory: A guide for the perplexed. *J. Chem. Theory Comput.*, 5(4):902–908, APR 2009.

[36] Ann E. Mattsson. In pursuit of the "divine" functional. *Science*, 298:759–760, 2002.

[37] J. Tao and al. Climbing the density functional ladder: Nonempirical Meta-Generalized Gradient Approximation Designed for Molecules and Solids. *Phys. Rev. Lett.*, 91:146401–1, 2003.

[38] Jianwei Sun, Adrienn Ruzsinszky, and John P. Perdew. Strongly constrained and appropriately normed semilocal density functional. *Phys. Rev. Lett.*, 115:036402, Jul 2015.

[39] John P. Perdew, Matthias Ernzerhof, and Kieron Burke. Rationale for mixing exact exchange with density functional approximations. *J. Chem. Phys.*, 105:9982, 1996.

[40] J. Paier, M. Marsman, K. Hummer, G. Kresse, I. C. Gerber, and A. G. Angyan. Screened hybrid density functionals applied to solids. *J. Chem. Phys.*, 124:154709, 2006.

[41] Leeor Kronik, Tamar Stein, Sivan Refaely-Abramson, and Roi Baer. Excitation gaps of finite-sized systems from optimally tuned range-separated hybrid functionals. *J. Chem. Theo. Comp.*, 8(5):1515–1531, 2012.

[42] Sivan Refaely-Abramson, Sahar Sharifzadeh, Manish Jain, Roi Baer, Jeffrey B. Neaton, and Leeor Kronik. Gap renormalization of molecular crystals from density-functional theory. *Phys. Rev. B*, 88:081204, Aug 2013.

[43] Daniel Lüftner, Sivan Refaely-Abramson, Michael Pachler, Roland Resel, Michael G. Ramsey, Leeor Kronik, and Peter Puschnig. Experimental and theoretical electronic structure of quinacridone. *Phys. Rev. B*, 90:075204, 2014.

[44] John F. Dobson and Bradley P. Dinte. Constraint satisfaction in local and gradient susceptibility approximations: Application to a van der waals density functional. *Phys. Rev. Lett.*, 76:1780–1783, 1996.

[45] M. Lein, J. F. Dobson, and E. K. U. Gross. Toward the description of van der waals interactions within density functional theory. *J. Comput. Chem.*, 20:12–22, 1999.

[46] J. Harl, L. Schimka, and Georg Kresse. Assessing the quality of the random phase approximation for lattice constants and atomization energies of solids. *Phys. Rev. B*, 81:115126, 2010.

[47] D C Langreth, B I Lundqvist, S D Chakarova-Käck, V R Cooper, M Dion, P Hyldgaard, A Kelkkanen, J Kleis, Lingzhu Kong, Shen Li, P G Moses, E Murray, A Puzder, H Rydberg, E Schröder, and T Thonhauser. A density functional for sparse matter. *J. Phys.: Condens. Matter*, 21:084203, 2009.

[48] Stefan Grimme. Density functional theory with london dispersion corrections. *Comput. Mol. Sci.*, 1:211–228, 2011.

[49] M. Dion, H. Rydberg, E. Schröder, D. C. Langreth, and B. I. Lundqvist. Van der Waals Density Functional for General Geometries. *Phys. Rev. Lett.*, 92:246401, 2004.

[50] Kyuho Lee, Éamonn D. Murray, Lingzhu Kong, Bengt I. Lundqvist, and David C. Langreth. Higher-accuracy van der waals density functional. *Phys. Rev. B*, 82(8):081101, Aug 2010.

[51] Y. Zhang and W. Yang. Comment on "Generalized Gradient Approximation Made Simple". *Phys. Rev. Lett.*, 80:890, 1998.

[52] T. Thonhauser, Valentino R. Cooper, Shen Li, Aaron Puzder, Per Hyldgaard, and David C. Langreth. Van der Waals density functional: Self-consistent potential and the nature of the van der Waals bond. *Phys. Rev. B*, 76:125112, 2007.

[53] J. F. Janak. Proof that $dE/dn_i = \varepsilon_i$ in density functional theory. *Phys. Rev. B*, 18:7165, 1978.

[54] J. P. Perdew, R. G. Parr, M. Levy, and J. L. Balduz. Density-functional for fractional particle number: Derivative discontinuities of the energy. *Phys. Rev. Lett.*, 49:1691, 1982.

[55] Oleg A. Vydrov, Gustavo E. Scuseria, and John P. Perdew. Tests of functionals for systems with fractional electron number. *J. Chem. Phys.*, 126:154109, 2007.

[56] J. P. Perdew and M. Levy. Physical content of the exact Kohn-Sham orbital energies: Band gaps and derivative discontinuities. *Phys. Rev. Lett.*, 51:1884, 1983.

[57] Fabien Tran and Peter Blaha. Accurate band gaps of semiconductors and insulators with a semilocal exchange-correlation potential. *Phys. Rev. Lett.*, 102(22):226401, 2009.

[58] Jochen Heyd, Gustavo E. Scuseria, and Matthias Ernzerhof. Erratum: "hybrid functionals based on a screened coulomb potential" [j. chem. phys. 118, 8207 (2003)]. *J. Chem. Phys.*, 124:219906, 2006.

[59] M. S. Hybertsen and S. G. Louie. First-principles theory of quasiparticles: Calculation of band gaps in semiconductors and insulators. *Phys. Rev. Lett.*, 55:1418, 1985.

[60] M. S. Hybertsen and S. G. Louie. Electron correlation in semiconductors and insulators: Band gaps and quasiparticle energies. *Phys. Rev. B*, 34:5390, 1986.

[61] Kurt Lejaeghere, Gustav Bihlmayer, Torbjörn Björkman, Peter Blaha, Stefan Blügel, Volker Blum, Damien Caliste, Ivano E. Castelli, Stewart J. Clark, Andrea Dal Corso, Stefano de Gironcoli, Thierry Deutsch, John Kay Dewhurst, Igor Di Marco, Claudia Draxl, Marcin Dułak, Olle Eriksson, José A. Flores-Livas, Kevin F. Garrity, Luigi Genovese, Paolo Giannozzi, Matteo Gianotomassi, Stefan Goedecker, Xavier Gonze, Oscar Grånäs, E. K. U. Gross, Andris Gulans, François Gygi, D. R. Hamann, Phil J. Hasnip, N. A. W. Holzwarth, Diana Iuşan, Dominik B. Jochym, François Jollet, Daniel Jones, Georg Kresse, Klaus Koepernik, Emine Küçükbenli, Yaroslav O. Kvashnin, Inka L. M. Locht, Sven Lubeck, Martijn Marsman, Nicola Marzari, Ulrike Nitzsche, Lars Nordström, Taisuke Ozaki, Lorenzo Paulatto, Chris J. Pickard, Ward Poelmans, Matt I. J. Probert, Keith Refson, Manuel Richter, Gian-Marco Rignanese, Santanu Saha, Matthias Scheffler, Martin Schlipf, Karlheinz Schwarz, Sangeeta Sharma, Francesca Tavazza, Patrik Thunström, Alexandre Tkatchenko, Marc Torrent, David Vanderbilt, Michiel J. van Setten, Veronique Van Speybroeck, John M. Wills, Jonathan R. Yates, Guo-Xu Zhang, and Stefaan Cottenier. Reproducibility in density functional theory calculations of solids. *Science*, 351(6280), 2016.

[62] N. Troullier and J. L. Martins. Efficient pseudopotentials for plane-wave calculations. *Phys. Rev. B*, 43:1993–2006, 1991.

[63] D. Vanderbilt. Soft self-consistent pseudopotentials in a generalized eigenvalue formalism. *Phys. Rev. B*, 41:7892, 1990.

[64] P. E. Blöchl. Projector augmented-wave method. *Phys. Rev. B*, 50:17953–17979, 1994.

[65] J. C. Slater. Wave functions in a periodic potential. *Phys. Rev.*, 51:846, 1937.

[66] D. Singh. *Planewaves, Pseudopotentials and the LAPW Method*. Kluwer Academic Publishers, Boston/Dordrecht/London, 1994. ISBN 0–7923–9412–7.

List of Figures